OLED DISPLAY FUNDAMENTALS AND APPLICATIONS

SECOND EDITION

Takatoshi Tsujimura



WILEY SID Series in **Display Technology**

Petitioner Samsung Ex-1009, 0001

OLED Display Fundamentals and Applications

Petitioner Samsung Ex-1009, 0002

Wiley-SID Series in Display Technology

Series Editors:
Anthony C. Lowe, The Lambent Consultancy, Braishfield, UK
Ian Sage, Abelian Services, Malvern, UK

A complete list of the titles in this series appears at the end of this volume.

Petitioner Samsung Ex-1009, 0003

OLED Display Fundamentals and Applications

Second Edition

Takatoshi Tsujimura

WILEY

Petitioner Samsung Ex-1009, 0004

This edition first published 2017
© 2017 John Wiley & Sons, Inc.

All rights reserved. No part of this publication may be reproduced, stored in a retrieval system, or transmitted, in any form or by any means, electronic, mechanical, photocopying, recording or otherwise, except as permitted by law. Advice on how to obtain permission to reuse material from this title is available at http://www.wiley.com/go/permissions.

The right of Takatoshi Tsujimura to be identified as the author(s) of this work has been asserted in accordance with law.

Registered Office
John Wiley & Sons, Inc., 111 River Street, Hoboken, NJ 07030, USA

Editorial Office
111 River Street, Hoboken, NJ 07030, USA

For details of our global editorial offices, customer services, and more information about Wiley products visit us at www.wiley.com.

Wiley also publishes its books in a variety of electronic formats and by print-on-demand. Some content that appears in standard print versions of this book may not be available in other formats.

Limit of Liability/Disclaimer of Warranty
The publisher and the authors make no representations or warranties with respect to the accuracy or completeness of the contents of this work and specifically disclaim all warranties; including without limitation any implied warranties of fitness for a particular purpose. This work is sold with the understanding that the publisher is not engaged in rendering professional services. The advice and strategies contained herein may not be suitable for every situation. In view of on-going research, equipment modifications, changes in governmental regulations, and the constant flow of information relating to the use of experimental reagents, equipment, and devices, the reader is urged to review and evaluate the information provided in the package insert or instructions for each chemical, piece of equipment, reagent, or device for, among other things, any changes in the instructions or indication of usage and for added warnings and precautions. The fact that an organization or website is referred to in this work as a citation and/or potential source of further information does not mean that the author or the publisher endorses the information the organization or website may provide or recommendations it may make. Further, readers should be aware that websites listed in this work may have changed or disappeared between when this works was written and when it is read. No warranty may be created or extended by any promotional statements for this work. Neither the publisher nor the author shall be liable for any damages arising here from.

Library of Congress Cataloguing-in-Publication Data

Names: Tsujimura, Takatoshi.
Title: OLED display fundamentals and applications / Takatoshi Tsujimura.
Description: Second edition. | Hoboken, New Jersey : John Wiley & Sons Inc., 2017. | Series: Wiley series in display technology | Includes bibliographical references and index.
Identifiers: LCCN 2016042831| ISBN 9781119187318 (hardback) | ISBN 9781119187486 (epub) | ISBN 9781119187325 (epdf)
Subjects: LCSH: Flat panel displays. | Electrtoluminescent devices. | Organic semiconductors. | Light emitting diodes. | BISAC: TECHNOLOGY & ENGINEERING / Electronics / General.
Classification: LCC TK7882.I6 T84 2017 | DDC 621.3815/422–dc23 LC record available at https://lccn.loc.gov/2016042831

Cover image: © Blend Images - Colin Anderson/ Gettyimages
Cover design by Wiley

Set in 10/12pt Warnock by SPi Global, Chennai, India

Printed in United States of America

10 9 8 7 6 5 4 3 2 1

Petitioner Samsung Ex-1009, 0005

Contents

About the Author *xi*
Preface *xiii*
Series Editor's Foreword to the Second Edition *xv*

1 Introduction *1*
References *5*

2 OLED Devices *7*
2.1 OLED Definition *7*
2.1.1 History of OLED Research and Development *7*
2.1.2 Luminescent Effects in Nature *8*
2.1.3 Difference Between OLED, LED, and Inorganic ELs *11*
2.1.3.1 Inorganic EL *11*
2.1.3.2 LED *11*
2.2 Basic Device Structure *12*
2.3 Basic Light Emission Mechanism *14*
2.3.1 Potential Energy of Molecules *14*
2.3.2 Highest Occupied and Lowest Unoccupied Molecular Orbitals (HOMO and LUMO) *15*
2.3.3 Configuration of Two Electrons *17*
2.3.4 Spin Function *20*
2.3.5 Singlet and Triplet Excitons *20*
2.3.6 Charge Injection from Electrodes *24*
2.3.6.1 Charge Injection by Schottky Thermionic Emission *25*
2.3.6.2 Tunneling Injection *28*
2.3.6.3 Vacuum-Level Shift *28*
2.3.7 Charge Transfer and Recombination *29*
2.3.7.1 Charge Transfer Behavior *29*
2.3.7.2 Space-Charge-Limited Current *29*
2.3.7.3 Poole–Frenkel conduction *32*
2.3.7.4 Recombination and Generation of Excitons *33*

Petitioner Samsung Ex-1009, 0006

2.4 Emission Efficiency *36*
2.4.1 Internal/External Quantum Efficiency *36*
2.4.2 Energy Conversion and Quenching *37*
2.4.2.1 Internal Conversion *37*
2.4.2.2 Intersystem Crossing *37*
2.4.2.3 Doping *38*
2.4.2.4 Quenching *40*
2.4.3 Outcoupling Efficiency of OLED Display *42*
2.4.3.1 Light Output Distribution *42*
2.4.3.2 Snell's Law and Critical Angle *43*
2.4.3.3 Loss Due to Light Extraction *44*
2.4.3.4 Performance Enhancement by Molecular Alignment *45*
2.5 Lifetime and Image Burning *46*
2.5.1 Lifetime Definitions *46*
2.5.2 Degradation Analysis and Design Optimization *47*
2.5.3 Degradation Measurement and Mechanisms *50*
2.5.3.1 Acceleration Factor and Temperature Contribution *50*
2.5.3.2 Degradation Mechanism Variation *50*
2.6 Technologies to Enhance the Device Performance *51*
2.6.1 Thermally Activated Delayed Fluorescence *51*
2.6.2 Other Types of Excited States *53*
2.6.2.1 Excimer and Exciplex *53*
2.6.2.2 Charge-Transfer Complex *53*
2.6.3 Charge Generation Layer *54*
References *56*

3 OLED Manufacturing Process *61*
3.1 Material Preparation *61*
3.1.1 Basic Material Properties *61*
3.1.1.1 Hole Injection Material *61*
3.1.1.2 Hole Transportation Material *62*
3.1.1.3 Emission Layer Material *62*
3.1.1.4 Electron Transportation Material and Charge Blocking Material *63*
3.1.2 Purification Process *67*
3.2 Evaporation Process *68*
3.2.1 Principle *68*
3.2.2 Evaporation Sources *72*
3.2.2.1 Resistive Heating Method *72*
3.2.2.2 Electron Beam Evaporation *75*
3.2.2.3 Monitoring Thickness Using a Quartz Oscillator *76*
3.3 Encapsulation *79*
3.3.1 Dark Spot and Edge Growth Defects *79*

Petitioner Samsung Ex-1009, 0007

3.3.2 Light Emission from the Bottom and Top of the OLED Device *80*
3.3.3 Bottom Emission and perimeter sealing *81*
3.3.4 Top Emission *82*
3.3.5 Encapsulation Technologies and Measurement *83*
3.3.5.1 Thin-Film Encapsulation *84*
3.3.5.2 Face Sealing Encapsulation *87*
3.3.5.3 Frit Encapsulation *88*
3.3.5.4 WVTR Measurement *88*
3.4 Problem Analysis *91*
3.4.1 Ionization Potential Measurement *91*
3.4.2 Electron Affinity Measurement *92*
3.4.3 HPLC Analysis *93*
3.4.4 Cyclic Voltammetry *94*
References *96*

4 OLED Display Module *99*
4.1 Comparison Between OLED and LCD Modules *99*
4.2 Basic Display Design and Related Characteristics *101*
4.2.1 Luminous Intensity, Luminance, and Illuminance *101*
4.2.1.1 Luminous Intensity *101*
4.2.1.2 Luminance *102*
4.2.1.3 Illuminance *103*
4.2.1.4 Metrics Summary *104*
4.2.1.5 Helmholtz–Kohlrausch Effect *106*
4.2.2 OLED Current Efficiencies and Power Efficacies *106*
4.2.3 Color Reproduction *109*
4.2.4 Uniform Color Space *115*
4.2.5 White Point Determination *116*
4.2.6 Color Boost *119*
4.2.7 Viewing Condition *120*
4.3 Passive-Matrix OLED Display *121*
4.3.1 Structure *121*
4.3.2 Pixel Driving *122*
4.4 Active-Matrix OLED Display *125*
4.4.1 OLED Module Components *125*
4.4.2 Two-Transistor One-Capacitor (2T1C) Driving Circuit *127*
4.4.3 Ambient Performance *136*
4.4.3.1 Living Room Contrast Ratio *136*
4.4.3.2 Chroma Reduction Due to Ambient Light *137*
4.4.4 Subpixel Rendering *138*
References *139*

Petitioner Samsung Ex-1009, 0008

5 OLED Color Patterning Technologies *143*
5.1 Color-Patterning Technologies *143*
5.1.1 Shadow Mask Patterning *143*
5.1.1.1 Shadow Mask Process *143*
5.1.1.2 Blue Common Layer *146*
5.1.1.3 Polychromatic Pixel *147*
5.1.2 White + Color Filter Patterning *148*
5.1.3 Color Conversion Medium (CCM) Patterning *149*
5.1.4 Laser-Induced Thermal Imaging (LITI) Method *149*
5.1.5 Radiation-Induced Sublimation Transfer (RIST) Method *151*
5.1.6 Dual-Plate OLED Display (DOD) Method *152*
5.1.7 Other Methods *153*
5.2 Solution-Processed Materials and Technologies *153*
5.3 Next-Generation OLED Manufacturing Tools *158*
5.3.1 Vapor Injection Source Technology (VIST) Deposition *158*
5.3.2 Hot-Wall Method *163*
5.3.3 Organic Vapor-Phase Deposition (OVPD) Method *164*
References *165*

6 TFT and Driving for Active-Matrix Display *167*
6.1 TFT Structure *167*
6.2 TFT Process *169*
6.2.1 Low-Temperature Polysilicon Process Overview *169*
6.2.2 Thin-Film Formation *172*
6.2.3 Patterning Technique *173*
6.2.4 Excimer Laser Crystallization *177*
6.3 MOSFET Basics *180*
6.4 LTPS-TFT-Driven OLED Display Design *183*
6.4.1 OFF Current *183*
6.4.2 Driver TFT Size Restriction *184*
6.4.3 Restriction Due to Voltage Drop *185*
6.4.4 LTPS-TFT Pixel Compensation Circuit *190*
6.4.4.1 Voltage Programming *190*
6.4.4.2 Current Programming *192*
6.4.4.3 External Compensation Method *193*
6.4.4.4 Digital Driving *194*
6.4.5 Circuit Integration by LTPS-TFT *197*
6.5 TFT Technologies for OLED Displays *200*
6.5.1 Selective Annealing Method *200*
6.5.1.1 Sequential Lateral Solidification (SLS) Method *200*
6.5.1.2 Selective Annealing by Microlens Array *200*
6.5.2 Microcrystalline and Superamorphous Silicon *202*
6.5.3 Solid-Phase Crystallization *205*

Petitioner Samsung Ex-1009, 0009

6.5.3.1 MIC and MILC Methods *205*
6.5.3.2 AMFC Method *205*
6.5.4 Oxide Semiconductors *207*
References *210*

7 OLED Television Applications *215*
7.1 Performance Target *215*
7.2 Scalability Concept *217*
7.2.1 Relationship between Defect Density and Production Yield *217*
7.2.1.1 Purpose of Yield Simulation *217*
7.2.1.2 Defective Pixel Number Estimation Using the Poisson Equation *217*
7.2.2 Scalable Technology *217*
7.2.2.1 Scalability *218*
7.3 Murdoch's Algorithm to Achieve Low Power and Wide Color Gamut *219*
7.3.1 A Method for Achieving Both Low Power and Wide Color Gamut *219*
7.3.2 RGBW Driving Algorithm *221*
7.4 An Approach to Achieve 100% NTSC Color Gamut With Low Power Consumption Using White + Color Filter *224*
7.4.1 Consideration of Performance Difference between W-RGB and W-RGBW Method *224*
7.4.1.1 Issues of White + Color Filter Method for Large Displays *224*
7.4.1.2 Analysis of W-RGBW Approach to Circumvent Its Trade-off Situation *224*
7.4.1.3 Design of a Prototype to Demonstrate That Low Power Consumption Can Be Achieved with Large Color Gamut *229*
7.4.1.4 Product-Level Performance Demonstration by the Combination of Scalable Technologies *230*
References *233*

8 New OLED Applications *235*
8.1 Flexible Display/Wearable Displays *235*
8.1.1 Flexible Display Applications *235*
8.1.2 Flexible Display Substrates *235*
8.1.3 Laser Liftoff Process *236*
8.1.4 Barrier Technology for Flexible Displays *240*
8.1.5 Organic TFTs for Flexible Displays *241*
8.1.5.1 Organic Semiconductor Materials *242*
8.1.5.2 Organic TFT Device Structure and Processing *243*
8.1.5.3 Organic TFT Characteristics *245*
8.2 Transparent Displays *245*

Petitioner Samsung Ex-1009, 0010

8.3 Tiled Display *247*
8.3.1 Passive-Matrix Tiling *247*
8.3.2 Active-Matrix Tiling *248*
References *252*

9 OLED Lighting *255*
9.1 Performance Improvement of OLED Lighting *255*
9.2 Color Rendering Index *257*
9.3 OLED Lighting Requirement *259*
9.3.1 Correlated Color Temperature (CCT) *260*
9.3.2 Other Requirements *262*
9.4 Light Extraction Enhancement of OLED Lighting *262*
9.4.1 Various Light Absorption Mechanisms *262*
9.4.2 Microlens Array Structure *266*
9.4.3 Diffusion Structure *266*
9.4.4 Diffraction Structure *268*
9.4.5 Reduction of Plasmon Absorption *268*
9.4.5.1 Plasmonic Loss Mechanism *268*
9.5 Color Tunable OLED Lighting *269*
9.6 OLED Lighting Design *272*
9.6.1 Resistance Reduction *272*
9.6.2 Current Reduction *272*
9.7 Roll-to-Roll OLED Lighting Manufacturing *273*
References *275*

Appendix *277*

Index *281*

Petitioner Samsung Ex-1009, 0011

About the Author

Takatoshi Tsujimura joined IBM Japan for TFT-LCD development and was selected as one of the "10 best engineers/researchers in the 10 best Japanese companies" by Nikkei Electronics Magazine. He demonstrated OLED's capability to be applied to large television by the world's largest 20-in. demonstration and received SID Special Recognition Award in 2008. He moved to Kodak as a director and developed 100% NTSC white + color filter OLED display with less power consumption than LCDs, which has become industry-standard technology for OLED TV over 50 in. He is currently general manager of OLED business unit, Konica Minolta Inc. He received SID Fellow Award in 2013. He is an SID executive and is a former SID Japan chapter chair. He received PhD in materials science and engineering.

Dr. Tsujimura holds 144 worldwide registered patents and 7 publications including the following:

T. Tsujimura, *OLED Display Fundamentals and Application*, SID-Wiley Series in Display Science, ISBN: 978-1-118-14051-2 (2012)
T. Tsujimura, *OLED Overview (Japanese),* Sangyo Tosho, ISBN: 978–4782855560 (2010)
T. Tsujimura, *OLED display overview (Korean),* Hantee Media, ISBN: 8964211766 (2013)
T. Tsujimura, *OLED display overview (Chinese),* Publication House of Electronics Industry, ISBN: 9787121262814 (2015)
T. Tsujimura, *Technology and Material Development,* CMC Technical Library (2010)
T. Tsujimura, *OLED Material Technology,* CMC Publishing (2004)
T. Tsujimura, *OLED Handbook,* Realize Science and Engineering (2004).

Petitioner Samsung Ex-1009, 0012

Preface

In the 30 years that have passed since the release of the "first OLED paper," there have been many publications promoting organic light-emitting diode (OLED) displays as a superior technology. Although many aspects of OLED performance are excellent, such as the ultimate high contrast provided by its self-emissive mechanism, it has not been an easy path to achieve wide acceptance in the industry. A decade ago, I was often told by my customers that they totally agree with the beauty of OLED screens, but they are not affordable for common display applications. It is always the case that emerging technology faces difficulty in the wide-scale adoption, in spite of its inherent advantages. The well-established liquid-crystal display (LCD) has been manufactured for a very long time, so it has already been progressively engineered to improve its shortcomings, such as viewing angle, response time, and cost. It was not easy for OLED to overcome such a situation.

What triggered OLED to become so popular was the rapid growth of smart phones. The touchscreen interface paired very well with the OLED screen, as OLED did not show any "touch mura," a smear-like contrast reduction caused by flow-induced liquid crystal deformation. LCD, in a short time, improved the touch mura, but OLED makers utilized this momentary advantage to obtain a chance of growth. From this penetration of OLED display screens, end customers had a chance to recognize the superior display image quality of OLED, especially the beauty of its high contrast. This fortunate circumstance was a major benefit to OLED technology.

More recently, OLED has also penetrated the large television market, taking advantage of the high color gamut white + color filter method we developed, which promises high-yield manufacturing. OLED technology offers many important features for good television, so we expect it will gradually become more popular as the manufacturing cost goes down.

It is still a very important phase for OLED technology to become more widely used. The purpose of this book is to provide necessary information for everyone

Petitioner Samsung Ex-1009, 0014

who is involved with this great technology, so that such knowledge can lead to further improvements. I also hope the contents will help readers to hit upon new great applications, taking advantage of the features of OLED devices.

Takatoshi Tsujimura

Petitioner Samsung Ex-1009, 0015

Series Editor's Foreword to the Second Edition

In the 4 years since the first edition of Dr Tsujimura's book was published, the status of OLED displays has undergone a transformation. Their development can be exemplified by two products; the introduction of OLED televisions with diagonal screen sizes and resolution fully matching those of LCD sets but with curved screens represented a striking innovation which at that time could not be provided by LCD panels. Many commentators were surprised by the speed with which LCD manufacturers responded to this challenge. On the other hand, OLED panels on flexible substrates provide thin, conformable displays offering excellent compatibility with touchscreen technologies, which many users regard as a benchmark for display performance on mobile electronic devices.

OLED devices are therefore showing their ability to drive customer expectations for display performance. OLED displays provide a performance lead in terms of thin profile, response speed, and black level dominated dark room contrast, which appear difficult to challenge, while brightness, stability, and manufacturing cost are relatively weaker points. Meanwhile, competition between OLED and LCD manufacturers has stimulated innovation in both technologies, driving improvement in key areas such as power efficiency, color gamut, and resolution. As self-emissive devices, OLEDs are also generating widespread interest for lighting applications where their ability to offer a large area source and to achieve high-quality color rendering and tunable color temperature promises an excellent quality of illumination.

This second edition of Dr Tsujimura's book recognizes all these advances through updating and revision of his earlier material, and the addition of extensive new sections covering advances in the technological exploitation of OLEDs. Some of the most prominent of these include approaches to improved power efficiency and color gamut for OLED television, and how to combine both of these key advances; materials and manufacturing methods for flexible OLED displays; roll-to-roll manufacture of OLED lighting panels; and structures of transparent OLED panels. The treatment of a number of the underlying scientific principles involved in device operation and efficiency is

Petitioner Samsung Ex-1009, 0016

also expanded, with new material on luminescence mechanisms, light trapping and extraction, the behavior of various pixel driver circuits, and numerous other topics. It is our hope that these changes will both maintain the currency of the volume and increase its value to a broad range of users.

Dr Tsujimura brings to his subject, the experience and background knowledge gained through his long career researching and developing active matrix technologies, liquid crystal displays, and OLEDs. His knowledge and enthusiasm for his subject are clear in this book, which I believe will continue to provide a most valuable resource both for those working on OLED technologies and their applications, and for scientists and engineers who wish to increase their knowledge of this important field.

Malvern, UK *Ian Sage, Series Editor*

Petitioner Samsung Ex-1009, 0017

1

Introduction

The basic structure of organic light-emitting diodes (OLEDs) was reported by Tang and Van Slyke at Eastman Kodak in 1987 [1]. This was a groundbreaking study and was later referred to as the "first OLED paper." Now, almost 30 years later, there is a large market for OLED devices. The first OLED product was developed by Pioneer for car audio. Then the first mass production of AMOLED by SK display (a joint manufacturing venture by Eastman Kodak and Sanyo Electric) for Kodak's LS633 digital camera (Figure 1.1) accelerated the use of OLED for display applications.

This was followed by the widescale development of many other OLED-based products, including cellular phones (Figure 1.2), smart watches (Figure 1.3), audio players (Figure 1.4), and portable global positioning satellite (GPS) devices, which now provide high-resolution displays in brilliant, multitone colors.

Larger-display products have also been introduced on the market, such as those shown in Figure 1.5. Much larger prototypes have also been developed (Figure 1.6). Because of their superior features such as slim flat-screen design and aesthetically pleasing screen image, and due to high-contrast image signal emission and very good response time, the current state of the art of OLED television technology that has debuted in the marketplace is indeed groundbreaking [2].

The main objective of this book is to explain the basics and application of this promising technology from various perspectives.

OLED Display Fundamentals and Applications, Second Edition. Takatoshi Tsujimura.
© 2017 John Wiley & Sons, Inc. Published 2017 by John Wiley & Sons, Inc.

Petitioner Samsung Ex-1009, 0018



Figure 1.1 The first active-matrix OLED display product on the market (Kodak LS633 digital camera).



Figure 1.2 Example of a cellular phone using active-matrix OLED (AMOLED) (Galaxy S7 smartphone by Samsung).

Petitioner Samsung Ex-1009, 0019



Figure 1.3 Example of a smart watch using active-matrix OLED (AMOLED) (Apple Watch Series 2 by Apple).



Figure 1.4 Example of an audio player using active-matrix OLED (AMOLED) (Sony Walkman NW-X-1050).

Petitioner Samsung Ex-1009, 0020



Figure 1.5 Example of a large television using active-matrix OLED (AMOLED) (65-in. curved OLED TV demonstrated in SID2015 by LG display).



Figure 1.6 111-in. dual-sided flexible OLED television prototype (LG Display at IMID2016).

Petitioner Samsung Ex-1009, 0021

References

1 C. W. Tang and S. A. Van Slyke, Organic electroluminescent diodes, *Appl. Phys. Lett.* **51**(12):913–915 (1987).
2 T. Tsujimura, W. Zhu, S. Mizukoshi, N. Mori, M. Yamaguchi, K. Miwa, S. Ono, Y. Maekawa, K. Kawabe, M. Kohno, and K. Onomura, Advancements and outlook of high performance active-matrix OLED displays, *SID 2007 Digest*, 2007, p. 84.

Petitioner Samsung Ex-1009, 0022

2

OLED Devices

2.1 OLED DEFINITION

2.1.1 History of OLED Research and Development

Before any in-depth discussion of OLED display structure, let us consider the initial origins of OLED technology, which are based on early observations of electroluminescence (EL). In the early 1950s, a group of investigators at Nancy University in France applied high-voltage alternating-polarity fields in air to thin films of cellulose or cellophane containing deposited or dissolved acridine orange and quinacrine, and observed light emission [1]. One mechanism identified in these reaction processes involved excitation of electrons. Then in 1960, a team of investigators at New York University (NYU) made ohmic (a nonrectifying charge injection, which shows linear current–voltage relationship) dark-injecting electrode contacts to organic crystals and described the necessary workfunctions (energy requirements) for hole and electron-injecting electrode contacts [2]. These contacts are the source of charge injection in all present-day OLED devices. The same NYU group also studied direct-current (DC) EL in vacuo on a single pure anthracene crystal and tetracene-doped anthracene crystals in the presence of a small-area silver electrode at 400 V [3]. The proposed mechanism for this reaction was termed *field-accelerated electron excitation of molecular fluorescence*. The NYU group later observed that in the absence of an external electric field, the EL in anthracene crystals results from recombination of electron and hole and that the conducting-level energy of anthracene is higher than the exciton energy level [4].

Because of the association between EL and later OLED development on the basis of these and other early EL studies, the term *organic EL* gradually emerged and is still used today. EL includes two basic phenomena:

1. Light emission due to the presence of excited molecules caused by accelerated electrons (i.e., electrons that are accelerated to higher energy levels)
2. Light emission due to electron–hole recombination, as in all light-emitting diodes (LEDs).

OLED Display Fundamentals and Applications, Second Edition. Takatoshi Tsujimura.
© 2017 John Wiley & Sons, Inc. Published 2017 by John Wiley & Sons, Inc.

Petitioner Samsung Ex-1009, 0024

Table 2.1 Differences between Liquid Crystal and OLED Displays

Parameter	LCD	OLED
Response time	Slow	Fast
Luminance boost	Difficult	Possible
Viewing angle	Narrower high contrast angle region	Lambertian distribution[a)]
Number of components	More	Fewer
Differential aging[b)]	Small	Larger
Susceptibility to water and O_2		Larger

a) Outgoing light distribution whose luminance is proportional to $\cos\theta$. To be discussed in Section 4.2.1.4.
b) Luminance reduction in terms of use of a particular pixel and between colors. To be discussed in Section 2.5.

Phenomenon 1 is the narrower definition. Current OLED devices, after Tang and Van Slyke's "first OLED paper," utilize exclusively LED-like emission mechanisms, that is, phenomenon 2.

Table 2.1 lists the differences between a liquid crystal display (LCD) and an OLED display. The OLED has a very short response time and is capable of using "punching" (an imaging technique for enhancing the local luminance to emphasize the highlighted region of an image). The punching technique is used in cathode ray tubes (CRTs), which can have much higher luminance of a dot than the screen luminance. An OLED can use a similar operation, while a normal LCD display cannot.

Table 2.2 outlines the chronological history of OLED technology development.

The chronological sequence of development listed in Table 2.2 reflects the emergence of some general terms of classification of OLED technologies, including the following:

- Small-molecule OLED (SMOLED) and polymer OLED (PLED)
- Passive-matrix OLED (PMOLED) and active-matrix OLED (AMOLED) displays
- Fluorescent emission and phosphorescent emission.

The developments listed here and in Table 2.2 indicate that the rapid advances in OLED technologies resulted from extensive experimental trial and error. Each technology is discussed in further detail later in the book.

2.1.2 Luminescent Effects in Nature

There are several kinds of "luminescence" in nature, which can be explained by a mechanism similar to that of an OLED.

Petitioner Samsung Ex-1009, 0025

Table 2.2 Timeline for OLED Technology Development

Year	Event[a)]	Company/Institute
1960–mid–1970s	D OLED crystal molecule, anthracene, etc.[b)]	NRC (Canada), RCA
1983	D First observation of electroluminescence from polymer film	National Physical Laboratory
1987	P OLED diode structure paper in *Appl. Phys. Lett.*[b)]	Eastman Kodak
1988	P Double heterojunction[c)]	Kyushu University
1990	P First PLED paper in *Nature*[b)]	Cambridge University
1994	P White OLED demonstration[c)]	Yamagata University
1996	P first AMOLED demonstration (QVGA)[b)]	TDK
1998	D first phosphorescence OLED[b)]	Princeton University
1999	D first passive OLED product	Pioneer
1999	D Color OLED display by white + color filter method[c)]	TDK
2001	D 0.72-in. headmount display by AMOLED on silicon[b)]	eMagin
2001	D 13-in. SVGA AMOLED prototype[b)]	Sony
2001	D 2.1-in. 130-ppi AMOLED prototype[b)]	Seiko Epson/CDT
2002	D 15-in. 1280×720 OLED prototype[b)]	Eastman Kodak/Sanyo
2002	P Tandem OLED device demonstration[c)]	Yamagata University
2003	D digital camera with 2.2-in. AMOLED display[b)]	Eastman Kodak
2003	D Tiled 24-in. AMOLED prototype with by 12-in. display[b)]	Sony
2003	D 20-in. phosphorescence AMOLED prototype by a-Si backplane[b)]	ChiMei/IDT/IBM
2006	P White OLED with phosphorescent emitter[c)]	UDC
2007	D 11-in. OLED Television product[c)]	Sony
2007	P White OLED by all phosphorescent emitters[c)]	Konica Minolta
2008	P 12-in. Transparent OLED prototype[c)]	Samsung
2008	P 4-in. Flexible OLED prototype[c)]	Samsung
2008	P 100% NTSC low power OLED by white + color filter method[c)]	Kodak
2009	D OLED lighting product[c)]	Philips
2009	P TADF OLED device[c)]	Kyushu University

Petitioner Samsung Ex-1009, 0026

Table 2.2 (Continued)

Year	Event[a)]	Company/Institute
2010	P White OLED over 100 lm/W	UDC
2011	D OLED lighting product by all phosphorescent emitters[c)]	Konica Minolta/Philips
2013	D 55-in. OLED Television product by white + color filter method[c)]	LG display
2013	P 4KOLED Television prototype[c)]	Sony/Panasonic
2014	D Flexible OLED display product[c)]	LG display
2014	D Flexible OLED lighting product by roll-to-roll manufacturing[c)]	Konica Minolta

a) *Abbreviations in this column*: a-si—amorphous silicon; AMOLED—active-matrix OLED; D—development of; P—publication or presentation/demonstration of; PLED—polymer (O)LED; ppi—pixels per inch; QVGA—quarter videographics array (320 × 240 pixels); SVGA—super videographics array (800 × 600 pixels).
b) SID International Symposium (2003), 40 Years of SID Symposia—Nurturing Progress in EL/OLED Technology, Baltimore, MD. http://sid.org/Portals/sid/Files/DisplayHistory/EL-OLED_History.pdf.
c) By Takatoshi Tsujimura, "Evolution and future of OLED lighting," OLED Forum Japan presentation, Kyushu University 11/12/2015.

A molecule has multiple discrete energy levels, each able to hold two electrons. When electrons fill these levels completely, beginning from the lowest in energy, the system is stable. This is called the ground state.

If an electron is moved to an upper empty energy level, the resulting configuration is called an excited state. The excited state is normally unstable, so the electron tends to release the energy and return to the ground state. In such a transition, the excess energy is released as light (called "luminescence") and/or heat.

Luminescence can be classified depending on how the energy is transferred to the system. Light emission by a firefly is a type of luminescence. Luciferin is oxidized to "oxyluciferin" in an excited state by luciferase enzyme in the presence of adenosine triphosphate. As the oxyluciferin converts to its ground state, the molecule loses energy that it emits as light. If an excited state created by a chemical reaction causes the photon emission as in this case, it is referred to as chemiluminescence.

Fluorescent paint shines when it is illuminated by short-wavelength light. By absorption of this light, an excited state is created and it causes light emission at a longer wavelength, termed photoluminescence (PL).

Petitioner Samsung Ex-1009, 0027

When energy is transferred to the molecule by an electric field or current, subsequent light emission is called EL.

There are also many other luminescence effects, such as mechanoluminescence, and so on. Many of these phenomena have similar mechanisms, in which excess energy is released as photons and the system relaxes to the ground state, as a result.

2.1.3 Difference Between OLED, LED, and Inorganic ELs

OLED, LED, and inorganic EL devices all emit light electrically, so the distinction between them may be confusing. Here, the features for each technology are summarized.

2.1.3.1 Inorganic EL

An inorganic EL device has a structure similar to an OLED, with emissive layers sandwiched by insulators and two electrodes. However, the emission mechanism is quite different.

An inorganic EL device's emissive layer is a mixture of a semiconductor and a metallic compound. Free electrons in the semiconductor are accelerated by an electric field and their kinetic energy is transferred to emission centers, which are excited by their impact. The excited emission center is unstable and loses its energy by emitting a photon.

If a DC voltage were used for electron acceleration, the emission would stop when the electric field in the semiconductor was sufficiently shielded by the electron movement. Therefore, inorganic EL devices are driven by an AC voltage so that the emission is continued.

2.1.3.2 LED

Normally, inorganic LEDs are simply called "LEDs." Though the materials are different, LEDs and organic LEDs have similar emission mechanisms.

Pure semiconductors normally have very few mobile charge carriers. For electronic purposes, doping of impurities into the semiconductor is frequently used to change its conductivity. The impurities may be of two kinds.

1. "Donor"-type impurities, which supply electrons to semiconductors. Electrons are the major charge carriers in this case and such semiconductors with donor impurities are called "n-type."
2. "Acceptor"-type impurities, which supply holes to semiconductors. (As a "hole" means "lack of an electron," supplying a hole is equivalent to accepting an electron.) Holes are then the major charge carriers and semiconductors with acceptor impurities are called "p-type."

If layers of n-type and p-type semiconductors are stacked together to form a junction with electrodes sandwiching the p/n junction layers, electrons from

Petitioner Samsung Ex-1009, 0028

the n-type semiconductor and holes from the p-type semiconductor recombine when electric current is applied between the two electrodes. Recombination in the p–n junction creates excited states that emit photons.

Thus, inorganic LEDs have a mechanism similar to that of organic LEDs, which also emit light due to electron–hole recombination. (To be precise, the conduction mechanisms of LEDs and organic LEDs are not the same. Inorganic semiconductor charge carriers are described by a band theory, in which the periodic potential of the semiconductor crystal leads to formation of a Bloch wave. This theory cannot normally be applied to the disordered layers formed by the organic molecules used for OLEDs. So LEDs and OLEDs operate by the same charge recombination route but due to different conduction mechanisms.)

2.2 BASIC DEVICE STRUCTURE

Emission from all OLED devices—whether of the small-molecular or polymer family—can be explained by the same principle. Through electron–hole recombination, a high-energy molecular state is formed. This state is called an *exciton*, as it behaves like a single molecule with high energy. This exciton emits light after an exciton lifetime period (Figure 2.1). (It should be noted that "exciton lifetime" is the exciton decay period and does not refer to the OLED device lifetime.) [Another type of emission, termed *photoluminescent* (PL) emission, is caused by light (e.g., UV)-induced molecular excitation.]

The wavelength of this light emission corresponds to the exciton energy, so it is possible to control the color of the emission by adjusting the molecular design of the color center. This feature is quite advantageous for OLED display applications.

In experiments using tetracene-doped anthracene crystals and materials, OLED emission had been observed before the so-called first OLED paper in 1987 [5] (see Row 1 in Table 2.2 [4]). However, the operating voltage and efficiency levels were insufficient for actual application. The structure depicted in Figure 2.2 and described in the Tang–Van Slyke paper [5] represents advanced concepts that remain valid today:

1. Significant enhancement of the recombination efficiency by using a layered structure using multiple different materials (heterostructure)
2. Fabrication of low-voltage, high-quality devices through evaporation
3. Appropriate choice of electron and hole injection materials and of work-functions for cathode/anode electrodes
4. High electric field obtained by ultrathin-film formation.

OLED devices could emit very dim light before these developments, but high-luminance operation was achieved only after the first OLED paper.

Petitioner Samsung Ex-1009, 0029

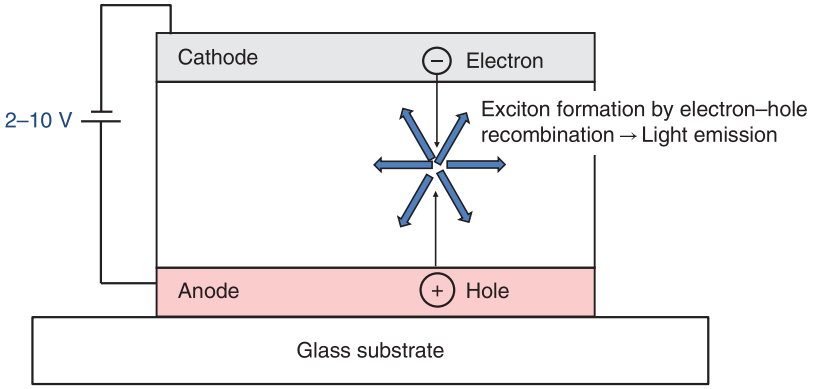


Figure 2.1 Diagram of the OLED emission mechanism.

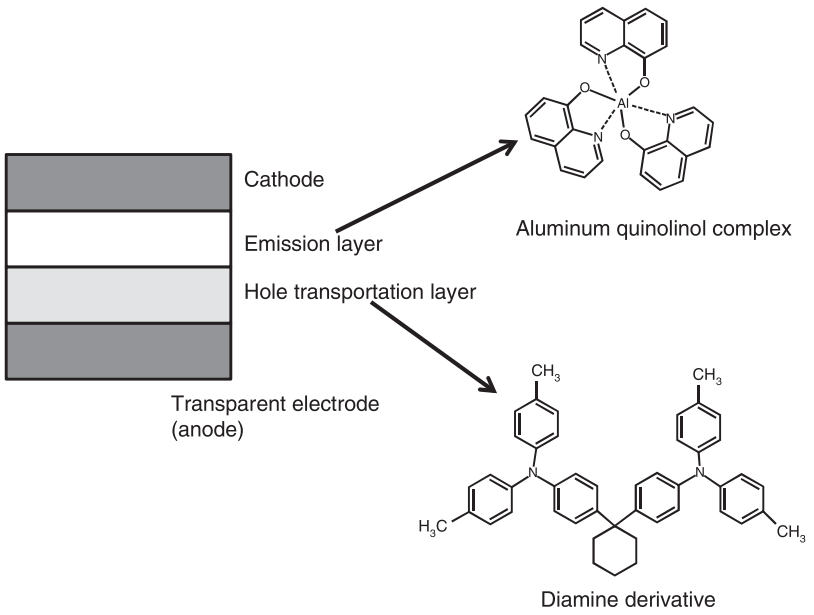


Figure 2.2 OLED device reported by Tang and Van Slyke in 1987 [5].

As mentioned earlier, the two basic families of OLED are small molecule and polymer (SMOLED and PLED). In SMOLED devices, a small molecule is deposited by evaporation technique, so the molecular size is small (however, the mass number of a small molecule can be relatively large). On the other hand, many PLED materials have structures containing chemical groups connected together, including structures that promote solubility and others that

Petitioner Samsung Ex-1009, 0030

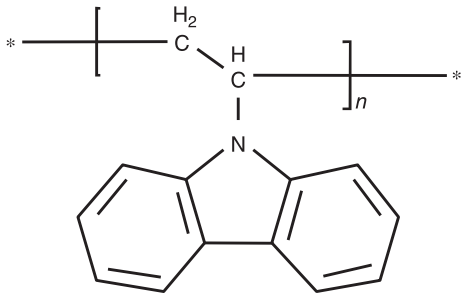


Figure 2.3 Example of a polymer OLED with polyvinylcarbazole molecular structure.

support light emission, the structure having a large overall molecular mass. Figure 2.2 shows typical examples of small-molecule OLED materials: Alq_3 and a diamine derivative. Figure 2.3 presents an example of a polymer OLED material: polyvinylcarbazole (PVK).

2.3 BASIC LIGHT EMISSION MECHANISM

The emission mechanism of OLED is discussed in this section.

2.3.1 Potential Energy of Molecules

When a molecule absorbs light, energy corresponding to the wavelength of light brings the molecule to metastable excited state through an electronic transition. For simplicity, a two-atom molecule, *A–B*, is assumed. When the distance between the two atoms is $r_{A\text{-}B}$, the potential energy *E* can be described by Figure 2.4 [6]. The lower curve represents the molecule in its electronic ground state. In the ground state, with a very short $r_{A\text{-}B}$, *E* increases rapidly. When $r_{A\text{-}B}$ is very long, the molecule will become dissociated. The most stable region is at the bottom of the valley in the potential energy curve. The parallel horizontal lines show the energies of different vibrational states. It can also be seen that the potential energy curves of Figure 2.4b also have similar vibrational states.

When a molecule absorbs light, according to the Franck–Condon principle, the molecule increases its energy without changing the interatomic distance. Therefore, the energy increase can be shown as a vertical arrow in Figure 2.4 (called a "vertical transition").

If the potential curve of the excited state does not have a minimum (Figure 2.4a), the excited state is unstable and will dissociate by the increase of $r_{A\text{-}B}$ with a corresponding decrease of potential energy. (This situation is called “Predissociation.”) In such cases, a continuous optical emission spectrum is observed.

When the excited state potential curve has a valley shape as in Figure 2.4b, the excited state is not easily dissociated; a metastable excited state is formed.

Petitioner Samsung Ex-1009, 0031

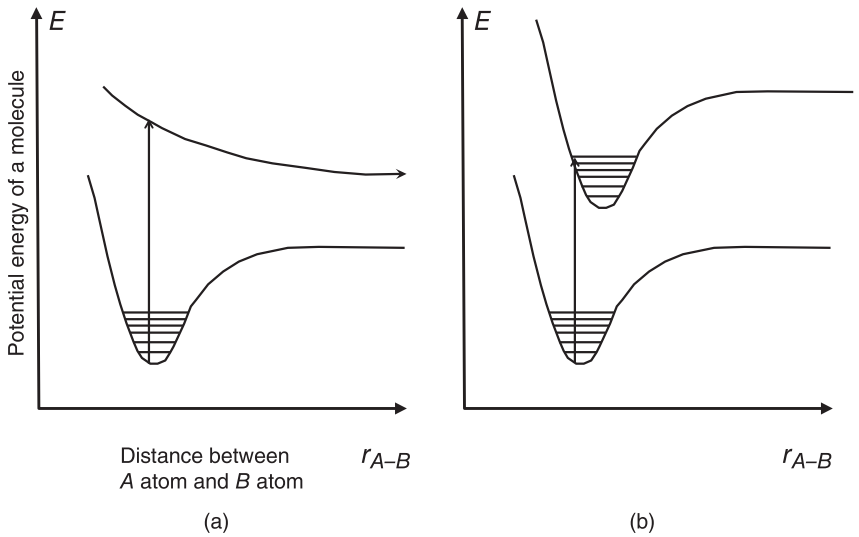


Figure 2.4 Potential curve of ground state and excited state in the case of a two-atom molecule.

As shown in Figure 2.5, several peaks often appear in the absorption spectrum, which correspond to different vibrational levels. (As shown in the figure, the shape of the fluorescent emission spectrum tends to resemble a mirror image of the absorption spectrum. This is because the vibrational level of the excited state and the ground state have similar structures.)

Immediately after light absorption, the interatomic distance in the excited molecule is the same as in the ground state (vertical transition). In a short time, it loses some vibration energy; atoms change their relative positions and the molecule relaxes to the lowest potential energy point along the excited state curve (called "internal conversion," and discussed in Section 2.4.2.1).

2.3.2 Highest Occupied and Lowest Unoccupied Molecular Orbitals (HOMO and LUMO)

When a ground state molecule absorbs light, the molecule changes to an excited state through electron reconfiguration. Using molecular orbital theory, a single covalent bond can be expressed as a linear combination of two electronic wavefunctions. In the case of a single bond, there is a bonding σ orbital with lower energy and an antibonding σ^* orbital with higher energy.

In the case of a double bond, the available energy levels can be shown as Figure 2.6, with σ and σ^* as bonding and antibonding orbitals, respectively, and also π and π^* bonding and antibonding orbitals, respectively.

Figure 2.7 shows the electron configuration of a more complicated molecule in the molecular orbital formalism.

Petitioner Samsung Ex-1009, 0032

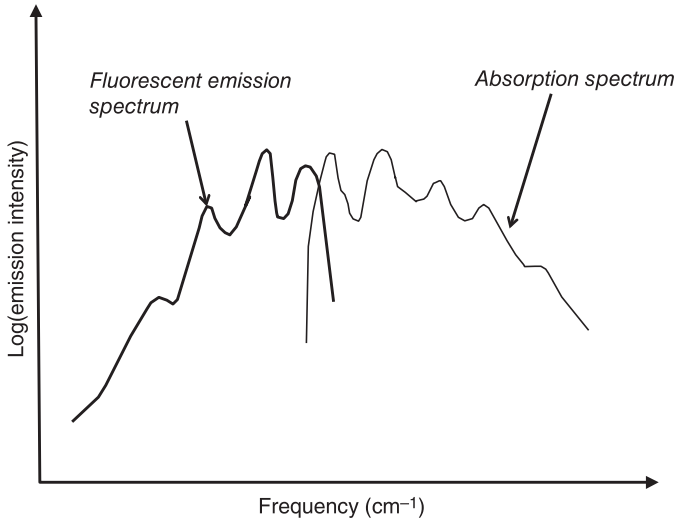


Figure 2.5 An example of absorption spectrum and fluorescent emission spectrum.

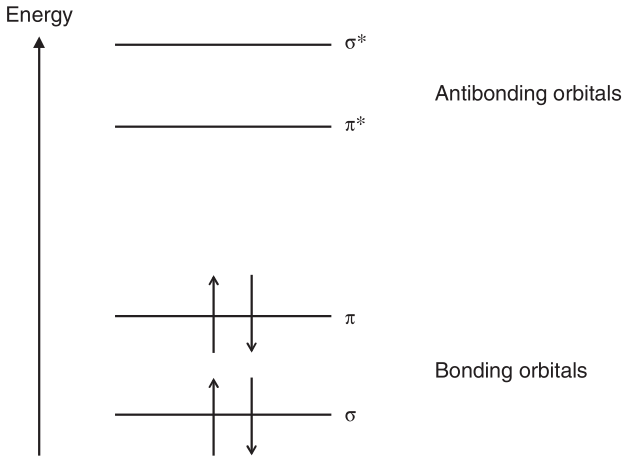


Figure 2.6 Electron configuration of double bond molecular orbital in molecular orbital.

Of all the electron-filled orbitals, the orbital having the maximum energy is called the *highest occupied molecular orbital* (HOMO). Conversely, among the unfilled electron orbitals, the orbital with the lowest electron energy is termed the *lowest unoccupied molecular orbital* (LUMO). The absolute values of the HOMO and LUMO energies relate to the ionization potential and electron affinity of the molecule. The ionization potential is the minimum energy

Petitioner Samsung Ex-1009, 0033

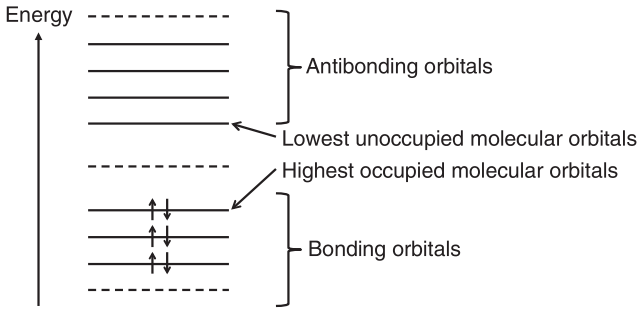


Figure 2.7 Electron configuration in molecular orbital.

required to extract one electron from the HOMO, and electron affinity is the energy released when one electron is added to the LUMO [7].

2.3.3 Configuration of Two Electrons

Before considering the OLED light emission mechanism, it is important for readers to understand the electron configuration in both the ground state and the excited state.

Let us assume that two electrons, 1 and 2, are located in different orbitals. Also, let us define H_1^0 and H_2^0 as Hamiltonians when electrons 1 and 2 exist without interacting:

$$H_1^0 = -\frac{\hbar^2}{2\mu}\nabla_1^2 - \frac{Ze^2}{r_1} \tag{2.1}$$

$$H_2^0 = -\frac{\hbar^2}{2\mu}\nabla_2^2 - \frac{Ze^2}{r_2} \tag{2.2}$$

$$H' = \frac{e^2}{r_{12}} \tag{2.3}$$

Here, H' is a perturbation due to interelectron repulsion.

When two electrons are allocated different orbitals, the Hamiltonian can be expressed as follows:

$$H = H_1^0 + H_2^0 + H' \tag{2.4}$$

If there is no perturbation, the solution of the wave equation can be expressed as follows:

$$\psi = C_1\chi_A(1)\chi_B(2) + C_2\chi_B(1)\chi_A(2) \tag{2.5}$$

The calculus of variations is useful here for solving the equation that accounts for perturbation as follows:

$$E\psi = (E^0 + E')\psi = H\psi \tag{2.6}$$

Petitioner Samsung Ex-1009, 0034

The energy E should be the minimized by the variation:

$$E = \frac{\int \psi H \psi \, d\tau}{\int \psi^2 d\tau} \tag{2.7}$$

As ψ_A, ψ_B are orthogonalized and normalized with respect to each other, the equation can be expressed as

$$\begin{aligned}\int \psi H \psi \, d\tau = \iint \{C_1 \chi_A(1)\chi_B(2) + C_2 \chi_B(1)\chi_A(2)\}(H_1^0 + H_2^0 + H') \\ \cdot \{(C_1 \chi_A(1)\chi_B(2) + C_2 \chi(1)\chi_A(2)\} d\tau_1 \, d\tau_2\end{aligned} \tag{2.8}$$

Here

$$\begin{aligned}&\iint \chi_A(1)\chi_B(2)(H_1^0 + H_2^0 + H')\chi_A(1)\chi_B(2) d\tau_1 \, d\tau_2 \\ &= \int \chi_A(1) H_1^0 \chi_A(1) d\tau_1 + \int \chi_B(2) H_2^0 \times \chi_B(2) d\tau_2 + J \\ &= E_A + E_B + J \\ &= E^0 + J\end{aligned} \tag{2.9}$$

and by applying the orthogonalization condition, we obtain

$$\begin{aligned}&\int \chi_A(1)\chi_B(1) d\tau_1 = 0 \\ &\int \chi_A(2)\chi_B(2) d\tau_2 = 0\end{aligned} \tag{2.10}$$

Therefore, Eq. (2.8) can be expressed as follows:

$$\int \psi H \psi \, d\tau = (C_1^2 + C_2^2)(E^0 + J) + 2C_1 C_2 K \tag{2.11}$$

Here, J is the Coulomb integral and K is the exchange integral, which can be expressed as follows:

$$\begin{aligned}J &= \iint \chi_A(1)\chi_B(2) H' \chi_A(1)\chi_B(2) d\tau_1 \, d\tau_2 \\ &= \iint \chi_B(1)\chi_A(2) H' \chi_B(1)\chi_A(2) d\tau_1 \, d\tau_2\end{aligned} \tag{2.12}$$

$$K = \iint \chi_A(1)\chi_B(2) H' \chi_B(1)\chi_A(2) d\tau_1 \, d\tau_2 \tag{2.13}$$

Petitioner Samsung Ex-1009, 0035

Using Eq. (2.7), we obtain

$$E = \frac{\int \psi H \psi \, d\tau}{\iint \{C_1 \chi_A(1)\chi_B(2) + C_2 \chi_B(1)\chi_A(2)\}^2 d\tau_1 \, d\tau_2}$$
$$= E^0 + H + \frac{2C_1C_2}{C_1^2 + C_2^2} K \tag{2.14}$$

According to the variational method, a condition for determining the minimum E value needs to be calculated.

A *minimum condition* occurs when the value of differentiation of E by C_1 and C_2 is zero:

$$\frac{\partial E}{\partial C_1} = \frac{\{2C_2(C_1^2 + C_2^2) - 2C_1C_2 \cdot 2C_1\}K}{(C_1^2 + C_2^2)^2} = 0 \tag{2.15}$$

Therefore,

$$\frac{2C_2(C_2^2 - C_1^2)K}{(C_1^2 + C_2^2)^2} = 0 \tag{2.16}$$

Then

$$C_2 = \pm C_1 \tag{2.17}$$

On the other hand, by applying the normalization condition, we obtain

$$\int \psi^2 d\tau = C_1^2 + C_2^2 = 1 \tag{2.18}$$

Therefore,

$$C_1 = \frac{1}{\sqrt{2}}, \quad C_2 = \pm\frac{1}{\sqrt{2}} \tag{2.19}$$

Using Eq. (2.14), we have

$$E' = E - E^0 = J \pm K$$

Also, by applying Eq. (2.5), we can obtain the following two wavefunctions:

$$\psi_s = \frac{1}{\sqrt{2}}\{\chi_A(1)\chi_B(2) + \chi_B(1)\chi_A(2)\} \tag{2.20}$$

$$\psi_a = \frac{1}{\sqrt{2}}\{\chi_A(1)\chi_B(2) - \chi_B(1)\chi_A(2)\} \tag{2.21}$$

Petitioner Samsung Ex-1009, 0036

2.3.4 Spin Function

The spin contribution to the molecular system must be considered in addition to the electron configuration determined in Section 2.3.3.

The wavefunction corresponding to a spin quantum number $\pm\frac{1}{2}$ (spin function) is expressed as α or β.

According to the same reasoning applied in Section 2.3.3, the characteristic spin function of a two-electron system can be expressed as follows:

$$\begin{aligned}
&\alpha(1)\alpha(2)\\
&\beta(1)\beta(2)\\
&\frac{1}{\sqrt{2}}\{\alpha(1)\beta(2)+\beta(1)\alpha(2)\}\\
&\frac{1}{\sqrt{2}}\{\alpha(1)\beta(2)-\beta(1)\alpha(2)\}
\end{aligned} \tag{2.22}$$

When the spin function is taken into account, the wavefunction must be antisymmetric with respect to electron exchange, as indicated in Eqs. (2.20) and (2.21); the wavefunction can then be expressed as follows:

$$\frac{1}{\sqrt{2}}\{\chi_A(1)\chi_B(2)+\chi_B(1)\chi_A(2)\}\cdot\frac{1}{\sqrt{2}}\{\alpha(1)\beta(2)-\beta(1)\alpha(2)\} \tag{2.23}$$

Three further degenerate states with respect to the wavefunctions can be expressed as follows:

$$\begin{aligned}
&\frac{1}{\sqrt{2}}\{\chi_A(1)\chi_B(2)-\chi_B(1)\chi_A(2)\}\alpha(1)\alpha(2)\}\\
&\frac{1}{\sqrt{2}}\{\chi_A(1)\chi_B(2)-\chi_B(1)\chi_A(2)\}\beta(1)\beta(2)\}\\
&\frac{1}{\sqrt{2}}\{\chi_A(1)\chi_B(2)-\chi_B(1)\chi_A(2)\}\cdot\frac{1}{\sqrt{2}}\{\alpha(1)\beta(2)+\beta(1)\alpha(2)\}
\end{aligned} \tag{2.24}$$

In total, four states, one in Eq. (2.23) and three in Eq. (2.24), are formed. Equation (2.23) represents *singlet state* and Eq. (2.24), the *triplet state*.

2.3.5 Singlet and Triplet Excitons

When $2n$ electrons are associated with the bonds in a molecule, $2n$ molecular orbitals are available to them. In the ground state, electrons occupy these from the lowest to higher energy orbitals in turn. Two electrons with opposite spin occupy each filled orbital as shown in the leftmost part of Figure 2.8. (This is the same case as Figure 2.7.) Normal molecules (those which have no unpaired electrons) have even numbers of electrons and the spins are paired as shown. This state is called S_0, the singlet ground state [6]. When a molecule absorbs light,

Petitioner Samsung Ex-1009, 0037

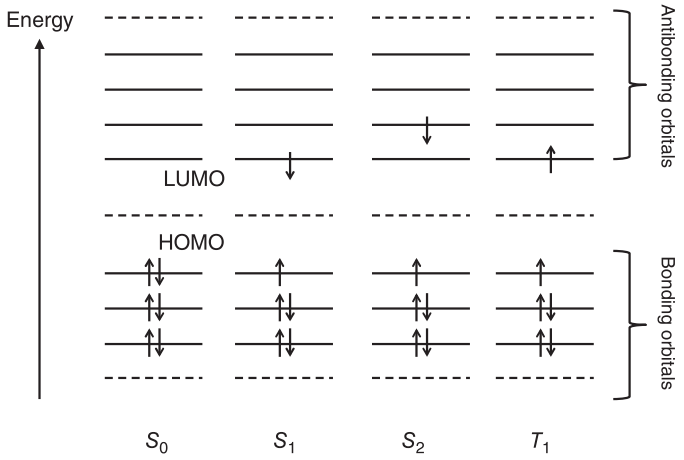


Figure 2.8 Electron configuration in ground state and excited states.

an electron changes its energy level from a bonding orbital to an antibonding orbital. When the electron changes its energy level to the lowest vacant orbital without changing its spin, as shown in the second left part of Figure 2.8, it is called S_1, the first excited singlet state. When a molecule is excited by a higher energy photon, that is, shorter wavelength light, the molecule can be changed to a higher energy state such as S_2, S_3, S_4, ...

If the electron changes its spin state on absorbing the photon energy, a triplet state results. If it changes its energy level to lowest vacant orbital and changes its spin, the resulting state is called T_1, the lowest excited triplet state, as shown in the rightmost part of Figure 2.8.

In reality, Figure 2.8 presents a simplified description. The excitation of electron(s) causes the molecule to change its configuration so that it becomes more stable in terms of energy, which also changes the energy levels of orbitals. Figure 2.9 shows the situation for an ethylene molecule. The energy gap is reduced by excitation. (This is why the energy difference between LUMO and HOMO is not in general the same as the energy difference between S_1 and S_0.)

Figure 2.10a shows the energy level of different molecular states. (This kind of energy level diagram of molecular states is called a Jablonski diagram. Jablonski diagrams are very useful to describe molecular state changes. It should be noted that the energy level in a Jablonski diagram shows the energy of molecular states. On the other hand, the energy levels in Figure 2.8 are those of orbitals.) As shown, triplet state T_1 has a lower energy than singlet state S_1. This cannot be explained by simple classical mechanics but requires a quantum mechanical discussion. Any two electrons of the same spin cannot occupy the same orbital, according to Pauli's exclusion principle, while two electrons with different spin states can exist in the same orbital. In a triplet state, where two electrons have

Petitioner Samsung Ex-1009, 0038

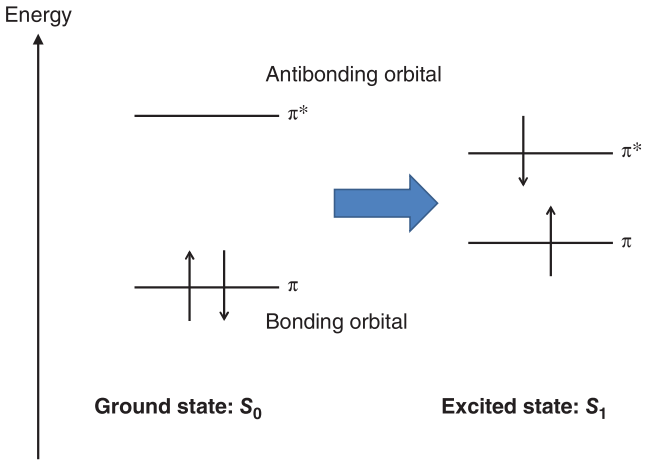


Figure 2.9 Electron configuration of ethylene molecule in S_0 ground state and in S_1 excited state.

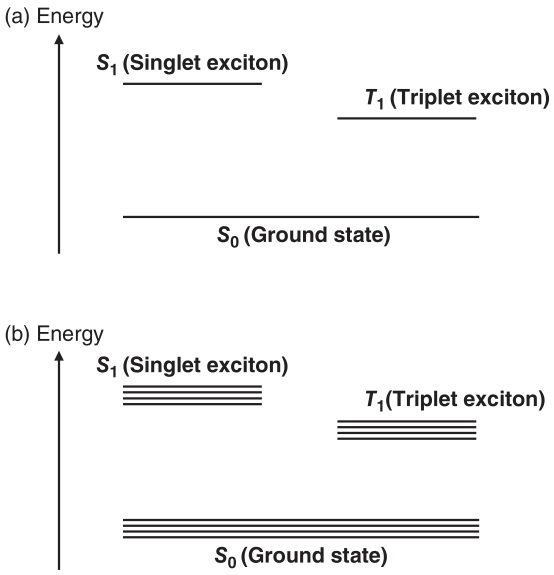


Figure 2.10 Energy state of each exciton (Jablonski energy diagram) (a) with and (b) without vibration states.

the same spin, the possibility of having the two electrons in the same location is zero. A quantum mechanical calculation also shows that the possibility of having the two electrons in the same vicinity is very low. In a singlet state where the electrons have different spins, the possibility of having them both in the same vicinity is much larger than in the case of a triplet. The difference in triplet

Petitioner Samsung Ex-1009, 0039

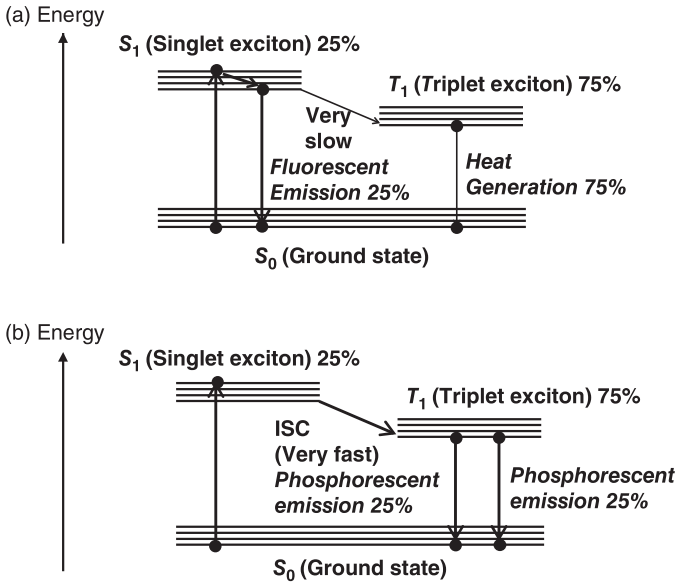


Figure 2.11 Emission mechanisms of (a) fluorescence (singlet) and (b) phosphorescence (triplet) (Jablonski energy diagram).

and singlet wavefunction distributions results in a lower repulsive energy in the triplet state compared to the singlet.

In a real molecule, there are various states due to the excitation of vibrations in the chemical bonds. Figure 2.10b shows the energy diagram taking vibrational states into account.

The excited molecules (excitons) lose their excess energy by one of the following routes (Figure 2.11):

(1) Energy loss by fluorescent light emission
(2) Energy loss by phosphorescent light emission
(3) Energy loss as heat by internal conversion (see Section 2.4.2.1)
(4) Energy causing a chemical reaction to form different molecules.

Regarding (1) and (2), light emission resulting from transition from a singlet state to the ground state is termed *fluorescent emission*; light emission from a triplet state to ground state transition is called *phosphorescent emission*

When two electrons are located in the same orbital, they form an *electron pair* with different spin states. This phenomenon is also known as the Pauli exclusion principle, which states that any two fermions (particles that follow the Fermi–Dirac statistics) of the same type (such as two electrons) cannot occupy the same quantum state simultaneously. Then, the spin direction must be reversed when the electron is changed from the T_1 to the S_0 state.

Petitioner Samsung Ex-1009, 0040

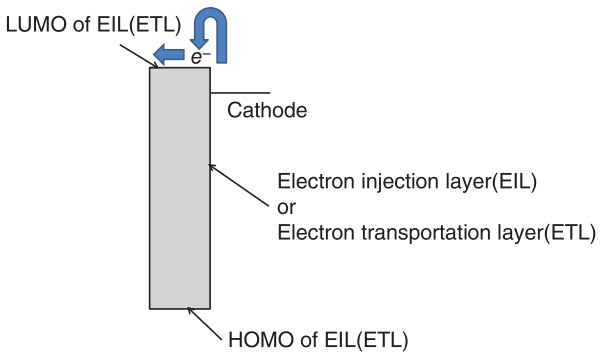


Figure 2.12 Electron injection from cathode to LUMO level of EIL(ETL) material.

Usually, this change is relatively slow, so the exciton lifetime (exciton decay time) of the triplet state is relatively long compared to that of singlet emission. Phosphorescent (triplet) light-emitting materials generally have complex metal structures including heavy metals such as iridium or platinum, as shown in Figure 3.7. These enable energy transfer between singlet and triplet (heavy-metal effect) that is normally prohibited. Due to the heavy-metal effect, both nonradiative transition from S_1 to T_1 (Intersystem crossing, discussed in Section 2.4.2) and radiative transition from T_1 to S_0 are accelerated. As triplet to singlet energy transfer, which is prohibited in the case of fluorescence, is allowed in phosphorescent case, high-efficiency emission is observed.

2.3.6 Charge Injection from Electrodes

Although an OLED device requires recombination of electrons and holes to emit light, normal OLED materials actually have very high resistance under weak electric fields and thus can be regarded as insulators. As discussed in Section 2.2, Tang and Van Slyke's work [5] was so successful because they introduced a very thin film to create strong electric fields and also chose structures and materials suitable for charge injection. State-of-the-art OLED devices also use the same concept. By means of a strong electric field, electrons are injected from a cathode to the LUMO level of the electron transport layer (Figure 2.12) and holes are injected from an anode to the HOMO level of the hole transport layer (HTL) (Figure 2.13).

The current–voltage curve of an OLED normally follows the space-charge-limited current (SCLC) equation (Eq. [2.45]) discussed in Section 2.3.7.2 with the charge injection mechanism discussed in this section.

To understand the mechanism of charge injection into an OLED device, it is very important to understand Schottky thermionic emission[8], tunneling injection[9, 10], and the vacuum-level shift model.

Petitioner Samsung Ex-1009, 0041

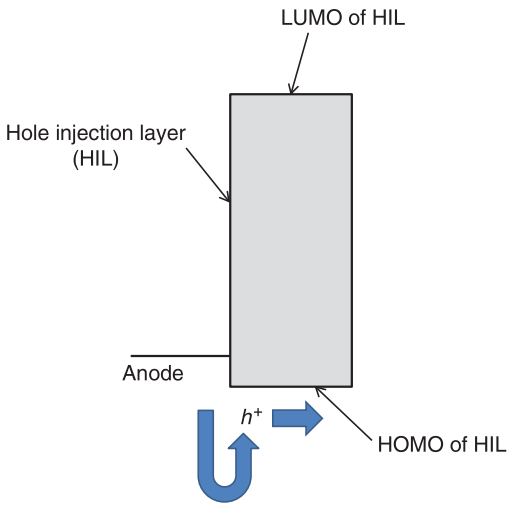


Figure 2.13 Hole injection from anode to HOMO level of HIL material.

2.3.6.1 Charge Injection by Schottky Thermionic Emission

A thermal electron emerges from the surface of a metal or semiconductor which is heated. The electrons require sufficient energy to cross the potential barrier to exit the electrode surface. When the temperature is increased, electrons possessing sufficient kinetic energy can reach and then exit the surface. This phenomenon is called *thermionic emission* or the *Richardson effect*.

The number of electrons with energy ranging between E and $E + dE$ that reach the metal surface can be expressed as

$$\Delta n(E)dE = 2v_{e,x}N(E)f(E)dE \tag{2.25}$$

where $v_{e,x}$ is the velocity component perpendicular to the surface where the electrons emerge, $N(E)$ the density state, and $f(E)$ the Fermi–Dirac distribution function of electron energy.

The total number of electrons that reach the surface per unit area and per unit time is expressed as

$$\begin{aligned} n &= \int \Delta n(E)dE \\ &= 2\int v_{e,x}N(E)f(E)dE \end{aligned} \tag{2.26}$$

The velocity of an electron can be expressed as follows:

$$mv_{e,x} = \hbar k_x = \hbar k\cos\theta$$

Petitioner Samsung Ex-1009, 0042

Then

$$n = \frac{2}{(2\pi)^3}\int v_{e,x} f(E(\vec{k}))d^3\vec{k} \tag{2.27}$$

$$= \frac{2}{(2\pi)^3}\int \frac{\hbar k\cos\theta}{m}\cdot\frac{1}{1+\exp\frac{\hbar^2k^2/2m-E_F}{k_BT}}k^2\sin\theta\,dk\,d\theta\,d\varphi \tag{2.28}$$

Electrons emitted thermionically must have sufficient kinetic energy orthogonal to the surface to penetrate the energy barrier. Therefore, the condition

$$\frac{(\hbar k_x)^2}{2m} = \frac{(\hbar k\cos\theta)^2}{2m} > E_F + \varphi \tag{2.29}$$

must be satisfied for the electrons to be emitted.

The lower bound of the integral in Eq. (2.28) should be

$$k_0 = \sqrt{\frac{E_F+\varphi}{\hbar^2\cos^2\theta/2m}}$$

Then

$$J = \frac{2e}{(2\pi)^3}\int_0^{2\pi}\int_0^{\pi/2}\int_0^{\infty}\frac{\hbar k\cos\theta}{m} \cdot\frac{1}{a+\exp\left(\frac{\hbar^2k^2/2m-E_F}{k_BT}\right)}k^2\sin\theta\,dk\,d\theta\,d\varphi \tag{2.30}$$

At sufficiently high temperatures, the Fermi–Dirac function follows the Maxwell–Boltzmann distribution function approximately. The Maxwell–Boltzmann distribution function can be expressed as

$$g(E) = \exp\left(-\frac{\hbar^2k^2/2m-E_F}{k_BT}\right) \tag{2.31}$$

so the electric current density of thermionic emission is

$$I = A_0T^2\exp\left(-\frac{\varphi}{k_BT}\right) \tag{2.32}$$

This is the *Richardson–Dushman equation*, where I is the saturated emission current density and A_0 is the Richardson constant, which can be expressed as follows:

$$A_0 = \frac{emk_B^2}{2\pi^2\hbar^3} = 120.4\ \ \mathrm{A/cm^2\ \ K^2} \tag{2.33}$$

In a practical electrode, the injection barrier will be lowered according to the image force principle. This is termed the *Schottky effect* or *barrier lowering* (Figure 2.14).

Petitioner Samsung Ex-1009, 0043

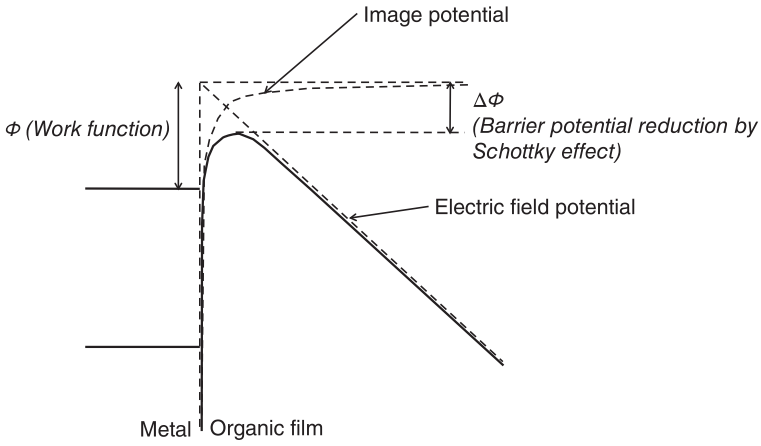


Figure 2.14 Barrier lowering due to image potential.

According to the Schottky effect, the apparent workfunction [11] is lowered by a quantity

$$\Delta\varphi = \sqrt{\frac{e^3 V}{4\pi\varepsilon_0}} \tag{2.34}$$

Therefore, the measured electric current value J can be expressed, using I in Eq. (2.32), as follows:

$$\begin{aligned} J &= I \exp \frac{\Delta\varphi}{k_B T} \\ &= I \exp \sqrt{\frac{e^3}{4\pi\varepsilon_0}} \cdot \frac{\sqrt{V}}{T} \end{aligned} \tag{2.35}$$

In a plot with $\sqrt{V}$ on the abscissa and J on the ordinate, the intercept of the ordinate displays the saturated emission current I. This format is known as a *Schottky plot*.

At the same time, by using the natural logarithm of Eq. (2.32), we can obtain

$$\ln \frac{I}{T^2} = -\frac{\varphi}{k_B} \cdot \frac{1}{T} + \ln A_0 \tag{2.36}$$

Assuming the slope of the graph to be a, with $1/T$ on the abscissa and the logarithm of I/T^2 on the ordinate, we can express the workfunction as

$$\varphi = a \cdot \frac{k_B}{e} \text{eV}$$

where k_B denotes the Boltzmann constant and e is the elementary unit charge. In graph format, this relationship is termed the *Richardson plot*.

In an actual OLED device, calculation using this method sometimes yields an apparent energy barrier lower than the theoretical value. Analysis of injection due to states altered by defects or impurities can explain this phenomenon.

Petitioner Samsung Ex-1009, 0044

2.3.6.2 Tunneling Injection

Some charge injection cannot be analyzed using the Schottky plot and can be better explained by tunneling injection.

Tunneling injection can be expressed by factoring in the Fowler–Nordheim current as

$$J = \frac{q^3 V^2 m_0}{8\pi h \Phi_{\mathrm{Bn}} m^*} \exp\left(-\frac{4\sqrt{2m^*}\Phi_{\mathrm{Bn}}^{1.5}}{3hqV}\right) \tag{2.37}$$

where m_0 is the free electron mass and m^* is the effective mass number. It should be noted that Eq. (2.37) contains no temperature contribution.

2.3.6.3 Vacuum-Level Shift

The vacuum-level shift model is often used to account for the electron injection mechanism to organic materials from a LiF/Al cathode, which is frequently used as an electron injection layer in OLED devices.

A metal/organic interface or metal halide/organic interface cannot be adequately explained by a Mott–Schottky model, which describes the Fermi energy level alignment by band bending. In the OLED device case, the vacuum-level shift caused by interface electric double layer formation [12–15] is dominant. Sometimes the shift can be as large as 1 eV or more, which cannot be disregarded.

Figure 2.15 shows the band diagram with and without vacuum-level shift [16]. The injection barrier height is lowered due to the electric double layer formed by the LiF/organic interface.

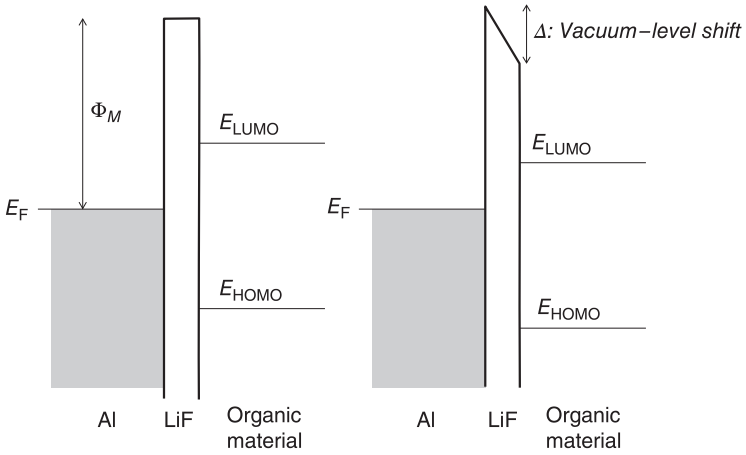


Figure 2.15 Band diagram with and without vacuum-level shift.

Petitioner Samsung Ex-1009, 0045

Hence, LiF significantly improves electron injection from Al to organic materials, so it is one of the most popularly used cathode electrodes.

Several explanations have been proposed of the vacuum-level shift between an electrode and an organic material [17]:

1. Polarization of the interface due to creation of chemical bonding or charge transfer
2. Polarization due to a mirror potential near the electrode
3. Reduction of the electric double layer due to push back of electrons spilling out into vacuum by Coulomb repulsion of organic molecules
4. Creation of an electric double layer due to charge exchange between interfacial states and the metal
5. Formation of an interfacial electric double layer due to the alignment of organic molecules having a permanent dipole.

Many models have been proposed. As the vacuum-level shift plays a very important role in OLED charge injection, a full understanding of its mechanism will lead to an improvement in OLED device performance.

2.3.7 Charge Transfer and Recombination

2.3.7.1 Charge Transfer Behavior

When a charge is injected into an electrode, if all the HOMO orbitals are occupied and cannot accept additional charge, the charge will be transferred into a LUMO in the case of an electron from a cathode. The electrons transferred from the cathode to LUMOs form an electric current (Figure 2.16). Similarly, holes are injected from the anode and transferred to HOMOs to form a hole current. (Figure 2.17. As a "hole" means the absence of an electron, this eventually means electron removal from an organic material and its transfer to the anode. This HOMO–LUMO charge transfer resembles charge transfer by conduction and valence bands in semiconductors.)

The mobility in OLED thin films ranges from about 10^{-3} to $\sim 10^{-6}$ cm/V·s, and as $\pi-\pi$ interaction is not significant in amorphous films, it is believed that the charges are transferred by hopping conduction, which often follows the space-charge-limited-current rule.

2.3.7.2 Space-Charge-Limited Current

As charge density in the organic material is normally small, when the amount of injected charge exceeds the internal charge amount, the conduction changes from ohmic to what is called "SCLC." To explain this term, when current flows through a vacuum between a cathode and an anode, the electrons carrying it form a space charge. This causes an alteration of the electric field near the cathode and limits the current that can flow. In an organic semiconductor, similar

Petitioner Samsung Ex-1009, 0046

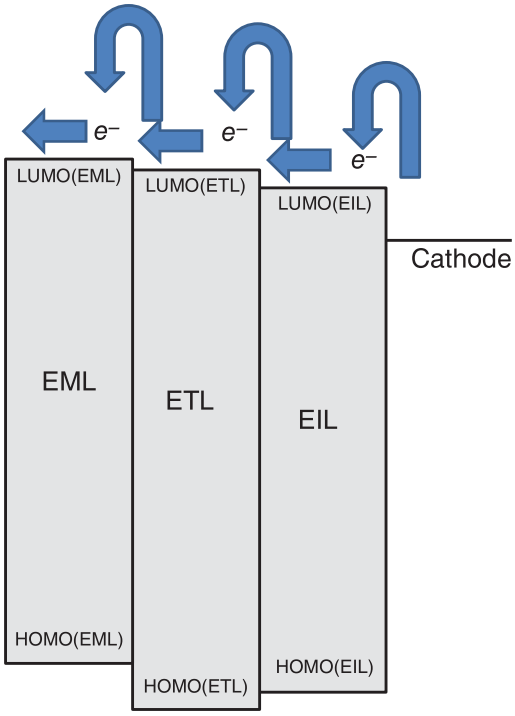


Figure 2.16 Electron transfer in EIL/ETL/EML.

effects occur. Charge carriers cause an electric polarization of the material, which behaves as a leaky dielectric and changes the internal field. Charge carriers can migrate significant distances through the dielectric but become trapped and cannot discharge at an electrode. Similar effects occur in an organic semiconductor. In other words, when charges flow in organic films, local polarization occurs in the organic materials. If charges are injected into the organic film before the polarization is relaxed, a polarized layer is created near the electrode. This is called the *space-charge* layer. Current flow is restricted by this space-charge layer, so it is called SCLC [18].

If charge transfer under an electric field (drift current) and by diffusion (diffusion current) is taken into account, and no charge trapping is assumed, the electric current can be expressed as

$$I = ne\mu E + eD\frac{dn}{dx} \tag{2.38}$$

where n is the charge density injected from the electrode into a thin film of thickness d. This follows the one-dimensional assumption, according to which the x axis is along the thickness direction, μ is the charge mobility, and D is the diffusion constant.

Petitioner Samsung Ex-1009, 0047

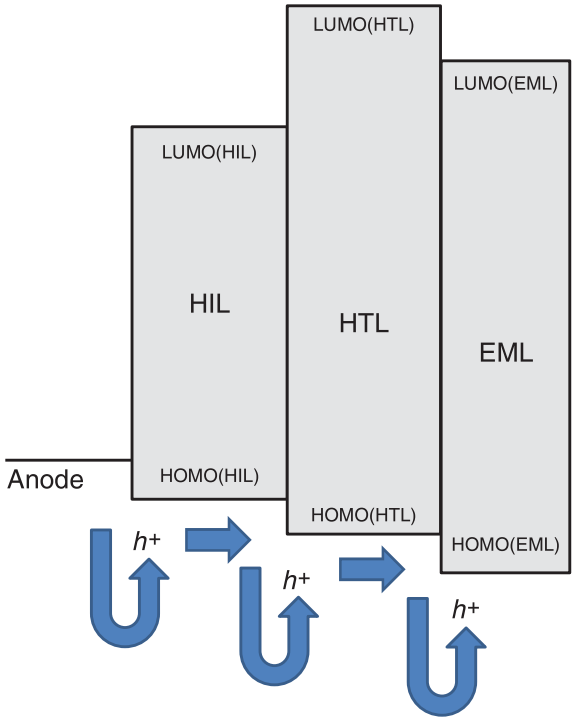


Figure 2.17 Hole transfer in HIL/HTL/EML.

Using the Poisson equation, we obtain

$$\frac{dE}{dx} = -\frac{en}{\varepsilon} \tag{2.39}$$

If an electric field E is applied to the material and if the drift current is sufficiently large compared to the diffusion current, the diffusion term can be neglected. Then, according to Eqs. (2.38) and (2.39), we obtain

$$I = -\varepsilon \mu E \frac{dE}{dx} \tag{2.40}$$

By integration, we then obtain

$$Ix = -\frac{\varepsilon \mu E^2}{2} + C \tag{2.41}$$

If $E = 0$ at $x = d$, then

$$E = \sqrt{\frac{2I(d-x)}{\varepsilon \mu}} \tag{2.42}$$

Petitioner Samsung Ex-1009, 0048

If the applied voltage is V, we obtain

$$V = \int_0^d E\,dx = \int_0^d \sqrt{\frac{2I(d-x)}{\varepsilon\mu}}dx = \frac{2}{3}\sqrt{\frac{2I}{\varepsilon\mu}}d^{3/2} \tag{2.43}$$

Then we can express the current density J, by factoring in the space-charge-limiting mechanism, as

$$J = \frac{9}{8}\frac{\varepsilon\mu V^2}{d^3} \qquad \text{(2.44, Space Charge Limited Current equation)}$$

where J is current density, μ carrier mobility, d thickness, V voltage, and ε the dielectric constant.

It is known that most of the current–voltage characteristics of OLED devices follow this SCLC equation.

These calculations were made assuming no charge trapping. In actual cases, taking trapping into account, the current density is expressed as

$$J = \frac{9}{8}\frac{\varepsilon\mu V^2}{d^3}\cdot\theta$$
$$\theta = \frac{N_c}{N_t}\exp\frac{E_t - E_c}{k_B T} \tag{2.45}$$

where N_c is the effective state density at the conduction band E_c and N_t is the state density of trapping state E_t.

According to Eq. (2.45), the electric current is proportional to the square of the voltage [19]. It should be noted that the current is not related to the carrier density but is proportional to the carrier mobility in this mechanism.

2.3.7.3 Poole–Frenkel conduction

Although Eq. (2.45) describes the behavior of most OLED devices, it was found that some systems such as ITO/PPV/Au do not obey it, especially in the higher electric field region. To explain the observed phenomena, the Poole–Frenkel conduction model, which has field-dependent mobility, was introduced [17].

Similar to the charge injection due to Schottky thermionic emission discussed in Section 2.3.6.1, the barrier height of the trapping state is lowered by

$$\Delta\phi_{PF} = \sqrt{\frac{qE}{4\pi\varepsilon\varepsilon_0}} \tag{2.46}$$

[20], where E is electric field.

Petitioner Samsung Ex-1009, 0049

Then the mobility can be expressed as follows:

$$\mu(E) = \mu_0 \exp\left(-\frac{E_a - q\Delta\phi_{PF}}{kT}\right)$$
$$= \mu_0 \exp\left(-\frac{E_a}{kT}\right) \cdot \exp\left(\frac{q}{kT}\beta\sqrt{E}\right)$$
$$= \mu_1 \cdot \exp\left(\frac{q}{kT}\beta\sqrt{E}\right) \tag{2.47}$$

where μ_1 is the mobility at zero electric field and can be expressed as

$$\mu_1 \equiv \mu_0 \exp\left(-\frac{E_a}{kT}\right) \tag{2.48}$$

and β is the Poole–Frenkel factor and is expressed as

$$\beta = \sqrt{\frac{e}{\pi\varepsilon\varepsilon_0}} \tag{2.49}$$

This is called the Poole–Frenkel conduction model.

The SCLC in Eq. (2.45) can be rewritten as

$$J(E) = \frac{9}{8}\varepsilon\frac{E^2}{d}\mu(0)\exp(\beta\sqrt{E}) \tag{2.50}$$

(SCLC with field-dependent mobility).

The actual situation is more complicated; the energy and location of trapping states have distributions, not a single value. There are several models to account for such cases. Among them, the "multiple trapping and release" (MTR) model is the most popularly used and can explain many of the phenomena. The MTR model assumes a narrow delocalized band with a high concentration of localized trapping levels [21]. During charge movement through the delocalized states, the charge is trapped and is then thermally released. As a result, the drift mobility μ_D due to the MTR mechanism can be expressed as

$$\mu_D = \mu_0\alpha \exp\left(-\frac{E_t}{kT}\right) \tag{2.51}$$

α is the ratio of density of states at the band edge to the trap concentration, in the case of a single trapping level. In the case of an energy-distributed trap, the drift mobility can be expressed by the same equation as Eq. (8.5) with E_t and α calculated by parameter fitting. (The MTR model can be also used for amorphous silicon TFTs.)

2.3.7.4 Recombination and Generation of Excitons

As shown in Figure 2.18, injected electrons and holes are transferred through their own charge transport layers in an OLED device. When an electron meets a hole, the electron and hole recombine and an exciton is formed. An exciton generates a photon whose wavelength corresponds to the energy gap after

Petitioner Samsung Ex-1009, 0050

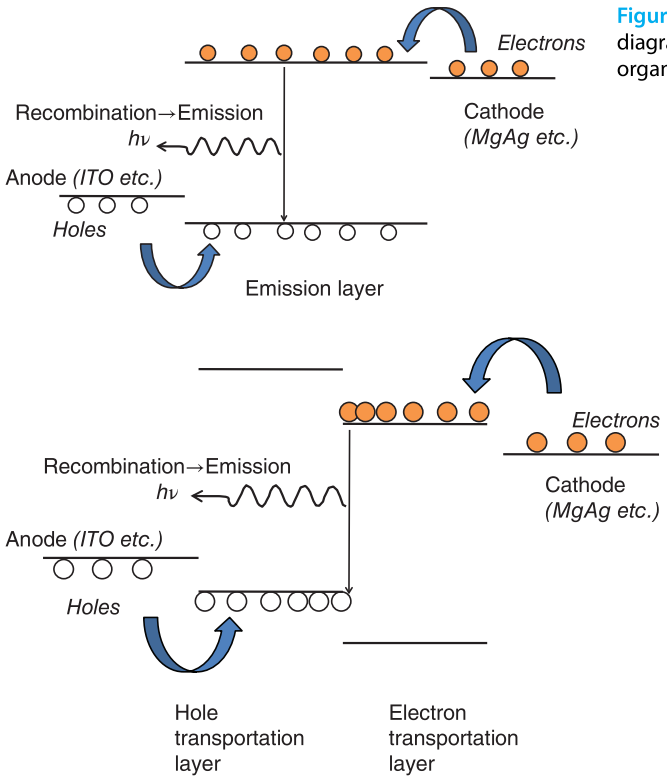


Figure 2.18 OLED band diagram for a single organic layer.

Figure 2.19 Enhancement of electron–hole recombination efficiency by multilayer structural configuration.

completion of its exciton lifetime or loses its energy due to internal conversion discussed in Section 2.4.2. If the probability of electron–hole recombination can be increased, more photons will be generated. So if electron and hole transport can be blocked (i.e., if their flow can be impeded) by the HOMO/LUMO band energy change at an interface between different material layers as shown in Figure 2.19, the location of their recombination can be controlled. As the charge carriers cannot easily pass through the entire device to reach the electrode [5], the recombination probability can be enhanced, and high efficiency can be achieved.

Recently developed OLED devices normally use structures that apply advanced modifications to this charge blocking principle to achieve efficient carrier recombination (Figure 2.20).

For example, the following are typical layers for an OLED device, using material suitable for each function:

- Electron injection layer (EIL)—for electron injection from the cathode

Petitioner Samsung Ex-1009, 0051

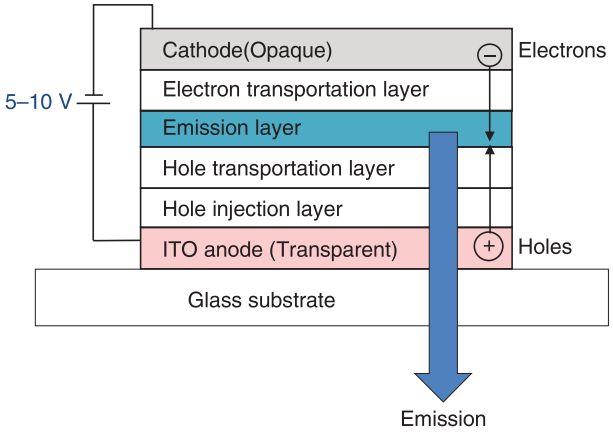


Figure 2.20 Example layout of an OLED device using role sharing by multiple layers.

- Electron transport layer (ETL)—for electron injection from the cathode and transport of electrons
- Hole blocking layer (HBL)—for blockage of hole transport
- Emission layer (EML)—electron/hole transport and their recombination to form an exciton, which generates light emission
- HTL—for hole transport from HIL to EML layer
- Hole injection layer (HIL)—for hole injection from the anode.

EIL and HBL can also be used to control the location where the excitons are formed by blocking hole transportation.

The choice of electrodes is also very important. For example, the HOMO level of NPB is −5.5 eV, and the workfunction of indium tin oxide (ITO) is about −4.7 eV. By solution modification, the workfunction of ITO can be changed to around −5.0 eV, which improves the hole injection efficiency; placement of a thin layer of CuPc (copper phthalocyanine) between ITO and NPB also helps improve the injection efficiency. (Regarding the anode preparation, see Section 6.2.2 for detail.)

Regarding the cathode side, as the LUMO of Alq_3 is around −3.3 eV, a MgAg alloy with a −3.8 eV workfunction is sometimes used as a cathode. It is also known that the injection efficiency using Al with workfunction −4.3 eV can be improved by placement of an LiF layer between Al and Alq_3. (See vacuum-level shift described in Section 2.3.6.3.)

Therefore, it is very important to design an OLED device by factoring in the relationships between workfunction, HOMO level, and LUMO level of each layer. To estimate such an energy level, ionization potential measurement is important (see the discussion in Section 3.4.1).

Petitioner Samsung Ex-1009, 0052

Since the 1980s, OLED device design has been significantly improved using the thin-film role sharing described above.

2.4 EMISSION EFFICIENCY

2.4.1 Internal/External Quantum Efficiency

To quantify how effectively an OLED device is emitting light, the internal quantum efficiency (IQE) and external quantum efficiency (EQE) are often calculated. Internal quantum efficiency η_{int} can be expressed by the following equation, which indicates how much light is generated from a given injected charge:

$$\eta_{\text{int}} = \gamma \zeta_{\text{s}} q \tag{2.52}$$

Here, γ is the electron hole balance (carrier balance), ξ_{s} the exciton generation efficiency (for singlet emitters, this is the singlet generation efficiency; in the case of triplet emission, this should be the sum of the singlet generation efficiency and the triplet generation efficiency), and q the fluorescence quantum efficiency for singlet (the efficiency to generate fluorescence light emission from the exciton) and phosphorescence quantum efficiency for triplet (the efficiency to generate phosphorescence emission). There are many reasons for an exciton to lose its energy without light emission, as discussed in Section 2.4.2.

In actual devices, a significant proportion of generated light is reflected, transferred, and absorbed in both the active layers and the substrate, so it is necessary to also consider the outcoupling efficiency (ratio of generated to extracted light) in order to understand the luminance when designing a display.

When the refractive index of a substrate is *n (refractive index refers to the ratio of light speed in vacuum divided by the phase velocity of light in the medium)*, outcoupling efficiency can be expressed as η_{o} (refer to Section 2.4.3 for further details).

External quantum efficiency can be expressed as follows:

$$\eta_{\text{int}} \cong \eta_{\text{o}} \gamma \zeta_{\text{s}} q \tag{2.53}$$

Using the most simplified outcoupling theory using classical reflection and refraction theory, η_{o} can be written as [21]

$$\eta_0 = 1/(2n^2) \tag{2.54}$$

In the case of fluorescent emission, the maximum value of the carrier balance is 100%, singlet generation efficiency is 25%, the maximum value of fluorescence quantum efficiency is 100%, and outcoupling efficiency is 20%, (n_{glass}=1.6 in Eq. [2.54]) the EQE limitation obtained using the fluorescent mechanism would

Petitioner Samsung Ex-1009, 0053

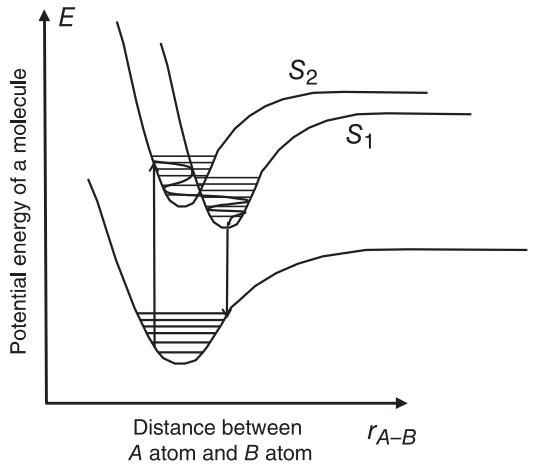


Figure 2.21 Explanation of internal conversion by potential curve.

be about 5% (=100% × 25% × 100% × 20%). In actual cases, quantum efficiency numbers higher than this have been observed due to, so-called, *delayed fluorescent emission* as discussed in Section 2.4.2.4.

According to similar calculations, the EQE limit for phosphorescence is thought to be around 20% (without light extraction structures, which are used for lighting, discussed in Section 9.4).

2.4.2 Energy Conversion and Quenching

2.4.2.1 Internal Conversion

There are several reasons for exciton energy loss after an electron–hole pair recombines. Figure 2.21 shows the conversion of an S_2 exciton to an S_1 exciton due to the crossover of potential curves [6]. Excitons in higher energy levels such as S_2 and T_2 have shorter lifetime than S_1 and T_1, so they tend to be converted to S_1 and T_1. At the point where the S_1 potential curve and the S_2 potential curve cross in Figure 2.21, S_1 and S_2 have the same potential energy and the same atom configuration. Therefore, S_2 can be easily converted to S_1 in this situation (called internal conversion; T_2 can be converted to T_1 in a similar way).

2.4.2.2 Intersystem Crossing

An S_1 exciton generated by direct excitation, carrier recombination or by internal conversion from a higher energy state (such as S_2) can be converted to T_1, due to crossing of the potential curves corresponding to the T_1 and S_1 states. (ISC: Intersystem crossing.) As S_1 has a single state and T_1 has three states, 25% of singlet and 75% of triplet exciton states can result at equilibrium (discussed in Sections 2.3.5 and 2.4.2.3). T_1 states normally cannot be converted to the S_0 ground state with emission of light, as a transition with a spin state change

Petitioner Samsung Ex-1009, 0054

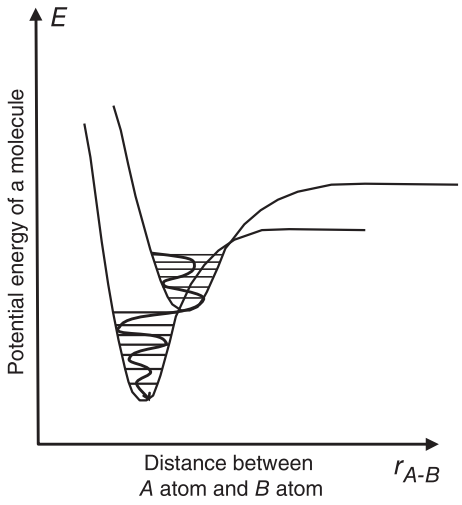


Figure 2.22 Explanation of radiationless deactivation by potential curve.

is forbidden. Thus, fluorescent system has 25% maximum internal quantum efficiency. In this case, the 75% of triplet excitons lose their energy as heat by radiationless deactivation (Figure 2.22). In the phosphorescent system, a phosphorescent emitter doped into the emissive layer converts T_1 to S_0 ground state with light emission; the transition becomes allowed through the heavy-metal effect, which is caused by spin-orbital interaction. Therefore, a phosphorescent system can provide 100% internal quantum efficiency due to emission from both S_1 and T_1 states (discussed in Section 2.4.2.3).

2.4.2.3 Doping

By adding a small quantity of emissive material, it is possible to improve the efficiency or to change the emission color. This is called *doping* [22, 23], and the materials used for doping are called *dopants*. This technique is especially useful for materials in which emission yield decreases at high density (this activity is referred to as *concentration quenching*). For example, in its original state Alq_3 is a green fluorescent emission material, but with the addition of small amount of rubrene, the emission color changes to yellow-orange. This is due to energy transfer from the Alq_3 exciton to the rubrene exciton. With the addition of a red fluorescent dopant to Alq_3 + rubrene system, such as DCJTB (4-(dicyanomethylene)-2-*tert*-butyl-6-(1,1,7,7,-tetramethyljulolidyl-9-enyl)-4*H*-pyran), further energy transfer occurs, and red emission is observed. Thus, it is possible to modify the color by converting the emission spectrum to a longer wavelength.

Figure 2.23 shows the doping emission mechanism in the case of fluorescence [23]. Host energy is transferred to the dopant by dipole–dipole coupling. This

Petitioner Samsung Ex-1009, 0055

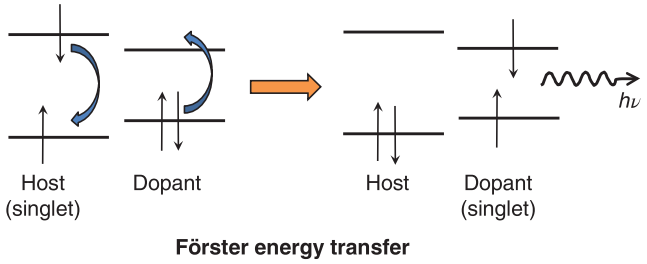


Figure 2.23 Doping emission by fluorescence mechanism.

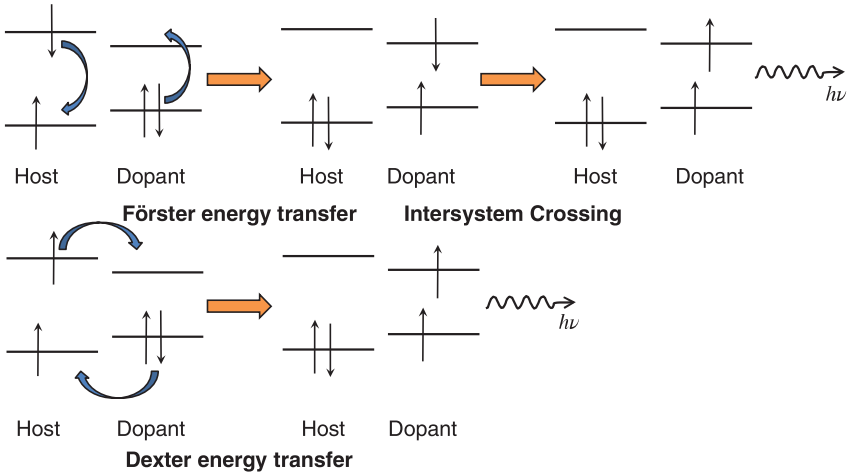


Figure 2.24 Doping emission by phosphorescence mechanism.

energy transfer can occur even when the excitons are separated by relatively long distances such as 100 Å (this is known as *Förster energy transfer*).

When this fluorescent emission mechanism is employed, only 25% of the excitons can be used because only singlet excitons contribute to the emission and the remaining 75% of excitons lose their energy by internal conversion (discussed in Section 2.4.2) to generate heat. For low power consumption and high luminance, emission yield must be improved.

Figure 2.24 shows an example of phosphorescent dopant emission reported by Baldo et al. [24]. They added approximately 6–8% of the phosphorescence dopant to the emissive layer such that both singlet and triplet excitons contributed to the emission. The energy transfer in this procedure [24] differs from Förster transfer, which uses dipole–dipole coupling. In the Dexter energy transfer method described by Baldo's group [24], energy transfer is effected by exciton hopping, in which case a shorter interexciton distance (e.g., ~10 Å) is necessary to make the transfer effective.

Petitioner Samsung Ex-1009, 0056

2.4.2.4 Quenching

Even if an exciton is in a radiative state, it may still lose its energy without emission if a quencher is present. The quencher can be included when the films are made and also can be created by electrical driving of the device or by aging. The likelihood of quenching tends to increase at higher exciton density (as the excitons have an increased chance to interact or to meet with quenchers, such as increased polaron).

Phosphorescent excitons have an especially long decay time, so are susceptible to energy loss by quenching.

The best-known quencher of phosphorescent emitters is oxygen. Oxygen's ground state is a triplet (the oxygen molecule has a peculiar biradical electron configuration, which has two unpaired electrons with the same spin, as the ground state. It has two electrons with the same state, namely triplet state), so the energy of a triplet exciton can be easily lost.

Other major causes of triplet exciton quenching include the following [25–27]:

1. Triplet–triplet annihilation (TTA)
   Triplet–triplet annihilation (TTA) is a conversion of two triplets into a ground state singlet and an excited singlet [28]. While there are a number of related processes, it has been reported that the process of donor molecule energy exchange, which was caused by two triplet excitons, to an excited acceptor molecule to form singlet state and triplet state according to the following formula, is dominant [29].

$$ {}^3A^* + {}^3A^* \rightarrow (4/9)^1A + (1/9)^1A^* + (13/9)^3A^* \tag{2.55} $$

   TTA causes efficiency loss at high current density due to the higher chance of triplet–triplet collision at the high triplet exciton densities found in phosphorescent devices. In the case of fluorescent emitters, triplet excitons are normally lost without emission, as the radiative transition from excited triplet to singlet ground state is forbidden. However, many cases have been reported, which exceed the quantum efficiency limit (25%) of fluorescent OLEDs [30, 31]. These observations can be interpreted as an efficiency increase due to TTA. According to (2.55), two triplet excitons (left) generate 1/9 singlet exciton and 13/9 triplet excitons, so in total and assuming the triplet excitons are recycled, five triplet excitons generate one singlet. The maximum internal quantum efficiency that can be achieved using fluorescent emitters then becomes 25% (singlet) plus one fifth of 75% (triplet) = 40%. This increase in emission occurs through TTA—contrary to the usual meaning of the word, so it is sometimes called triplet–triplet fusion (TTF). The singlet excitons generated by TTF decay later than those derived directly from carrier recombination, so delayed emission is observed from this effect. This type of efficiency increase is therefore called delayed fluorescence.

Petitioner Samsung Ex-1009, 0057

2. Triplet–polaron quenching (TPQ)
   When a triplet exciton interacts with a charged molecule, the energy of a donor molecule can be transferred to the charged molecule.
3. Field-induced quenching [32]
   At a high electric field, the decrease in electrophosphorescence is observed. Also neat solid film also decreased phosphorescence at high electric field. This phenomenon is interpreted that the electron–hole pairs are coulombically dissociated by electric field [33].
   Among these exciton quenching effects, it is reported that only TTA has an important effect on the OLED efficiency [34].

Poor OLED performance and OLED device degradation can sometimes be explained by a quenching mechanism. To analyze the system, it is important to know what will happen if a quencher is added to the OLED emissive system.

When a quencher is added to a photochemical system, the following elementary reactions occur [6]:

1. Photon absorption:

$$A_0 \xrightarrow{h\nu} A^* \tag{2.56}$$

2. Photo emission:

$$A^* \xrightarrow{k_e} A_0 + h\nu \tag{2.57}$$

3. Quenching:

$$A^* + A \xrightarrow{k_q} A_0 + A^* \tag{2.58}$$

4. Other deactivation:

$$A^* \xrightarrow{k_d} A_0 + \text{Heat} \tag{2.59}$$

5. Reaction:

$$A^* \xrightarrow{k_r} P(\text{Product}) \tag{2.60}$$

The rate of each reaction can be written as I_a, $k_e[A^*]$, $k_q[A^*][Q]$, $k_d[A^*]$, and $k_r[A^*]$, respectively.

The rate of excited state generation can be written as

$$\frac{d[A^*]}{dt} = I_a - (k_e + k_q[Q] + k_d + k_r)[A^*] \tag{2.61}$$

When the system is in equilibrium, left term equals zero.

Therefore,

$$I_a = (k_e + k_q[Q] + k_d + k_r)[A^*] \tag{2.62}$$

Petitioner Samsung Ex-1009, 0058

When φ_r is the quantum yield of the reaction and φ_{r0} is the quantum yield without quencher,

$$\begin{aligned} {}^{\phi_{r0}}/_{\phi_r} &= \frac{k_\mathrm{r}}{k_\mathrm{e}+k_\mathrm{d}+k_\mathrm{r}} \cdot \left(\frac{k_\mathrm{r}}{k_\mathrm{e}+k_\mathrm{q}[Q]+k_\mathrm{d}+k_\mathrm{r}} \right)^{-1} \\ &= 1 + \frac{k_\mathrm{q}}{k_\mathrm{e}+k_\mathrm{d}+k_\mathrm{r}}[Q] = 1 + k_\mathrm{q}\tau_0[Q] \end{aligned} \tag{2.63}$$

where τ_0 is the exciton lifetime of A^*.

When total reaction constant of exciton decay is $k[A^*]$("Photon emission" + "Other deactivation".)

$$\phi_r = \frac{k_\mathrm{r}}{k_\mathrm{r}+k_\mathrm{d}+k_\mathrm{q}[Q]} \tag{2.64}$$

Therefore,

$${}^{1}/_{\phi_r} = \alpha + \beta \cdot [Q] \tag{2.65}$$

where

$$\alpha = 1 + \frac{k_\mathrm{d}}{k_\mathrm{r}} \quad \text{and} \quad \beta = \frac{k_\mathrm{q}}{k_\mathrm{r}}$$

When a photochemical reaction is caused by a single excited state, the graph $1/\varphi r$ versus $[Q]$ shows linear behavior. This graph is called a Stern–Volmer plot.

When photochemical reaction contains multiple phenomena, the Stern–Volmer plot can show nonlinear relationship. For example, at low quencher density, the amount of quenching is proportional to the frequency of collision (dynamic quenching) between an emissive exciton and a quencher, then the Stern–Volmer plot shows linear relationship. However, in the case when the quencher forms nonemissive stable complex (static quenching), Stern–Volmer plot shows superlinear relationship due to two quenching mechanisms. In other cases, for example, when there are singlet and triplet excitons and only triplet excitons are quenched, the Stern–Volmer plot shows saturation at a certain efficiency value, as the quencher volume is increased.

To determine whether poor device performance is due to a quencher, a Stern–Volmer plot analysis is effective.

2.4.3 Outcoupling Efficiency of OLED Display

2.4.3.1 Light Output Distribution

Light generated by excitons travels via various paths. Some of the light reaches the human eye, but a significant portion of the light diminishes by propagation in the thin film (waveguide mode) or by propagation in substrate (substrate mode).

Petitioner Samsung Ex-1009, 0059

Meerheim et al. made quantitative analysis of energy loss mechanism in OLED [35]. The energy applied is used for the following:

(1) Electrical losses
(2) Nonradiative losses
(3) Absorption
(4) Surface plasmons
(5) Waveguided-mode losses
(6) Substrate-mode losses
(7) Outcoupled light, extracted to outside.

Especially, surface plasmons, waveguided mode, and substrate mode are the three major reasons of losses in OLED devices. It is important to make countermeasure for each light loss mechanism to achieve highly efficient devices. (Light extraction enhancement in the case of OLED lighting is discussed in Section 9.4.)

The basic characteristics of optics are discussed as follows.

2.4.3.2 Snell's Law and Critical Angle

Denoting the incident angle as θ_i the reflection angle as θ_r, and the refraction angle of the transmitted light as θ_t, then according to Snell's law (Figure 2.25), we have

$$\frac{\sin\theta_i}{\sin\theta_t} = \frac{n_2}{n_1} \tag{2.66}$$

where n_1 and n_2 are the refractive indices of materials 1 and 2, respectively.

When θ_i is larger than the critical angle θ_C, the incident light causes total reflection. The critical angle is expressed as follows:

$$\theta_C = \sin^{-1}\frac{n_2}{n_1} \tag{2.67}$$

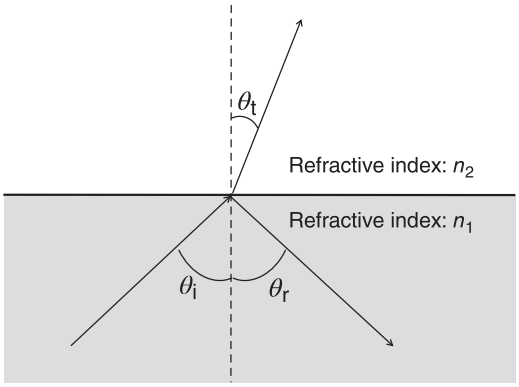


Figure 2.25 Schematic representation of Snell's law.

Petitioner Samsung Ex-1009, 0060

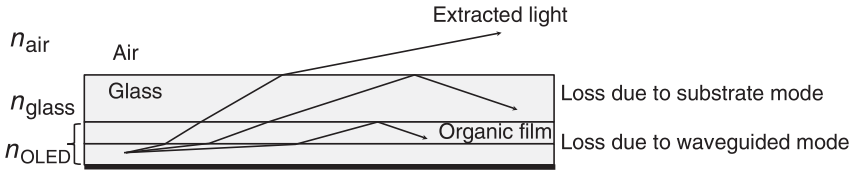


Figure 2.26 Schematic representation of light extraction loss.

If the light in high refractive index keeps its incident angle larger than critical angle, the light never comes out and is lost. This is the major cause of waveguided-mode loss and substrate-mode loss.

2.4.3.3 Loss Due to Light Extraction

For a point light source, the light extraction outcoupling efficiency η_o is

$$\eta_o = \frac{2\pi I_0 \int_0^{\theta_B} \sin\theta \, d\theta}{2\pi I_0 \int_0^{\pi/2} \sin\theta \, d\theta} = 1 - \sqrt{1 - \left(\frac{n_{air}}{n_{OLED}}\right)^2} \tag{2.68}$$

Here, I_0 is the luminous intensity toward the front direction. For a diffusion surface, we obtain

$$\eta_o = \frac{2\pi I_0 \int_0^{\theta_B} \cos\theta \sin\theta \, d\theta}{2\pi I_0 \int_0^{\pi/2} \cos\theta \sin\theta \, d\theta} = \left(\frac{n_{air}}{n_{OLED}}\right)^2 \tag{2.69}$$

For example, if the refractive index of air is $n_{air} = 1.0$ and the OLED organic film refractive index is $n_{OLED} = 1.75$ (Alq_3), the light extraction efficiency is very low: approximately 17.9% for the point light source and 32.6% for the diffusion surface (Figure 2.26).

Figure 2.26 is a very simplified hypothetical depiction of light extraction loss, and, in actual cases, the optical properties of multiple films, electrodes, and multiple interference effects must be accounted for. Mikami et al. [36] derived the following equation to determine the energy extracted from the device in this kind of system:

$$E = \frac{(1 - |\rho_0|^2\{1 - |\rho_0|^2 + 2|\rho_0| \exp i(2\delta_1 - \varphi_1)\}}{1 + |\rho_0||\rho_1| - \sqrt{|\rho_0||\rho_1|} \exp i(2\delta_0 - \varphi_0 - \varphi_1)} \tag{2.70}$$

Here, E is extracted energy, ϕ_0 the phase shift due to front surface reflection, ϕ_1 the phase shift due to rear surface reflection, $|\rho_0|^2 = R_0$ the energy reflection ratio of the front boundary layer, $|\rho_1|^2 = R_1$ the energy reflection of the rear

Petitioner Samsung Ex-1009, 0061

boundary layer, Δ_0 the phase shift due to thickness of the EML, and Δ_1 the phase shift that results between the EML and the rear layers.

By adjusting the parameters to ensure uniformity of the light phase, which may be modified by the multilayer reflection, one can utilize the resonance effect (microcavity effect) to achieve high efficiency and color purity in OLED devices. Especially for the top emission case (emission from the top of the structure), the resonance effect can be utilized by using a semitransparent thin metal film for the top electrode. However, the microcavity effect causes significant alteration of characteristics due to thickness variation; thus, precise thickness control is necessary for manufacturing.

In the bottom emission case (i.e., light emission from the bottom of the structure), it is also possible to apply the microcavity effect by using a semitransparent bottom electrode or by employing a Bragg reflector.

Other approaches for enhancement of light extraction have been reported, including microlens arrays, micropyramidal structure, diffraction structure, and photonic arrays. These designs are discussed in further detail in Section 9.4.

2.4.3.4 Performance Enhancement by Molecular Alignment

Since "first OLED paper" was released in 1987, in most cases, the performance of OLED was discussed based on the single molecular behavior. Different from inorganic semiconductors, which has strong interaction between atoms that clearly defines the band structure according to the Bloch theory, the interaction between organic molecules is much weaker due to poor molecular orbital overlap with adjacent molecules. Also it has been proved that amorphous organic film deposition gives large benefit in device fabrication, due to uniformity and prevention of electric shortage between anode and cathode electrodes, so it was perceived as pointless to discuss about the orientation of molecules in the past.

However, it was gradually proved that a sort of orientation in amorphous film is playing an important role in the device performance these days [37].

In general, rod-shaped molecules in amorphous film show horizontal molecular orientation, while molecules in polycrystalline film show vertical orientation [38]. There are two major reasons why horizontal molecular alignment gives better OLED device performance.

1. *Electrical advantage:* Horizontal molecular orientation increases the π–π overlap between adjacent molecules and decreases the disorder in the film, which improves the charge transportation toward thickness direction.
2. *Outcoupling advantage:* Molecules emit light to perpendicular direction to its dipole moment, so the light from horizontal molecular orientation gives smaller incident angle when it arrives to the film interface. The small incident angle avoids the total reflection caused by the refractive index difference (Figure 2.25). If such horizontally aligned molecules would be fabricated by

Petitioner Samsung Ex-1009, 0062

some method, it also brings merit to avoid the absorption loss by the circular polarizer (discussed in Section 4.1) because such aligned molecules cause polarized emission.

To make such oriented or aligned molecules happen, several processes have been proposed, such as substrate temperature control during vacuum evaporation [38], rubbing of molecules [39], electric field [40], and stretching [41].

Horizontal alignment of the emitter is also effective to suppress the plasmon-related energy loss. The topic is discussed in Section 9.4.5.1.

2.5 LIFETIME AND IMAGE BURNING

2.5.1 Lifetime Definitions

According to the driving stress, OLED device decays its luminance. The decrease in luminance of the device not only causes the luminance reduction of a display but also causes the luminance difference between the pixels according to the amount of total driving stress applied to the pixels (picture elements). As a result, pixels of a pattern that was displayed for a long period remains as luminance decrease and creates image burning, where black-and-white-reversed image of the displayed pattern remains when the display is operated. This is called differential aging (Figure 2.27).

Figure 2.28 shows the variation in luminance of an OLED device with constant current operation, in which a perylene-doped BAlq layer functions as the EML. As indicated in the graph, the time spent prior to the 50% luminance decay is denoted T_{50} (also as LT_{50}). Similarly, the time spent prior to the 30%

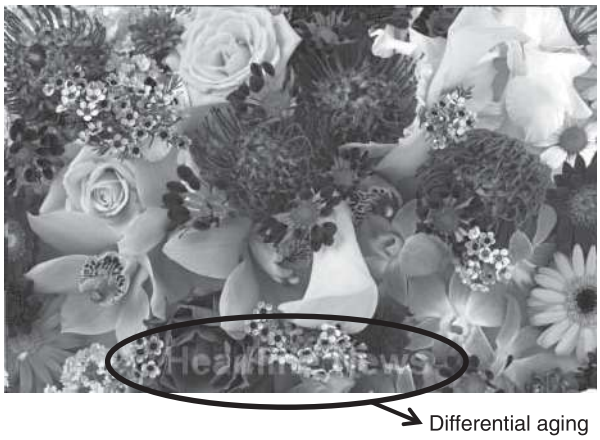


Figure 2.27 Image sticking on a display caused by the differential aging.

Petitioner Samsung Ex-1009, 0063

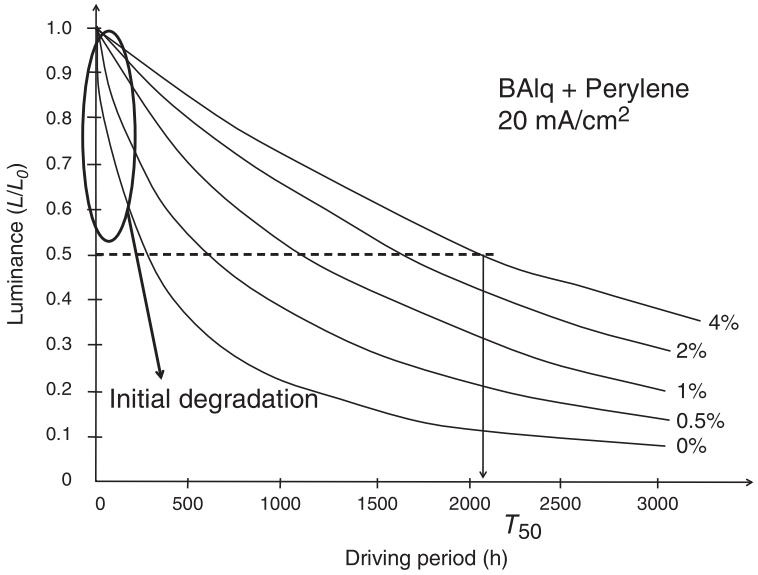


Figure 2.28 Luminance decay curve.

luminance decay is denoted T_{70}; the time prior to 5% decay, T_{95}; and the time prior to 3% decay, T_{97}. Previously T_{50} was used most frequently; however, as OLED lifetime increases every year, and as 50% luminance degradation is seldom acceptable from a product perspective, many OLED display and OLED lighting users now employ T_{70}. Standards T_{95} and T_{97} are also used to show how a display is likely to cause *image burning* because 3–5% display luminance change is close to the perception limit of the human eye. This luminance difference almost corresponds to the color difference $\Delta E = 1$ in uniform color space (discussed in Section 4.2.4). The luminance difference is not associated with color, so this corresponds to $L^* = 1$. The uniform color space concept is very important for determining the allowable limitation as to the luminance decay and color change.

2.5.2 Degradation Analysis and Design Optimization

A closer look at the 0% doping curve in Figure 2.28 reveals a gradual decrease in the rate of degradation from the left to right of the graph [42]. One can also note a sharp drop in the initial decay rate with a decrease in perylene doping. This initial reduction in the decay rate results in total lifetime decrease as well as image burning; these effects can be minimized by fine-tuning the device design and process.

During operation of an OLED display, any color shift should be minimized as well. The pixel is composed of red, green, and blue subpixels as shown in

Petitioner Samsung Ex-1009, 0064

Figure 2.29. After operation, these red, green, and blue subpixels (spatially located primary color elements in a pixel) are degraded as shown in Figure 2.30. As white is expressed by the mixture (Figure 2.28) of red, green, and blue (the calculation method is discussed in Section 4.2.5.), the white point (color coordinate of white) in the display is shifted on color coordinate if the primary color luminance has been changed.

To avoid the white point shift, the aperture may be adjusted (aperture adjustment, Figure 2.31) according to variation in the degradation curve for individual colors (Figure 2.30).

When the current density is J, the lifetime of an OLED device decreases in proportion to $1/J^n$ ($n = 1.2–1.9$, called the acceleration factor, discussed in Section 2.5.3.1.). By adjustment of the aperture ratio, the current density can be controlled, so the decay curve for each color—red, green, and blue—can be adjusted to a similar curve as shown in Figure 2.32, and white point shift can be reduced.

However, the most recent types of display, such as those for high-resolution mobile phone applications, have design restrictions such as shadow mask intolerance and negligible flexibility for aperture ratio adjustment for each color.

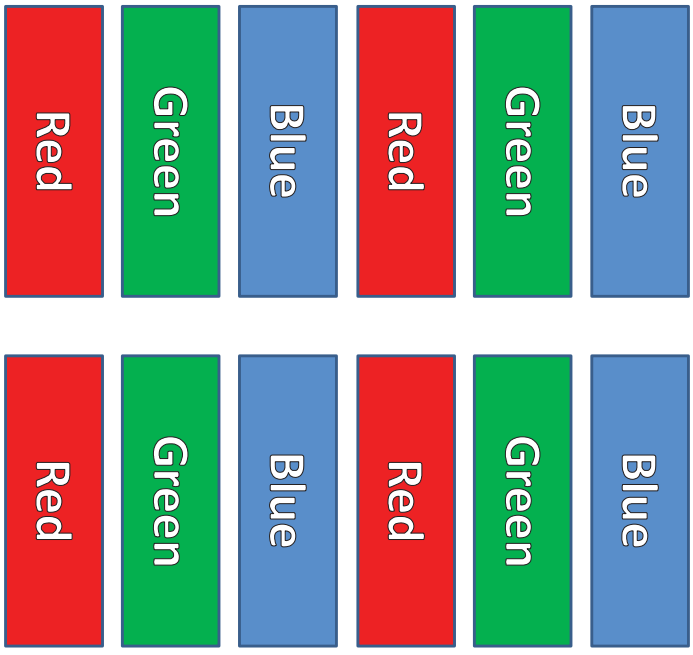


Figure 2.29 Pixel arrangement without aperture adjustment.

Petitioner Samsung Ex-1009, 0065

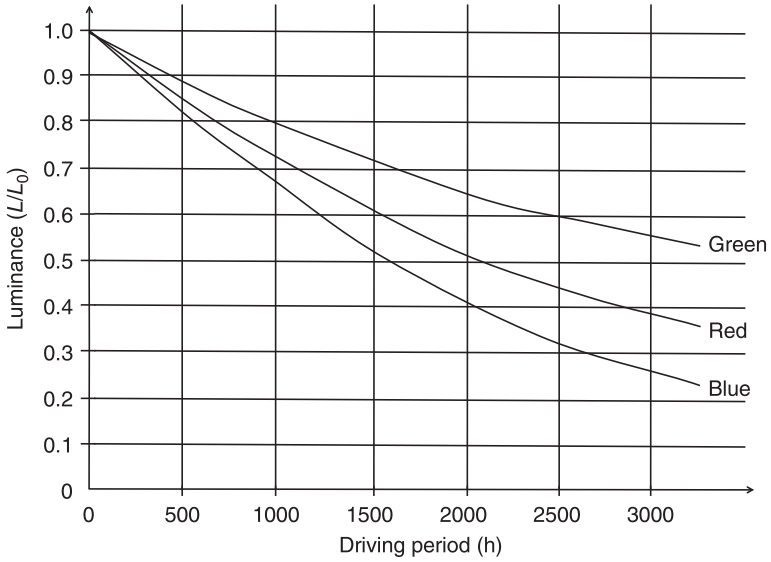


Figure 2.30 Individual degradation curves for three colors.

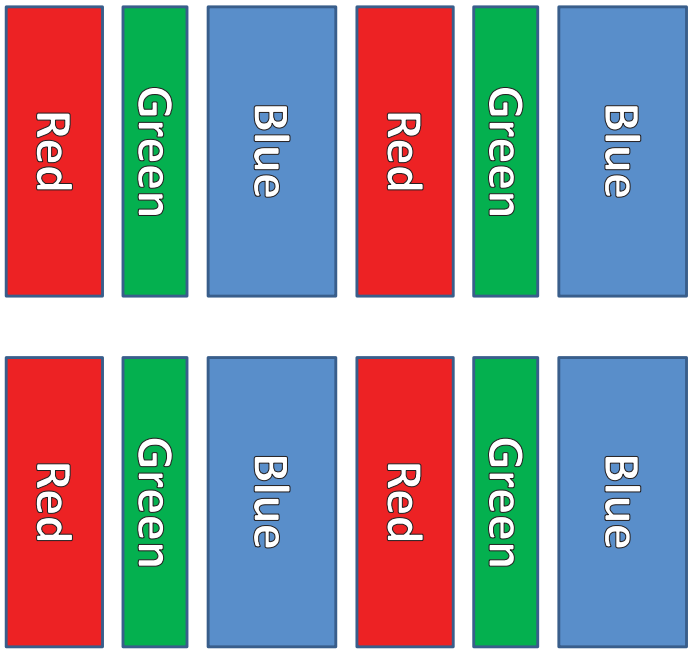


Figure 2.31 Pixel arrangement with aperture adjustment.

Petitioner Samsung Ex-1009, 0066

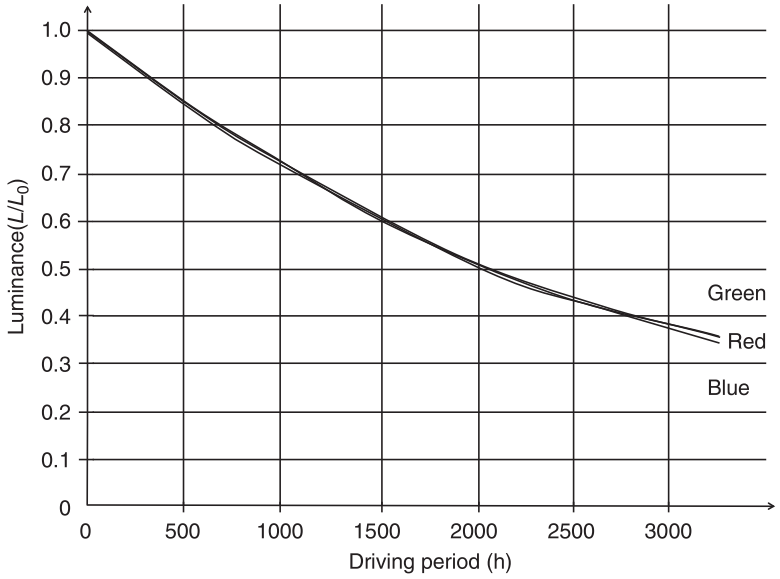


Figure 2.32 OLED pixel display curve for a display with aperture adjustment.

2.5.3 Degradation Measurement and Mechanisms

2.5.3.1 Acceleration Factor and Temperature Contribution

As OLED is a current-driven device, a molecule would be affected by the passing charges. Negative charge would provide reduction stress and positive charge would give oxidation stress to the molecule. With that simple assumption, the electrical damage of OLED device should be proportional to the number of passing charges, hence proportional to the electric current. However, in reality, the damage is proportional to J^n whose n is greater than one. One possible cause of this deviation would be joule heating of the device caused by the electric current. Yoshioka et al. made an analysis to decouple the contribution between non-joule-heat component and joule-heat component of the OLED device degradation [43]. The result shows that the acceleration factor is decreased when the joule-heat contribution is eliminated; however, the acceleration factor without self-joule heating is $n = 1.20 \pm 0.10$, which is not one. This implies that there still remains non-joule-heating acceleration mechanism of device degradation.

2.5.3.2 Degradation Mechanism Variation

For good OLED device performance, it is very important to understand what is happening in the fabricated device. There are many articles describing the cause of OLED device degradation.

Petitioner Samsung Ex-1009, 0067

Aziz et al. explored the degradation study of OLED device and categorized it into three mechanisms: (1) dark-spot degradation, (2) catastrophic failure, and (3) intrinsic degradation [44].

Burrows et al. made a comparison of the degradation behavior of encapsulated device and nonencapsulated device [45]. They found that the encapsulated device has two orders of magnitude longer lifetime than that of nonencapsulated ones. The encapsulation issue is discussed in Section 3.3.

To understand the cause of encapsulated OLED device degradation, Kondakov et al. made an analysis on the OLED device after 312 h operation at 80 mA/cm^2 stress [46]. The derivatives detected by HPLC and the expected precursors of the detected materials were assumed as quenchers in the study. It was found that the monotonic increase in the extent of NPB chemical degradation coincide with the monotonic decrease in luminous efficacy, which indicates that the nonradiative NPB derivatives created by driving stress cause the quenching of excitons in the system.

Meerheim et al. made an analysis on the hole blocking layer (HBL) dependence of phosphorescent OLED device systems [47]. When BPhen is used as an HBL layer, the OLED device lifetime is much shorter (1/50) in than the case of BAlq HBL. The paper concludes the difference is due to two mechanisms, the BPhen's dimer acting as a quencher and also BPhen acting as a ligand of Iridium, which is causing the nonradiative recombination center.

So et al. made a comparison between small-molecule OLED and polymer OLED in the degradation mechanism [48]. In the small-molecule case, the accumulation of degradation products are causing both luminous efficacy loss and operating voltage increase. In the case of polymer OLED, charge-transport and injection properties affect the device lifetime. It was also pointed out that charge balance plays a very important role in having a good lifetime of the device, as surplus carriers damage the organic materials.

2.6 TECHNOLOGIES TO ENHANCE THE DEVICE PERFORMANCE

2.6.1 Thermally Activated Delayed Fluorescence

As discussed in Section 2.4.2.2, by means of phosphorescent emitter such as Iridium complex, high internal quantum efficiency near 100% is possible, which enables conversion between singlet and triplet by means of intersystem crossing. However, the triplet excitons by phosphorescent emitters have several issues such as triplet exciton quenching (Section 2.4.2.4) and high cost due to Iridium compound, so new method to achieve high quantum efficiency has been suggested.

Petitioner Samsung Ex-1009, 0068

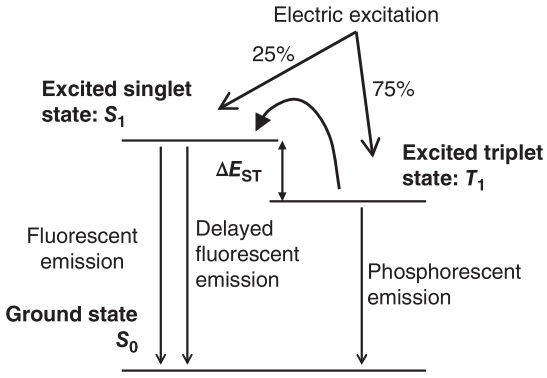


Figure 2.33 Energy diagram of TADF system.

Figure 2.33 shows the energy diagram to explain the light emission mechanism from S_1 and T_1 states. In fluorescent system, phosphorescent emission from T_1 to S_0 is forbidden, so 75% of excitons in the triplet state cannot contribute to the emission normally. To allow such a triplet state to emit light, there are two approaches possible, other than the phosphorescent mechanism.

1. Delayed fluorescence by TTA (TTA, discussed in Section 2.4.2.4)
2. Upconversion of exciton from T_1 to S_1 state by thermal energy.

The second approach is called TADF (Thermally Activated Delayed Fluorescence). It has been known that several materials, such as porphyrin derivatives, show the TADF emission. However, as it is a thermally activated mechanism, which requires T_1 state to acquire energy ΔE_{ST} in Figure 2.33, the emission becomes smaller as the temperature is decreased. Therefore, to make TADF emission large enough to apply to the OLED device for realistic applications, it is necessary to secure the emission at lower temperature.

Adachi's group made a major breakthrough in this issue and made the TADF molecule usable for OLED device application for normal temperature range [49]. To minimize the temperature dependence of TADF method, it is necessary to minimize the $\Delta E_{ST.}$ The ΔE_{ST} can be written using exchange integral, K (see Section 2.3.3 for details) as follows.

$$\Delta E_{ST} = 2K \tag{2.71}$$

$$K = \iint \chi_A(1)\chi_B(2)\frac{1}{r_{12}}\chi_A(2)\chi_B(1)d\tau_1 d\tau_2 \tag{2.72}$$

This means that as the wavefunction overlap between ground state and excited state becomes smaller, ΔE_{ST} would be reduced. Therefore, orthogonal wavefunction would give smaller ΔE_{ST}, which will avoid the temperature dependence. However, there is an issue when such a molecule is to be designed. Radiation rate can be written by transition dipole moment μ as the following

Petitioner Samsung Ex-1009, 0069

formula, which has very similar equation to (2.72); then the radiation would be decreased as ΔE_{ST} in most molecular designs.

$$I_{rad} \propto \mu^2 = \left\{ \iint \chi_A(1)\chi_B(2) r_{12} \chi_A(2)\chi_B(1) d\tau_1 d\tau_2 \right\}^2 \tag{2.73}$$

To make large enough radiation with minimum ΔE_{ST}, formula (2.72) must be small, while (2.73) is kept large. To make that happen, Adachi's group connected donor molecule and acceptor molecule by a chemical group with a steric hindrance. As a result, internal quantum efficiency near 100% was achieved using the TADF method [49].

Thus, TADF can make 100% internal quantum efficiency, but it is still ongoing R&D topic and many advanced approaches have been proposed. For example, TAF (TADF-assisted fluorescence) uses TADF molecule as an assist dopant of fluorescent OLED device. Molecule designs for small ΔE_{ST} generally tend to cause slower fluorescent emission, so the singlet state can be downconverted into triplet states before fluorescence. In the TAF system, fluorescent emitters with fast decay receive energy from TADF molecule and quickly decay, so it can avoid the high energy excitons to degrade the OLED device [50].

2.6.2 Other Types of Excited States

2.6.2.1 Excimer and Exciplex

A transient aggregate of excited singlet state ($^1C^*$) and ground state of the same molecule is called excimer. (It should be noted that excimer is an aggregate of excited state and is not applied to an aggregate of ground state.)

$$C + h\nu \rightarrow {}^1C* \overset{C}{\rightarrow} {}^1(C-C)*$$

Excimer is often observed in condensed aromatic compounds.

If similar situation happens between different molecules, it is called exciplex. The excited state of charge-transfer complex (discussed in Section 2.6.2.2) is a kind of this excimer. A high-efficiency emission mechanism using the exciplex formation has been proposed [51].

2.6.2.2 Charge-Transfer Complex

When an electron-donating compound and electron-accepting compound are located adjacently, new absorption peak appears due to the charge transfer between two molecules. This type of molecular compound is called charge-transfer complex or CT complex Figure 2.34 shows the energy diagram of CT complex.

CT complex can be used to enhance the charge injection from the electrode (Figure 3.4 in Section 3.1.1.1) and also can be used as charge generation layer to form a tandem device (discussed in Section 2.6.3).

Petitioner Samsung Ex-1009, 0070

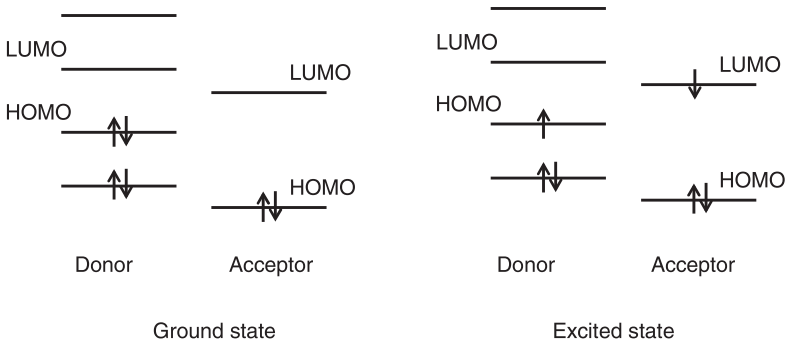


Figure 2.34 Ground state and excited state of CT complex.

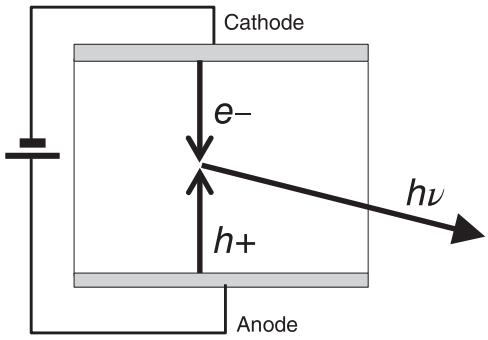


Figure 2.35 Schematic representation of a conventional OLED device.

With CT complex configuration, organic materials can have electrical conductivity (discussed in Section 8.1.5.1). Based on this mechanism, famous organic conductor TTF-TCNQ was developed, which shows metallic conduction mechanism (see Figure 8.8).

2.6.3 Charge Generation Layer

As discussed in Section 6.4.3, voltage drop is a significant issue in larger OLED displays. To reduce the voltage drop, tandem OLED device (also called multiphoton device) is effective, which increases the current efficiency (further discussed in Section 6.4.3).

Figure 2.35 shows a conventional OLED device, which sandwiches organic layers between the cathode and anode. Photons are generated in the organic layers by electron–hole recombination.

Figure 2.36a shows a two-unit tandem OLED structure, in which two organic layers are connected by an intermediate layer (known as a *connector layer* or a *charge generation layer* [CGL]) and the serial connection of organic layer units are sandwiched between the anode and cathode. Figure 2.36b shows a five-unit case.

Petitioner Samsung Ex-1009, 0071

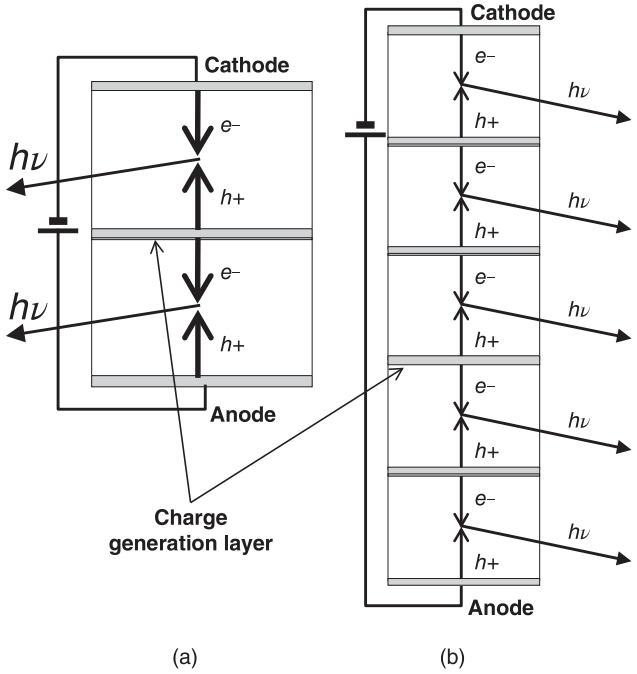


Figure 2.36 Schematic examples of a tandem OLED device with (a) two-layer and (b) five-layer serial connections.

With the tandem structure, by means of electrons and holes generated from the connector layer, photons are created in each organic layer unit, as if a charge were generating multiple photons. Ideally, the electric current of a tandem structure is the same as the current of the one-unit case and the voltage is N times greater than in the one-unit case. Therefore, current efficiency is N times greater, but power efficacy (luminous efficacy) is almost the same as that of the one-unit OLED device. (In power efficacy case, voltage increase cancels the emission increase in the equation.)

Ideally, with the same electric current, the N-unit tandem OLED device can deliver N times more luminance. The tandem device can be used in another way as well. The N-unit tandem OLED device can achieve the same luminance as the one-unit OLED device with $1/N$ times the electric current.

To make this operation happen, the CGL needs to have capability to produce electrons and holes and inject them into adjacent emissive units. Such CGLs are normally by either (1) conducting materials, such as ITO, or (2) insulating materials, such as V_2O_5 and 4 F-TCNQ, which forms CT complex with the adjacent material, such as aryl amine compound (discussed in Section 3.1.1.1) [52]. As both electrons and holes need to be injected from a common material to the

Petitioner Samsung Ex-1009, 0072

adjacent layers, there occurs a large potential barrier for the carrier injection, especially for electrons. To facilitate the electron injection, alkhali dopants, organic dopants, and materials that induce vacuum-level shift are used.

References

1 A. Bemanose, M. Comte, and P. Vouaux, *J. Chim. Phys.* **50**:64 (1953); A. Bemanose, *J. Chim. Phys.* **52**:396 (1955); A. Bemanose and P. Vouaux, *J. Chim. Phys.* **52**:509 (1955).

2 H. Kallmann and M. Pope, *J. Chem. Phys.* **32**:300 (1960); H. Kallmann and M. Pope, *Nature* **186**(4718): 31 (1960).

3 M. Pope, H. Kallmann, and P. Magnante, *J. Chem. Phys.* **38**(8):2042 (1963).

4 M. Sano, M. Pope, and H. Kallmann, *J. Chem. Phys.* **43**(8):2920 (1965).

5 C. W. Tang and S. A. Van Slyke, Organic electroluminescent diodes, *Appl. Phys. Lett.* **51**(12):913–915 (1987).

6 T. Matsuura, *Photochemistry*, Kagaku Dojin, p. 11 (1970).

7 H.Inoue, et al., *Photochemistry I*, Maruzen, p. 103 (1999).

8 E. L. Murphy and R. H. Good, Thermionic emission, field emission, and the transition region, *Phys. Rev.* **102**(6):1464–1473 (1956).

9 P. S. Davids, S. M. Kogan, I. D. Parker, and D. L. Smith, Charge injection in organic light-emitting diodes: tunneling into low mobility materials, *Appl. Phys. Lett.* **69**(15): 2270 (1996).

10 B. K. Crone, I. H. Campbell, P. S. Davids, and D. L. Smith, Charge injection and transportation in single-layer organic light-emitting diodes, *Appl. Phys. Lett.* **73**(21):3162 (1998).

11 M. E. Kiziroglou, X. Li, A. A. Zhukov, P. A. J. de Groot, and C. H. de Groot, Thermionic field emission at electrodeposited Ni-Si Schottky barriers, *Solid-State Electron.* **52**(7):1032–1038 (2008).

12 H. Ishii, K. Sugiyama, E. Ito, and K. Seki, Energy level alignment and interfacial electronic structures at organic/metal and organic/organic interfaces, *Adv. Mater.* **11**:605 (1999).

13 N. Hayashi, H. Ishii, E. Itoh, and K. Seki, Electronic structure of organic/metallic interface observed by Kelvin method—band bending and large surface potential creation, *Appl. Phys. Mag.* **71**:1488 (2002).

14 H. Ishii, Metal-molecular interface electronic structure for organic molecular electronics, *Solid Phys.* **40**:375 (2005).

15 I. G. Hill, A. Rajagopal, A. Kahn, and Y. Hu, Molecular level alignment at organic semiconductor–metal interfaces, *Appl. Phys. Lett.* **73**:662 (1998).

16 I. G. Hill and A. Kahn, Energy level alignment at interfaces of organic semiconductor heterostructures, *J. Appl. Phys.* **84**(10): 5583 (1998).

17 C. Adachi et al., *Device Physics of Organic Semiconductors*, Kodansha Ltd., p. 33 (2012).

Petitioner Samsung Ex-1009, 0073

18 P. Mark and W. Helfrich, Space-charge-limited currents in organic crystals, *J. Appl. Phys.* **33**:205 (1962).

19 N. F. Mott and R. W. Gurney, *Electronic Processes in Ionic Crystals*, Oxford University Press, London and New York, 1940.

20 G. Horowitz, Organic field-effect transistors, *Advanced Materials*, **10**(5):365 (1998).

21 P. G. Le Comber and W. E. Spear, Electronic transport in amorphous silicon films, *Phys. Rev. Lett.* **25**:509–511 (1970).

22 C. W. Tang, S. A. Van Slyke, and C. H. Chen, Electroluminescence of doped organic thin films, *J. Appl. Phys.* **65**:3610–3616 (1989).

23 C. W. Tang, C. H. Chen, and R. Goswami, Electroluminescent Device with Modified Thin Film Luminescent Zone, US Patent 4,769,292 (1988).

24 M. A. Baldo, D. F. O'Brien, Y. You, A. Shoustikov, S. Sibley, M. E. Thompson, and S. R. Forrest, Highly efficient phosphorescent emission from organic electroluminescent devices, *Nature* **395**:151–154 (1998).

25 C. Ganzorig and M. Fujihira, A possible mechanism for enhanced electrofluorescence emission through triplet–triplet annihilation in organic electroluminescent devices, *Appl. Phys. Lett.* (**17**):3137 (2002).

26 Z. D. Popovic and H. Aziz, Delayed electroluminescence in small-molecule-based organic light-emitting diodes: evidence for triplet-triplet annihilation and recombination-center-mediated light-generation mechanism, *J. Appl. Phys.* **98**:13510 (2005).

27 S. Reineke, K. Walzer, and K. Leo, Triplet-exciton quenching in organic phosphorescent light-emitting diodes with Ir-based emitters, *Phys. Rev.* **75**:125328 (2007).

28 The IUPAC Gold book, http://goldbook.iupac.org/T06505.html.

29 S. M. Bachilo and R. B. Weisman, Determination of triplet quantum yields from triplet-triplet annihilation fluorescence, *J. Phys. Chem. A* **104**:7711-7714 (2000).

30 D. Kondakov, Characterization of triplet-triplet annihilation in organic light-emitting diodes based on anthracene derivatives, *J. Appl. Phys.* **102**:114504 (2007).

31 M. Funahashi, H. Yamamoto, N. Yabunouchi, K. Fukuoka, H. Kuma, and C. Hosokawa, Highly efficient fluorescent deep blue dopant for "super top emission" device, *SID Symposium Digest*, Vol.**39**, Issue 1, pp. 709-711, (2008).

32 X. Zhou, J. Blochwitz, M. Pfeiffer, A. Nollau, T. Fritz, K. Leo, Enhanced hole injection into amorphous hole-transport layers of organic light-emitting diodes using controlled p-type doping, *Adv. Funct. Mater.* **11**(4):10-314 (2001).

33 J. Kalinowski,W. Stampor, J. Mezyk, M. Cocchi, D. Virgili, V. Fattori, and P. Di Marco, Quenching effects in organic electrophosphorescence, *Phys. Rev. B* **66**:235321 (2002).

Petitioner Samsung Ex-1009, 0074

34 M. Baldo, C. Adachi, and S. Forrest, Transient analysis of organic electrophosphorescence. II. Transient analysis of triplet-triplet annihilation, *Phys. Rev. B* **62**:10967 (2000).

35 R. Meerheim, M. Furno, S. Hofmann, B. Lüssem, and K. Leo, Quantification of energy loss mechanisms in organic light-emitting diodes, *Appl. Phys. Lett.* **97**:253305 (2010).

36 A. Mikami, S. Nakajima, and A. Okada, Flexible polymer electroluminescent device with PVCz light-emitting layer on high-index of refraction substrate, *IDW 2002 Digest*, pp. 1139–1142 (2002).

37 D. Yokoyama, Molecular orientation in small-molecule organic light-emitting diodes, *J. Mater. Chem.* **21**:19187 (2011).

38 D. Yokoyama, Y. Setoguchi, A. Sakaguchi, M. Suzuki, and C. Adachi, Orientation control of linear-shaped molecules in vacuum-deposited organic amorphous films and its effect on carrier mobilities, *Adv. Mater.* **20**(3):386-391 (2010).

39 M. Era, T. Tsutsui, and S. Saito, Polarized electroluminescence from oriented p-sexiphenyl vacuum-deposited film, *Appl. Phys. Lett* **67** (17):2436-2438 (1995).

40 T. Cremoux, M. Dussauze, E. Fargin, T. Cardinal, D. Talaga, F. Adamietz, and V. Rodriguez, Trapped molecular and ionic species in poled borosilicate glasses: toward a rationalized description of thermal poling in glasses, *J. Phys. Chem. C* **118**:3716–3723 (2014).

41 P. Dyreklev, M. Berggrem, W. Inganas, M. Andersson, O. Wennerstrom, and T. Hyertberg, Polarized electroluminescence from an oriented substituted polythiophene in a light emitting diode, *Adv. Mater.* **7**:43–45 (1995).

42 T. Tsujimura, K. Furukawa, H. Ii, H. Kashiwagi, M. Miyoshi, S. Mano, H. Araki, and A. Ezaki, World's first all phosphorescence OLED product for lighting application, *IDW 2011 Digest* (2011).

43 T. Yoshioka, K. Sugimoto, K. Katagi, Y. Kitago, M. Tajima, S. Miyaguchi, T. Tsutsui, R. Iwasaki, and Y. Furukawa, An improved method for lifetime prediction based on decoupling of the joule self-heating effect from coulombic degradation in accelerated aging tests of OLEDs, *SID 2014 Digest*, pp. 642-645 (2014).

44 H. Aziz and Z. Popovic, Degradation phenomena in small-molecule organic light-emitting devices, *Chem. Mater.* **16**(23):4522-4532 (2004).

45 P. Burrows, B. Bulovic, S. Forrest, L. Sapochak, D. McCarthy, and M. Thompson, Reliability and degradation of organic light emitting devices, *Appl. Phys. Lett.* **65**(23):2922-2924 (1994).

46 D. Kondakov and R. Young, Role of chemical transformations of hole transport materials in operational degradation of the current generation of highly efficient fluorescent OLEDs, *SID Symposium Digest*, Vol. **40**, Issue 1, pp. 687-690 (2009).

Petitioner Samsung Ex-1009, 0075

47 R. Meerheim, S. Scholz, S. Olthof, G. Schwartz, S. Reineke, K. Walzer, and K. Leo, Influence of charge balance and exciton distribution on efficiency and lifetime of phosphorescent organic light-emitting devices, *J. Appl. Phys.* **14**:014510 (2008).
48 F. So and D. Kondakov, Degradation mechanisms in small-molecule and polymer organic light-emitting diodes, *Adv. Mater.* **22**:3763-3777 (2010).
49 H. Uoyama, K. Goushi, K. Shizu, H. Nomura, and C. Adachi, Highly efficient organic light-emitting diodes from delayed fluorescence *Nature* **492**:234–238 (2012).
50 H. Nakanotani, T. Higuchi, T. Furukawa, K. Masui, K. Morimoto, et al., High-efficiency organic light-emitting diodes with fluorescent emitters, *Nat. Commun.* **5**:4016 (2014).
51 S. Seo, T. Takahashi, H. Nowatari, S. Hosoumi, T. Ishisone, T. Watabe, S. Mitsumori, N. Ohsawa and S. Yamazaki, Efficiency enhancement in phosphorescent and fluorescent OLED utilizing energy transfer from exciplex to emitter, *SID 2015 Digest*, Vol. **46**, Issue 1, pp. 605-608 (2015).
52 J. Kido, High performance OLEDs for displays and general lighting, *SID Symposium Digest of Technical Papers*, Vol. **39**, Issue 1, pp. 931–932 (2008).

Petitioner Samsung Ex-1009, 0076

3

OLED Manufacturing Process

The process for manufacturing high-quality OLED devices is discussed in this chapter.

3.1 MATERIAL PREPARATION

3.1.1 Basic Material Properties

As discussed in Section 2.3, OLED devices consist of multiple layers that have different functions. It is very important to design layers by selecting material in terms of their inherent properties and compatibility (e.g., with respect to their HOMOs and LUMOs) with other layers.

3.1.1.1 Hole Injection Material

The term *hole injection* refers to the injection of holes from an anode, namely, ejection of electrons to the anode. The mechanism is discussed in Section 2.3.6. Hole injection material is used to reduce the height of the barrier (also termed a *potential barrier*) against hole injection from anodes [1, 2]. The material layer involved in this process is called the *hole injection layer* (HIL).

Hole injection material is often selected so that the HOMO level is located between the HOMO of the hole transportation material (HTM) and the work-function of the anode (Figure 3.1).

Figure 3.2 shows typical hole injection materials.

There is another type of HIL used popularly, such as $HAT(CN)_6$ (Figure 3.3). $HAT(CN)_6$ is known to form charge-transfer complex (discussed in Section 2.6.2.2.) with aryl amine compounds, such as NPB. Figure 3.4 shows the case when $HAT(CN)_6$ is used as HIL and NPB is used as HTL. Electrons are extracted from the interface due to charge-transfer mechanism and conduct toward the anode. Also holes, created by electron extraction, conduct toward the cathode . (Act as a kind of charge generation layer, discussed in Section 2.6.3.) As a result, effective hole injection can make happen for high-performance OLED operation.

OLED Display Fundamentals and Applications, Second Edition. Takatoshi Tsujimura.
© 2017 John Wiley & Sons, Inc. Published 2017 by John Wiley & Sons, Inc.

Petitioner Samsung Ex-1009, 0078

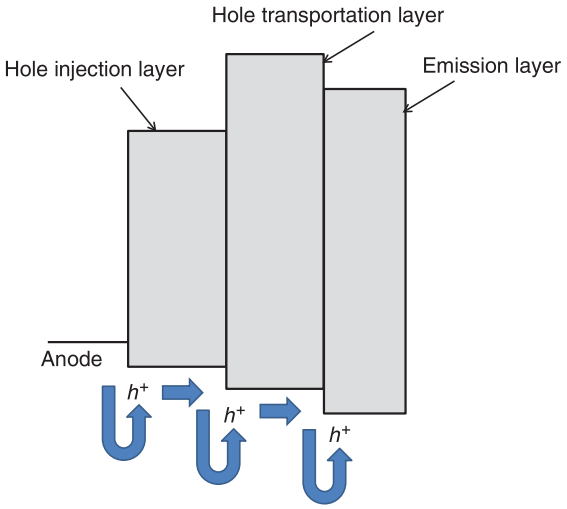
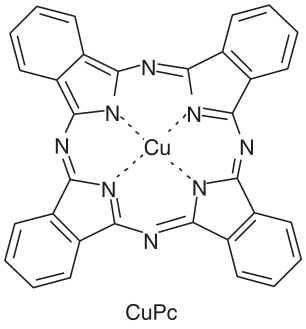
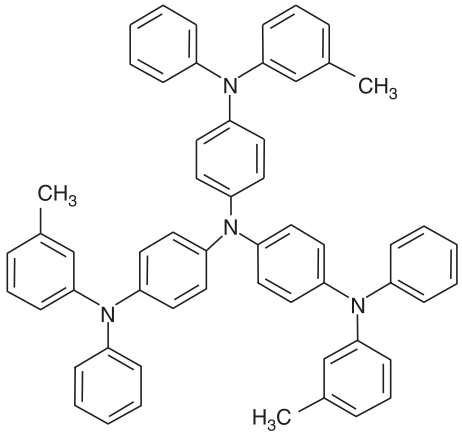


Figure 3.1 Example of energy diagram using HIL layer with stepwise energy location mechanism.



CuPc



m-MTDATA

Figure 3.2 Example structures of hole injection material.

3.1.1.2 Hole Transportation Material

HTM is used to transport holes to the emission layer (EML) [3]. This layer is called the *hole transport layer*, which is usually designed with a higher exciton energy than EML to ensure that the excitation energy of the EML is not transferred to the transport layer.

Figure 3.5 shows the structures of typical HTMs.

3.1.1.3 Emission Layer Material

The layer from which light is emitted is referred to as the EML [4, 5]. The electron transportation and hole transport layers can also function as EMLs.

Petitioner Samsung Ex-1009, 0079

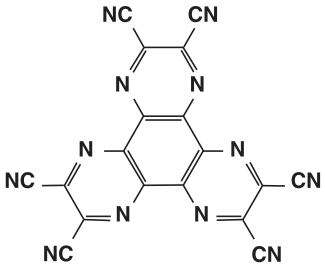


Figure 3.3 Structure of $HAT(CN)_6$. hole injection material.

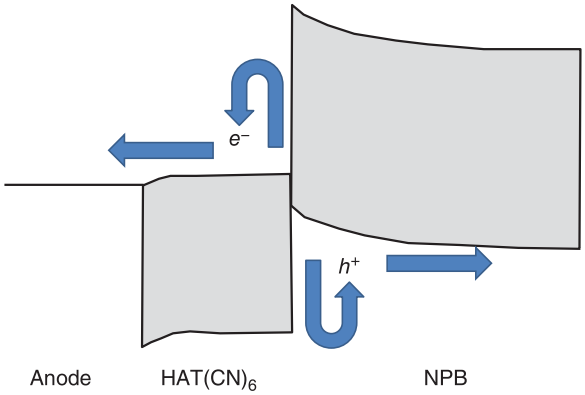


Figure 3.4 Example of energy diagram using HIL layer with charge-transfer complex mechanism.

Host material normally has light emission capability, but doping (Section 2.4.2.3) of the host material is a very useful approach when emission from the host material causes concentration quenching (quantum yield loss at high concentration) or when the color needs fine-tuning. In such cases, the bandgap of the host material should be wider than that of the dopant.

Figure 3.6 shows typical fluorescent light-emitting materials.

Phosphorescent materials [6, 7] are also used for the EML. Normally, light emission from the triplet state is prohibited. However, with the use of heavy-metal complexes containing iridium and platinum, for example, light emission is allowed as a result of spin–orbit coupling, due to the heavy-metal effect (discussed in Section 2.4.2.3). Figure 3.7 shows the structure of a typical phosphorescent dopant. For phosphorescent emission, the triplet bandgap of the host needs to be wider than that of the dopant, so a host material specifically designed for phosphorescent emission is sometimes used (Figure 3.8) [8].

3.1.1.4 Electron Transportation Material and Charge Blocking Material

Electron transportation material is used to transport electrons injected from the cathode [9–11]. This layer, called the *electron transport(ation) layer* (ETL), is sometimes used with the *electron injection layer* (EIL), such as LiF, which induces vacuum-level shift (Section 2.3.6.3) when it is allocated with organic

Petitioner Samsung Ex-1009, 0080

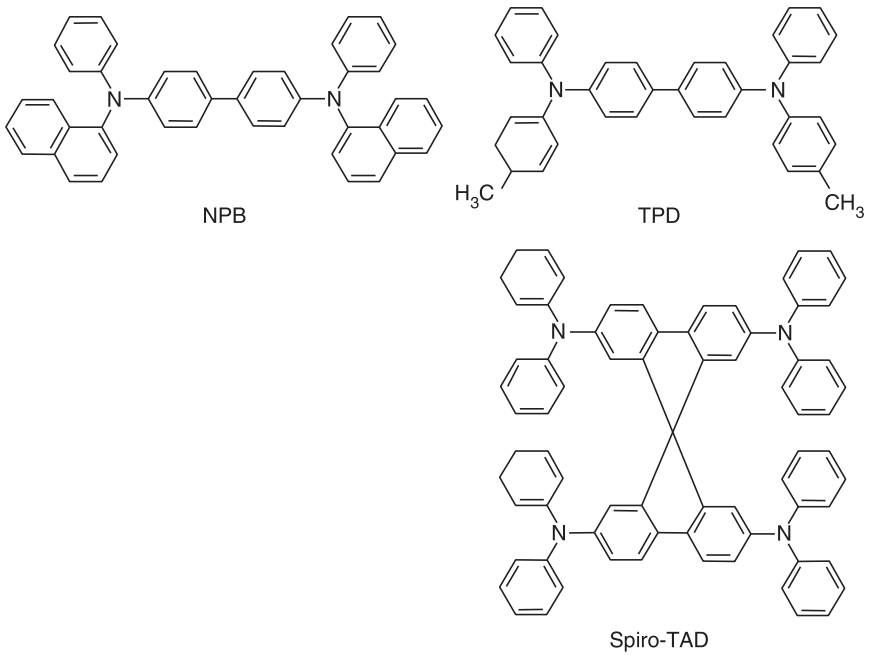


Figure 3.5 Example structures of hole transportation material.

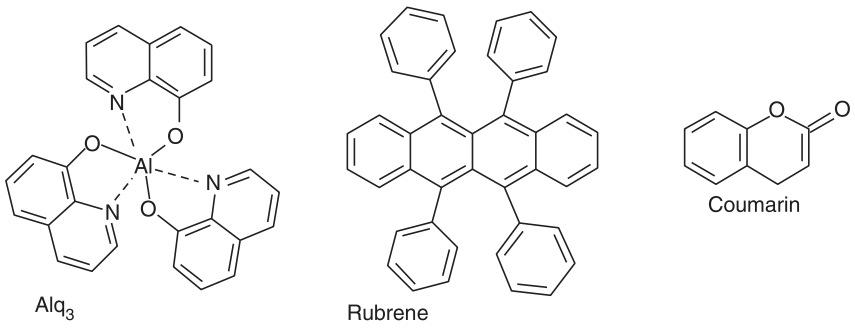


Figure 3.6 Example structures of fluorescent light-emitting materials.

materials, or alkhali dopants, such as Li, Ca, or organic materials such as Liq_3 with smaller electron affinity than the electrode, to increase the electron injection capability (the injection mechanism is discussed in Section 2.3.6.). Sometimes, the ETL is used without EIL when the cathode workfunction matches with the LUMO of the ETL.

Petitioner Samsung Ex-1009, 0081

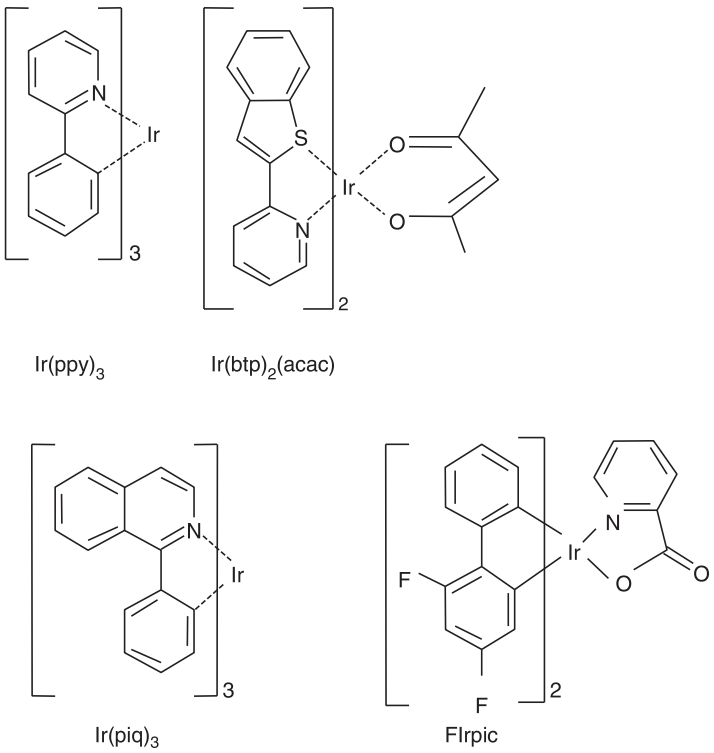
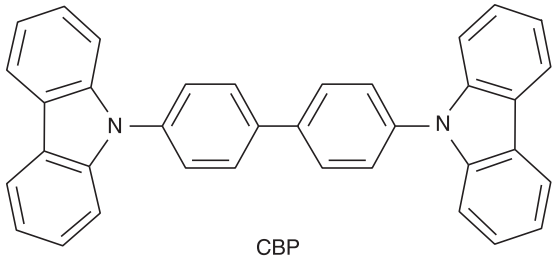


Figure 3.7 Example structures of phosphorescent dopant materials.

Figure 3.8 Example structure of a phosphorescent host material.



Just like the hole transport layer, the electron transport layer should have a higher exciton energy than that of the EML. The electron transport layer also sometimes blocks exciton and hole movement to enhance emission efficiency.

Figure 3.9 shows a typical example of the electron transport layer. BCP(bathocuproine) is also known as a popular *hole blocking material* (HBM). The hole blocking layer (HBL), a layer of HBM material, is used to block the hole transfer so that the charge is accumulated in the EML layer.

Petitioner Samsung Ex-1009, 0082

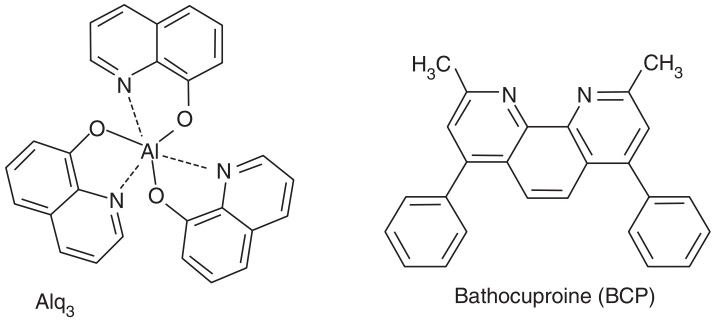


Figure 3.9 Example structures of electron transportation material.

Figure 3.10 shows a simple two-layered OLED device without HBL. Generally speaking, organic material conducts more holes than electrons. Therefore, the amount of holes accumulated in the hole transportation layer/EML interface is normally higher than the amount of electrons accumulated in the same interface. The electric field caused by the accumulated holes facilitates the electron transport, which results in good carrier balance. The holes that meet with electrons would successfully recombine and most of them would create photons for emission. However, especially when EML has high hole conduction, such as due to Ir-complex molecule doping, excessive holes increase the leakage current. Such leakage current reduces the OLED device efficacy and also causes undesired light emission from unexpected layers.

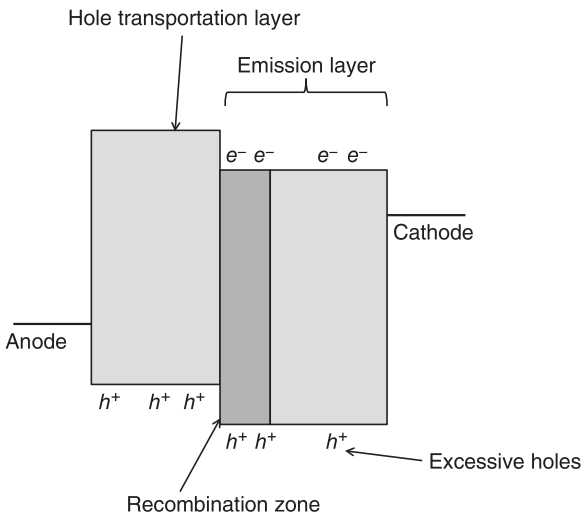


Figure 3.10 Schematic representation of energy diagram using two-layer OLED device without hole blocking layer.

Petitioner Samsung Ex-1009, 0083

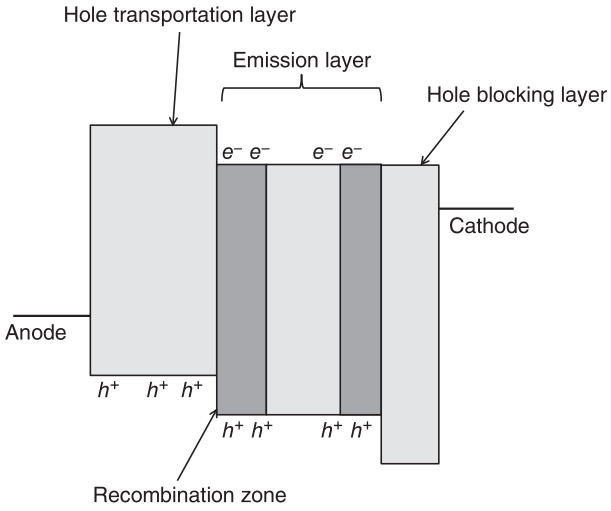


Figure 3.11 Schematic representation of energy diagram using two-layer OLED device with hole blocking layer.

To circumvent the situation, HBL is used. In the case of OLED device shown in Figure 3.11, excessive holes meet with energy barrier at EML/HBL interface. As the electric field created by blocked holes suppresses the hole injection from the hole transport layer to EML, the amount of holes in EML is maintained. As a result, two recombination zones are established. Due to the recombination location control, efficacy loss due to leakage current can be suppressed. Also emission from unexpected layers can be avoided. By accumulation of charge, effective electron–hole recombination can be made to achieve high efficiency by means of better carrier balance, as discussed in Section 2.4.1.

3.1.2 Purification Process

The characteristics and lifetime of an OLED device depend significantly on the purity of the materials used. For this reason, sublimation purification is often used to increase the purity of the materials. Figure 3.12 shows a simplified layout for typical equipment employed for sublimation purification. This equipment consists of a quartz tube, a metal tube attached to the quartz tube (the metal tube is used to set the temperature gradient), and a band heater.

Several grams of material to be purified are heated by the band heater. The greater the distance between the material and the band heater, the lower the temperature, so sublimed material is transferred to the lower-temperature location. Nonvolatile impurities remain in the boat, and high-mass material is extracted in the high-temperature region. Low-mass material is extracted in the low-temperature region, so mass separation is possible using this

Petitioner Samsung Ex-1009, 0084

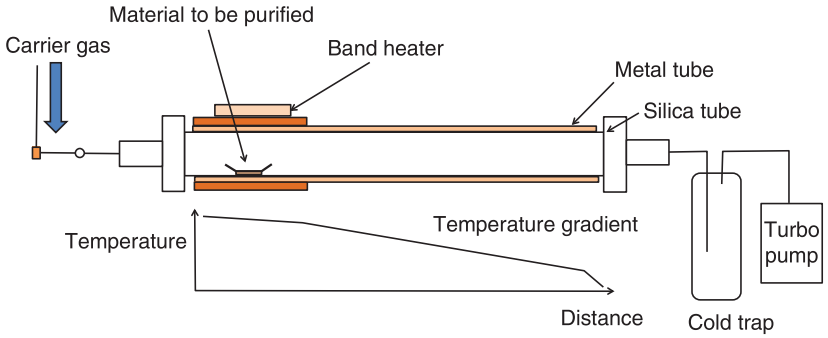


Figure 3.12 Schematic representation of sublimation purification equipment.

method. During OLED device fabrication, even if the material is uniform, any impurities that it contains can significantly influence the characteristics of the OLED device. In that sense, sublimation purification is very important.

3.2 EVAPORATION PROCESS

3.2.1 Principle

The *evaporation* process [12] involves conversion of a solid or a liquid to the vapor state by heating the material in an evaporation source. A material that is transformed directly into vapor, bypassing the liquid phase, is called a sublimation-type material. On the other hand, a material type that turns into liquid and then evaporates is called a melting-type material (further discussed in Section 3.2.2.1). The simplest evaporation source is called a "boat": a boat-shaped vessel made of metal, such as tungsten, which also acts as a resistive heating source to raise the temperature of the material in the vessel to vaporize it. The heat can also be applied by electron beam (EB) evaporation; however, a high-energy electron, ion, or X-ray can damage the TFT substrate and OLED device, so resistive heating is more commonly used. The basic structure of evaporation equipment, using a boat for the evaporation source, is shown in Figure 3.13. For organic materials, an evaporation crucible is popular for manufacturing (Figure 3.14), as it can apply heat more uniformly than a boat. In the case of the crucible, heat is applied by the resistive-heating filament, which is normally placed outside the crucible.

The basic parameters of the evaporation process can be described as follows. By applying the kinetic theory of gases, we can express the number of molecules evaporated per unit evaporation area per unit time (/m^2s), when the material

Petitioner Samsung Ex-1009, 0085

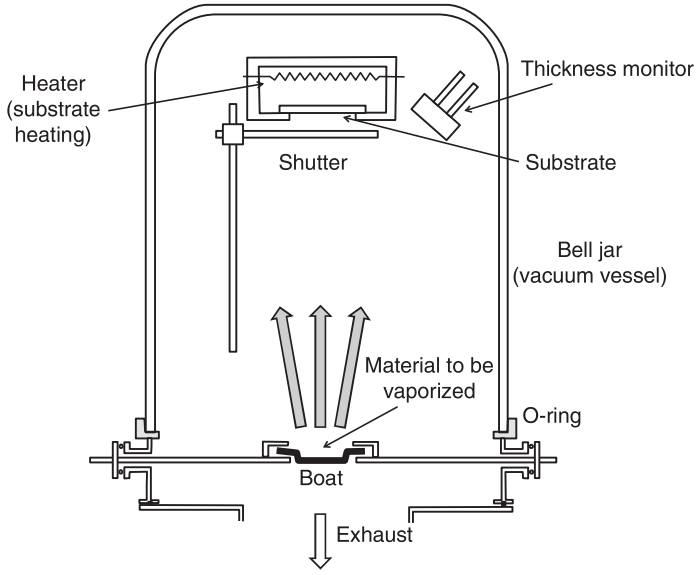


Figure 3.13 Basic structure of an evaporation source.

is heated and then extracted by evaporation, as

$$J = \frac{1}{4}\alpha n\bar{v} = 2.6 \times 10^{24} P\sqrt{MT} \tag{3.1}$$

where n is the number of molecules per unit volume, $\bar{v}$ the average velocity, P the pressure, M the molecular mass, and α the cohesion coefficient (α is almost 1).

In Eq. (3.1), as the temperature increases, vapor pressure also increases, so the deposition rate is increased. An OLED device normally requires precise evaporation speed control, so a Knudsen cell (Figure 3.14) (sometimes called a "K cell," a crucible used to apply more uniform temperature gradient) is often used for manufacturing.

The mean free path can be expressed by the equation

$$\lambda = \frac{1}{\sqrt{2}\pi n D^2} \tag{3.2}$$

where λ is the mean free path (m), n the molecular number density in vacuum, and D the molecular diameter (m). For example, if the molecular diameter is 1.4 nm (Alq_3), the vacuum level must be larger than 10^{-4} Pa when the distance between crucible and substrate is 30 cm. The purpose of a high vacuum is to

Petitioner Samsung Ex-1009, 0086

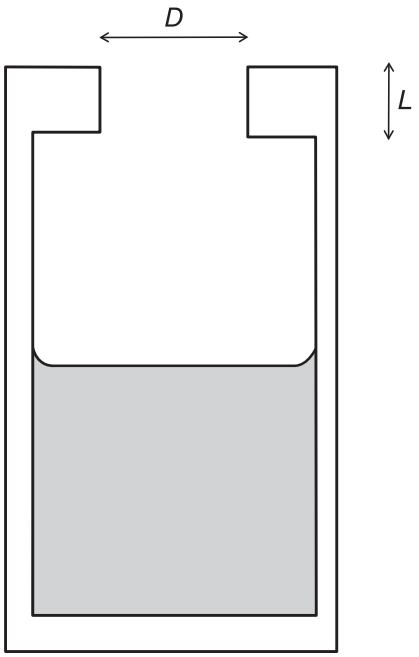


Figure 3.14 Schematic representation of a Knudsen cell (where D = diameter, L = length).

lengthen the mean free path to avoid any impurities being included in the film, such as oxygen, which causes oxidization.

The amount of material deposited on the substrate is determined by the evaporation angle and source–substrate distance. Here, we assume that the evaporated molecule originated from a point source. Isotropic evaporation is also assumed.

The number of molecules evaporated into the solid angle $d\omega$ is

$$dN = \frac{Nd\omega}{4\pi} \tag{3.3}$$

where N is the total number of evaporated molecules per second (Figure 3.15).

The frequency of incident evaporation molecules at point A in Figure 3.16 is

$$n = \frac{N\cos\phi}{4\pi r^2} \tag{3.4}$$

Here, we assume that the substrate is located immediately above the evaporation source at a distance h.

In the θ direction, h and θ can be described as

$$h = r\cos\theta$$
$$\theta = \phi$$

Petitioner Samsung Ex-1009, 0087

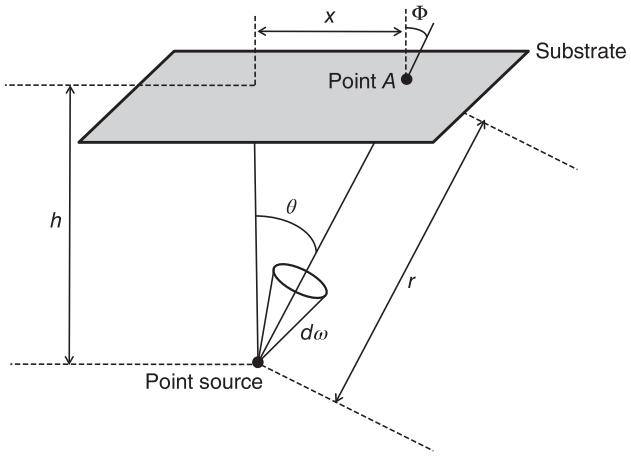


Figure 3.15 Incident evaporation molecule to substrate at point *A* from point source.

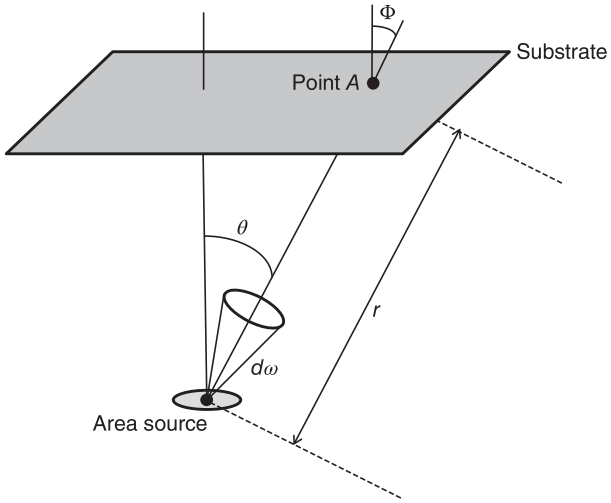


Figure 3.16 Incident evaporation molecule to substrate at point *A* from area source.

Using Eq. (3.4), we note that the thickness of the deposited layer is proportional to $1/\cos^3\theta$. The thickness distribution $d(x)$, at a distance x from the right (point A in Figure 3.16) below the evaporation source, can be expressed as

$$d(x) = d(0)\left\{1 + \frac{x^2}{h^2}\right\}^{-(3/2)} \tag{3.5}$$

Petitioner Samsung Ex-1009, 0088

On the other hand, if a very small area evaporation source, not a point source, is assumed, then, according to the rule of cosines, we obtain

$$dN = \frac{N \cos\theta \, d\omega}{\pi} \tag{3.6}$$

Therefore, we can express n as

$$n = \frac{N \cos\theta \cos\phi}{\pi r^2} \tag{3.7}$$

The thickness distribution is now proportional to $1/\cos^4\theta$. Then, according to this formula, the thickness distribution $d(x)$ of area source (Figure 3.16) at a distance x can be expressed as follows:

$$d(x) = d(0)\left\{1 + \frac{x^2}{h^2}\right\}^{-2} \tag{3.8}$$

The simulated thickness distribution for the point source (Eq. [3.5]) and for the area source with a very small area (Eq. [3.8]) is plotted in Figure 3.17. Normally, an OLED device requires precise thickness control with variation within several percent of thickness (requirements for microcavities are tighter), so the variation shown in Figure 3.17 renders the thickness distribution in OLED devices nonuniform and thus unsuitable for this display application.

To correct the variation in thickness distribution, the following strategies are recommended:

- Increasing source to substrate distance (T/S); this distance is also known as *target–source distance* (T/S).
- Rotation of substrate.
- Offset positioning from the rotation center (Figure 3.18).

As the T/S of a point source needs to be long, a large amount of material is deposited on the chamber wall and shield plate, so the material utilization level tends to be low.

3.2.2 Evaporation Sources

3.2.2.1 Resistive Heating Method

In resistive heating, the most frequently used evaporation method, Joule heating due to electric current flow through the resistance of a high-melting-point metal, such as tungsten, tantalum, or molybdenum, is used to cause evaporation of the material. There are two methods of implementation: (1) using high-melting-point metal as a filament to create heating and (2) using the metal as a boat itself. If method 2 is used, it is important to ensure compatibility between the boat material and the evaporation material in order to avoid interaction between these two materials.

Petitioner Samsung Ex-1009, 0089

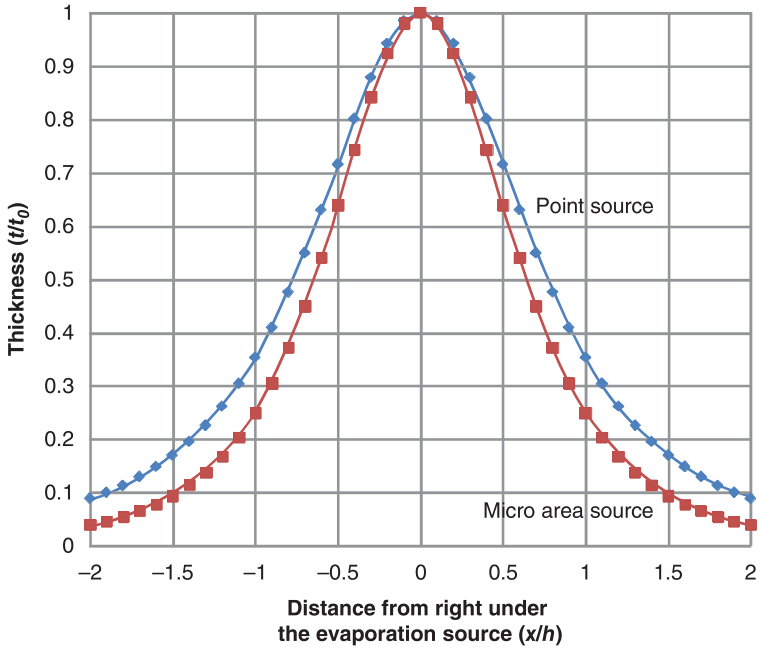


Figure 3.17 Thickness distribution in the case of motionless evaporation.

In another method, in the case of filament implementation, a boron nitride (BN), quartz, or graphite crucible is heated by a tungsten filament heater.

It is also possible to deposit a mixture such as by the doping method using multiple crucibles. (Normally, multiple materials contained in one crucible cannot be evaporated as a mixture. This is because the evaporation pressure values of different materials vary, so only one material will be evaporated while the others are not, as in a distillation process.)

All OLED materials can be classified into one of the following two groups: (1) melting-type material, which evaporates after melting, and (2) sublimation-type material, which sublimes without melting, as discussed in Section 3.2.1. The evaporation source should be selected according to the evaporation parameters of the specific material.

If evaporation is carried out by only one evaporation source for 1 week, the OLED device characteristics may change during operation of the evaporation equipment or the material to be evaporated may become depleted. To avoid such problems, a revolver (also known as a *turret*) mechanism (Figure 3.19) is often used.

Figure 3.20 shows the transformation of an evaporation source material during operation. OLED materials seldom have high thermal conductance, so the

Petitioner Samsung Ex-1009, 0090

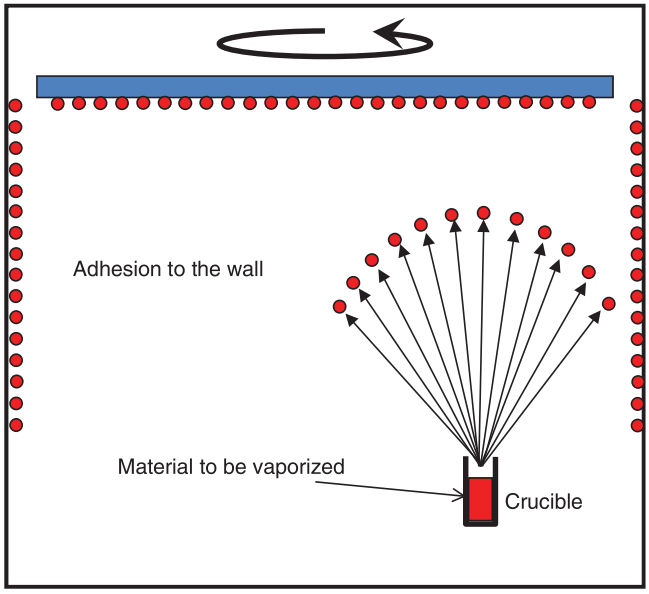


Figure 3.18 Schematic example of evaporation with offset and substrate rotation.



Figure 3.19 Evaporation equipment using a revolver apparatus.

Petitioner Samsung Ex-1009, 0091

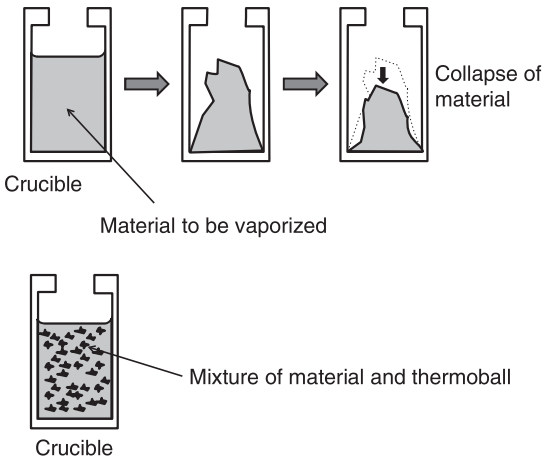


Figure 3.20 Schematic representation of material in an evaporation source.

material near the wall tends to be evaporated more rapidly than that in the center area. Moreover, the stacked, accumulated material may suddenly collapse, resulting in a significant change in evaporation rate, which is problematic for manufacturing.

As the material near the wall is consumed more rapidly, the heater temperature must be higher than the normal evaporation temperature of the material to ensure adequate evaporation speed. However, this higher temperature can degrade the material's properties.

To overcome this problem, a material known as a *thermoball* (see the lower diagram in Figure 3.20; photo in Figure 3.21), which has a high thermal conductance, with thermal stability at the evaporation temperature, is sometimes mixed with the material to be vaporized. Because of the high thermal conductance, issues such as sudden change in evaporation speed or material decomposition due to overheating can be avoided.

A linear evaporation source (see Figures 3.22 and 3.23) is also used to increase manufacturability [13, 14]. With a linear source, uniform deposition can be achieved even when the source is very close to the substrate, so this feature is advantageous in terms of material utilization. However, as the source is close to the substrate, this can lead to OLED device degradation due to radiative heating and shadow mask deformation as a result of thermal expansion. Also, because of the thermal conductance problems of the material, it is not easy to evaporate materials uniformly along the whole length of the linear source , so material utilization is not always as high as expected.

3.2.2.2 Electron Beam Evaporation

Use of the resistance heating method can result in contamination of the evaporated material. In EB evaporation, an accelerated EB is emitted toward the target material to evaporate it. This method can be used to produce high-quality

Petitioner Samsung Ex-1009, 0092



Figure 3.21 A thermoball.

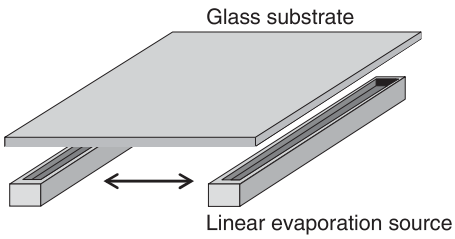


Figure 3.22 Thin-film evaporation by linear source.

films but may also result in damage to the TFT and OLED device due to the ultraviolet light and X-ray radiation created.

3.2.2.3 Monitoring Thickness Using a Quartz Oscillator

In an actual full-length evaporation operation, the evaporation rate fluctuates. To ensure accurate thickness measurement, feedback control is necessary for

Petitioner Samsung Ex-1009, 0093



Figure 3.23 Linear source evaporation equipment.

monitoring the thickness. A quartz oscillator is often used to measure the thickness (Figure 3.24).

In thickness measurement using a quartz oscillator, the oscillation frequency of the quartz is reduced because of the effective change in mass due to the film formation. As the Q value of the quartz oscillator exceeds 10^6, this method has about 0.5 nm sensitivity.

Petitioner Samsung Ex-1009, 0094

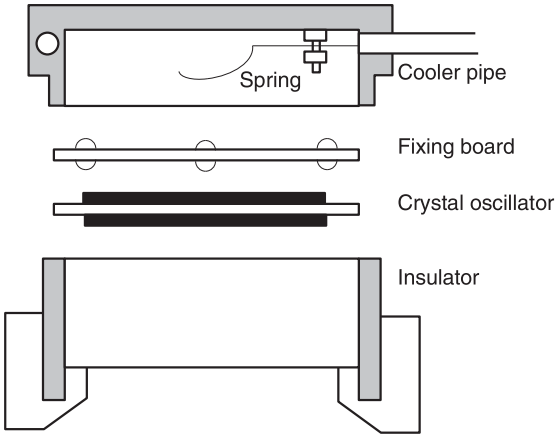


Figure 3.24 Schematic representation of a thickness monitoring apparatus using a quartz crystal oscillator.

The correlation between resonant frequency f_q of the quartz oscillator and thickness t_q can be expressed as follows:

$$f_q \cdot t_q = \frac{v_q}{2} = N_q = 1.69 \times 10^3 \ \text{(m/s)} \tag{3.9}$$

If the oscillation frequency of the quartz oscillator without film formation is f_c, then

$$\rho_f t_f = \rho_q t_q \frac{f_q - f_c}{f_q} \tag{3.10}$$

where ρ_q and ρ_f are density of the quartz oscillator and density of the deposited film, respectively, and t_q and t_f are thicknesses of the quartz oscillator and the deposited film.

When the film is thick, this equation is no longer valid, and

$$\rho_f t_f = \rho_q t_q \frac{f_q - f_c}{f_c} \tag{3.11}$$

should be used instead.

Here, the Z ratio is defined as follows:

$$Z = \frac{\rho_q v_q}{\rho_f v_f} \tag{3.12}$$

Then

$$\rho_f t_f = \frac{\rho_q t_q}{\pi Z(1-F)} \tan^{-1}\{Z \tan(\pi F)\} \tag{3.13}$$

In this equation, we have

$$F = \frac{f_q - f_c}{f_q} \tag{3.14}$$

Petitioner Samsung Ex-1009, 0095

According to this equation, thickness can be calculated from the frequency difference. Although the crystal thickness monitoring method is able to provide continuous measurement during operation, to keep the measurement accuracy, frequent quartz replacement is required, which causes suspension of the manufacturing process. Therefore, newer deposition method is proposed, which uses ellipsometry or a Pirani gauge (Section 5.3.1) to measure the thickness during operation, circumventing this issue.

3.3 ENCAPSULATION

3.3.1 Dark Spot and Edge Growth Defects

To produce high-quality OLED displays, defects should be avoided in terms of manufacturing and reliability. An OLED is highly vulnerable to water damage, so it is important to protect the device from humidity.

Figure 3.25 shows a defect called a *dark spot (also called "black spot" or "black dot")*, which is believed to be caused by the cathode peeling or by organic material degradation due to the presence of pinholes (Figure 3.26) created by several mechanisms, such as irregularities of the substrate surface or of the anode, or the protrusion structure of organic film [15, 16].

When encapsulation is insufficient, the nonemissive area gradually increases, as shown in Figure 3.27. As a result, effective pixel size decreases; this is called *pixel shrinkage* or *edge growth*.

Moisture in the OLED display panel does not only come from the outside. Especially when polymer resin is used for planarization or edge insulation, the material and baking conditions should be carefully investigated to ensure that the presence of the polymer does not result in excess moisture.

Schaer et al. have made an experiment to investigate how dark spots are grown in controlled atmosphere [17]. In the experiment, it was found that the degradation of OLED in water vapor is very much different from the degradation in pure oxygen, and the degradation speed by water is faster by three orders of magnitude than oxygen. Normally, aluminum cathode shows excellent protection against water and oxygen; however, when the pinholes exist due to particles, dark spots are created. In the case of degradation due to water vapor, delamination of cathode is observed, which is possibly due to the bubble burst, caused by hydrogen evolution, which is created by electrochemical reduction of water. The delamination of cathode inhibits the electron injection of cathode to organic layers, which prevents the OLED emission in the region.

The growth of dark spot follows the following equation:

$$D(t) = D_0 e^{kt}$$

where D is the dark spot diameter, D_0 the initial dark spot diameter, and k the growth rate.

Petitioner Samsung Ex-1009, 0096

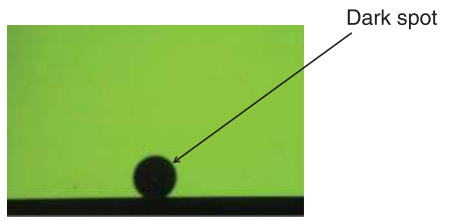


Figure 3.25 Dark spot formation.



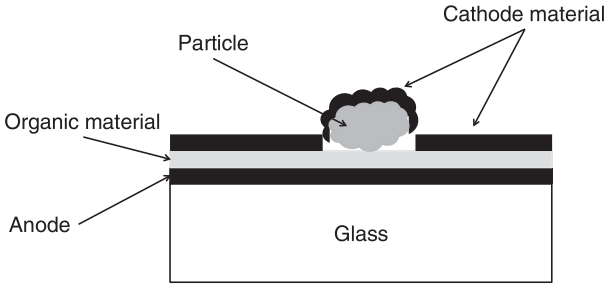


Figure 3.26 Schematic representation of dark spot formation mechanism.

According to [17], the growth rate of dark spot is

$$k = 2 \times 10^{-4} \ [\mathrm{s}^{-1}]$$

This value changes depending on the condition.

As the time goes on, visible dark spot number is increased and the appearance of a display is deteriorated, so it is very important to avoid internal and external moisture in manufacturing high-quality OLED displays.

3.3.2 Light Emission from the Bottom and Top of the OLED Device

An encapsulation strategy to protect an OLED display panel from moisture and oxygen is very important for fabricating a good OLED display.

Figure 3.28 shows light emission structures using both bottom and top emission methods.

Petitioner Samsung Ex-1009, 0097

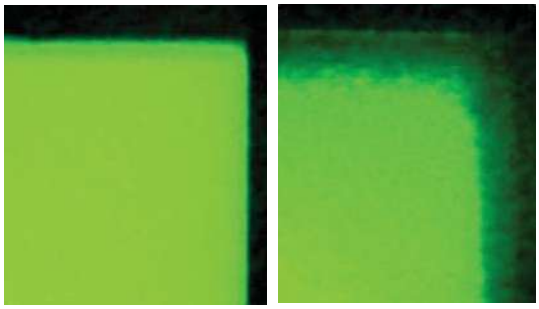


Figure 3.27 Edge growth (a) before and (b) after high-temperature/high-humidity testing (sample with encapsulation).

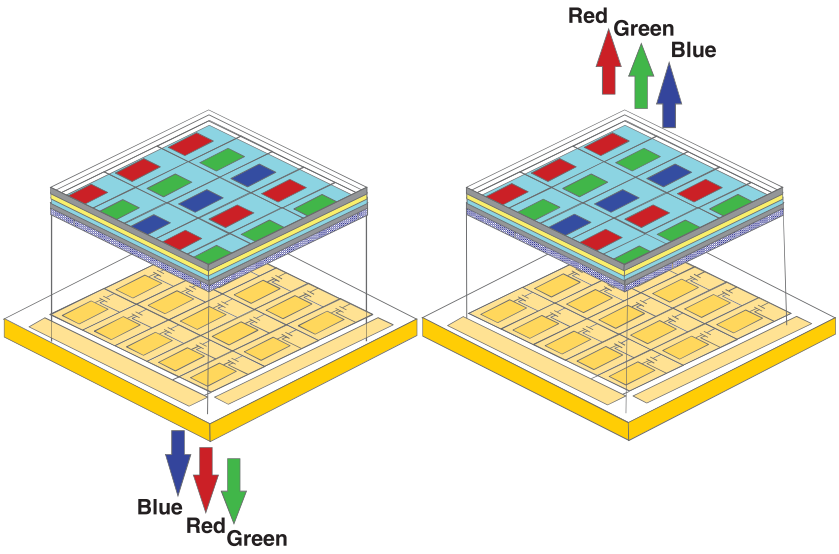


Figure 3.28 Light emission from (a) bottom and (b) top of the OLED structure.

3.3.3 Bottom Emission and perimeter sealing

Bottom emission structure has been used since the first commercialization of OLED display and is a mature technology.

For the bottom structure, opaque aluminum is used for the upper electrodes (normally cathodes) of the OLED device, and a transparent electrode such as ITO is used for the lower electrodes (normally anodes). In that case, the light

Petitioner Samsung Ex-1009, 0098

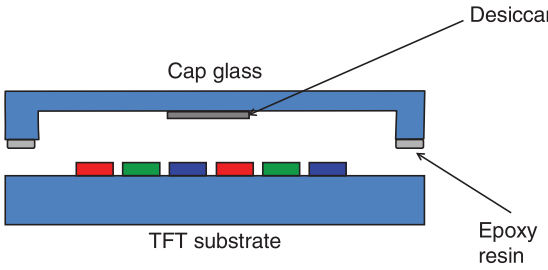


Figure 3.29 Schematic example of bottom emission sealing.

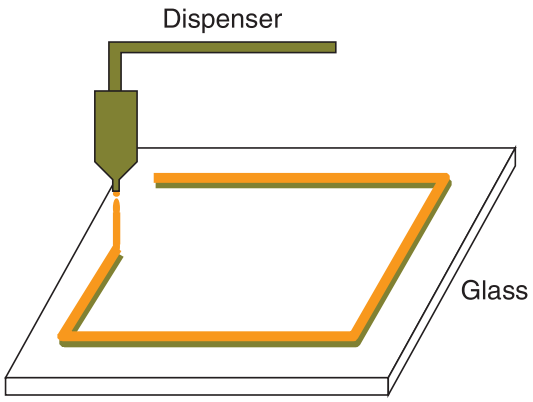


Figure 3.30 Schematic representation of seal dispensing.

generated in the OLED device passes through the glass and is emitted to outside. In the bottom emission structure, perimeter sealing plus a desiccant have been used for most of the products. A desiccant is inserted between the OLED device substrate and the counter substrate using a hollow device called a *cap glass* or a cap metal, to absorb any moisture in the display device (Figure 3.29). Epoxy resin is distributed by a dispenser (Figure 3.30) or by screen printing along the edge of the cap substrate to form the perimeter seal, which is then attached to the OLED device substrate. The perimeter seal is cured by UV or heat (Figure 3.31).

3.3.4 Top Emission

To allow a high-resolution display to have enough aperture ratio in a pixel, top emission structure is often used. Especially, when an active-matrix OLED display needs to have compensation circuit (discussed in Section 6.4.4.), the circuitry occupies significant portion of a pixel, so the aperture ratio becomes very small in the case of bottom emission. Using top emission, the pixel electrode can be placed above the circuitry, so the aperture ratio is not reduced regardless of the complexity of the circuitry.

Petitioner Samsung Ex-1009, 0099

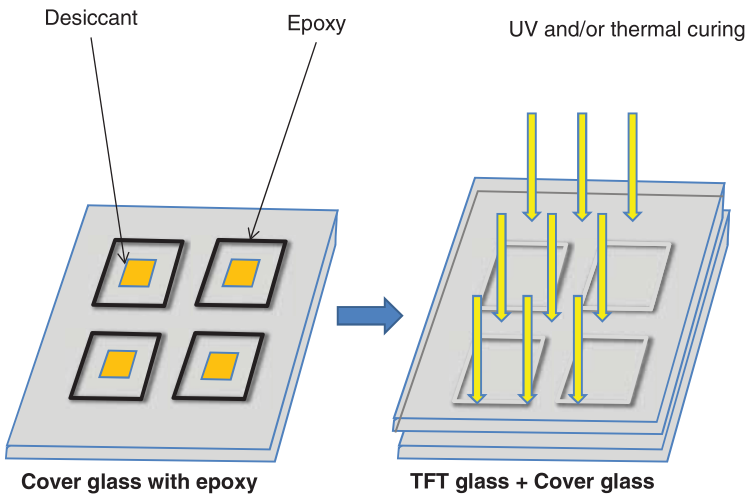


Figure 3.31 An example of perimeter-sealing process (bird's-eye view).

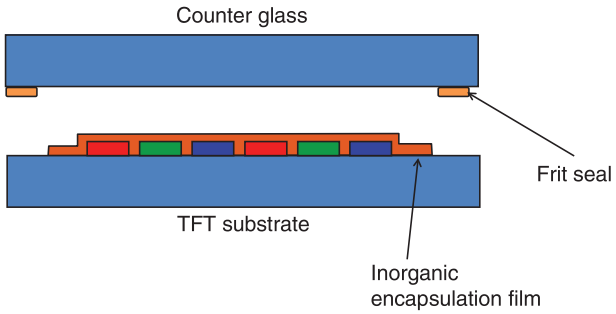


Figure 3.32 Schematic example of top emission encapsulation.

In a top emission structure, it is not possible to place opaque desiccants within the emissive device. (Use of a transparent desiccant has been proposed but is not widely applied in actual manufacturing.) Without a desiccant, more strict moisture control is necessary than for a bottom emission device. Thin-film encapsulation is used for many of the top emission OLED devices in combination with perimeter sealing, face sealing, and frit sealing technologies.

Figure 3.32 shows an example of top emission structure encapsulation, which uses a combination of thin-film encapsulation and frit sealing.

3.3.5 Encapsulation Technologies and Measurement

To encapsulate OLED device from moisture and oxygen, several techniques are used. Also WVTR measurement is used to evaluate the barrier performance.

Petitioner Samsung Ex-1009, 0100

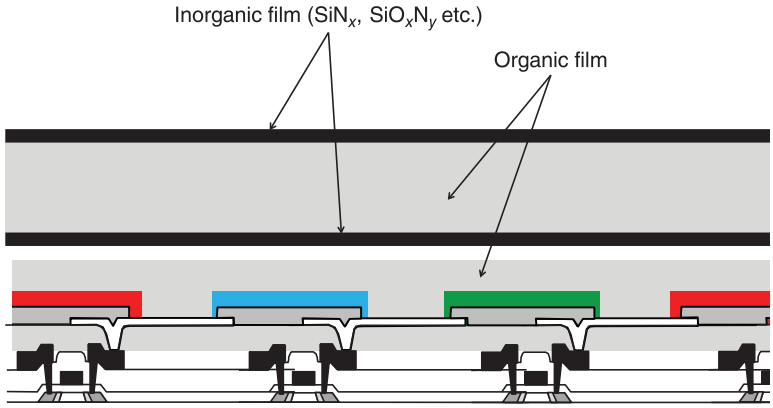


Figure 3.33 Schematic representation of film encapsulation by inorganic–organic repetition.

3.3.5.1 Thin-Film Encapsulation

Inorganic films, such as SiN_x or SiN_xO_y, are known to protect OLED devices from moisture and oxygen. (In the case of triplet emission, exciton is susceptible to quenching by oxygen's triplet state, as discussed in Section 2.4.2.) However, the inorganic films for barrier purpose usually have pinholes, which leak the moisture and oxygen. To circumvent the situation, alternate deposition of inorganic and organic films (Figure 3.33) is often used.

Organic films tend to have good step coverage but poor protection capability against humidity. On the other hand, inorganic film tends to have poor step coverage but shows great barrier property when it once covers. As such, organic/inorganic film repetition can achieve good barrier performance despite the existence of pinholes [18].

Prins et al. made a modeling of humidity penetration through barrier film pinholes [19]. With organic/inorganic repetition structure, organic layer does not block the humidity/oxygen penetration. Inorganic layer basically blocks the humidity/oxygen penetration, but pinholes in inorganic layer leak the moisture/oxygen. As pinholes of different inorganic layers exist in different locations, the humidity/oxygen needs to travel long distance until it gets out of the barrier film structure. Due to the long distance, the conductance of humidity/oxygen flux is suppressed and it enhances the barrier property. This is called "Labyrinth effect" or "Tortuous path effect."

The technique can also be applied to barrier film (discussed in Section 8.1.4), which is normally fabricated by depositing barrier layers on plastic film.

In most cases, the thin-film barrier layers are normally deposited by CVD (Figure 6.7), sputtering (Figure 6.7) or ion plating. Figures 3.34 and 3.35 show the SiO_2 film deposited on aluminum wiring with and without taper shape,

Petitioner Samsung Ex-1009, 0101

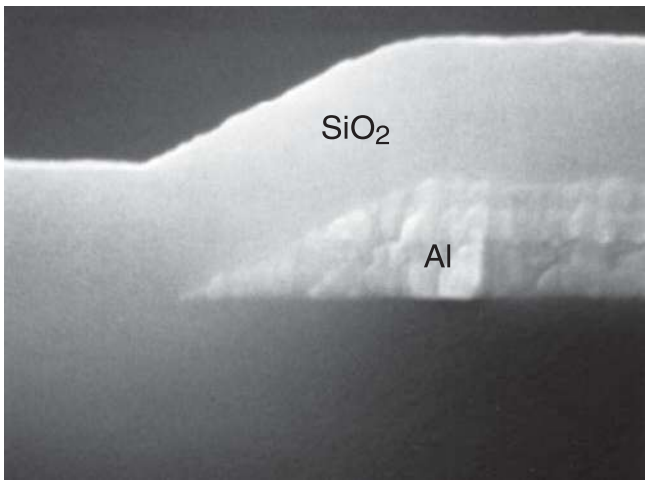


Figure 3.34 SiO_2 film deposited by CVD on tapered aluminum [20].

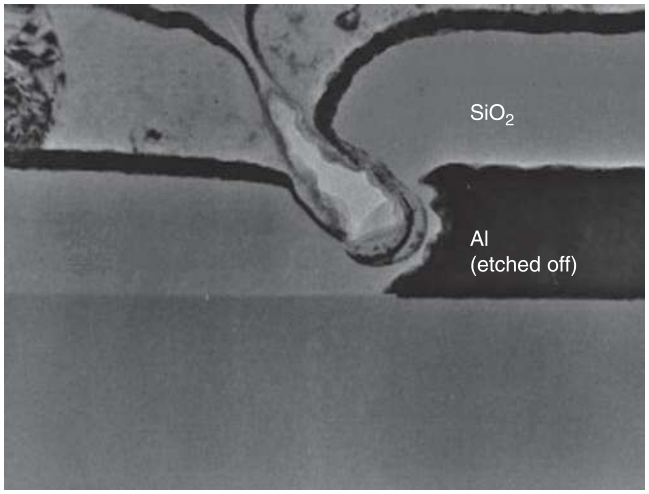


Figure 3.35 SiO_2 film deposited by CVD on nontapered aluminum [20].

respectively [20]. It can be clearly shown that the coverage of CVD SiO_2 film is not good enough when wiring is not tapered (Figure 3.35). Same situation can happen when film is deposited on a particle. If coverage is good enough, the particle can be covered so that the number of leakage path can be minimized. However, if the coverage is insufficient, water leakage path is created, which causes dark spot growth. It is known that normally CVD film coverage is better

Petitioner Samsung Ex-1009, 0102

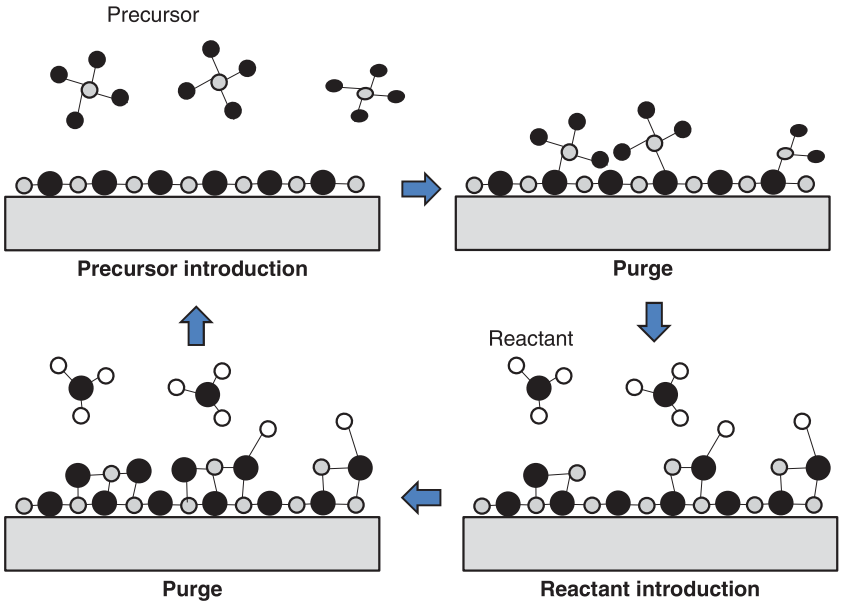


Figure 3.36 Schematic depiction of the reaction mechanism of the atomic layer deposition (ALD) method.

than that of film by sputtering method. Said that, even CVD does not provide perfect coverage over particles.

To improve the coverage issue on a particle, ALD (atomic layer deposition) deposition is attracting attention.

Figure 3.36 illustrates the reaction mechanism of the ALD method. Following introduction of the precursor gas to the film, the monolayer molecule is adsorbed. After the precursor gas is purged by the pump, reactant gas is introduced that reacts with reactant adsorbed precursor to form a monolayer film. This two-step procedure is repeated to form a high-quality film. As the interaction happens even beneath the particle, ALD deposition can make very good coverage happen on a particle even with very thin layer. Although this method yields high-quality film, the deposition rate obtained using the ALD method is low. To circumvent this issue, parallel processing of the ALD method, such as batch processing, can be used. To further improve the productivity, a high-speed ALD method termed *spatial ALD* (Figure 3.37) is attracting attention as a possible means of addressing this issue [21]. Spatial ALD uses a principle to transfer substrate on various gas flows so that the monolayer film is deposited sequentially. Spatial isolation of reactive gas enables layer-by-layer deposition without a time-consuming purging process,

Petitioner Samsung Ex-1009, 0103

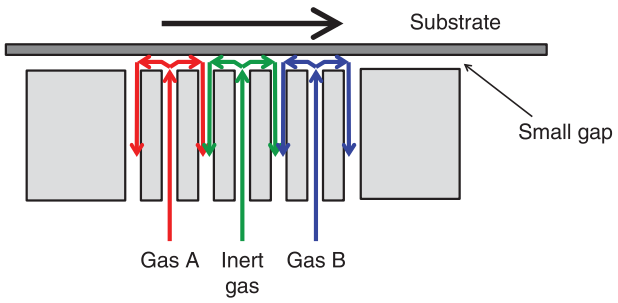
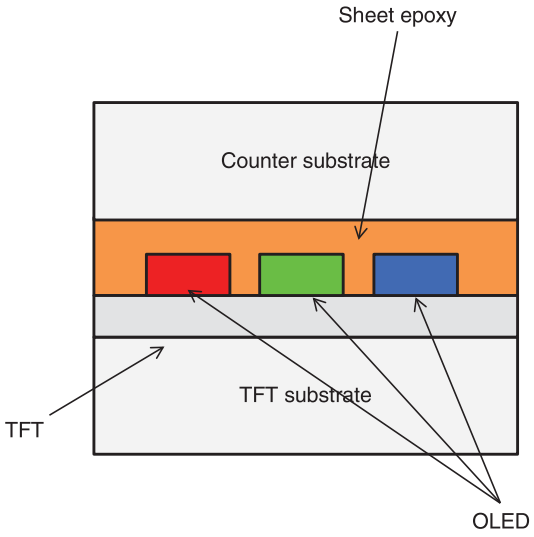


Figure 3.37 Schematic depiction of spatial ALD system.

Figure 3.38 An example of face sealing encapsulation structure (cross-sectional view).



which is necessary in the case of the normal ALD method. Therefore, spatial ALD offers both high productivity and high-quality film formation capability.

3.3.5.2 Face Sealing Encapsulation

The device in Figure 3.38 has counterplate and substrate sandwiching the OLED device and is glued together by the blanket sealing material. The structure is called "face sealing [22]." The face sealing does not have any cavity in its structure, so it very well matches with flexible OLED device. Also, as the display size becomes larger, it becomes difficult to sustain the counterplate by peripheral structure. In such cases, face sealing technology can bring mechanically robust feature.

Petitioner Samsung Ex-1009, 0104

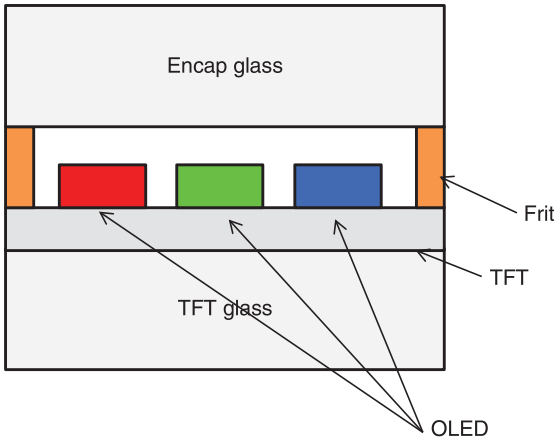


Figure 3.39 An example of face-frit encapsulation structure (cross-sectional view).

Sheet adhesive or "Dam-fill" structure (hermetic adhesive + filling material) is used for this purpose.

3.3.5.3 Frit Encapsulation

Figure 3.39 shows the frit sealing structure [23]. Glass frit, with 8–20 μ height and 0.5–5.0 mm width, is dispensed on the cover glass as shown in the left side of Figure 3.40. Then, cover glass is attached on the OLED substrate and the frit portion is cured by moving laser irradiation. The frit glass reaches softening point by laser and is cooled down to make hermetic sealing of the device.

With frit sealing method, frit hermetic seal basically has very high barrier property, so very long reliability can be obtained for glass-substrate-based OLED devices.

3.3.5.4 WVTR Measurement

As discussed, a barrier layer for an OLED needs to provide a high protection capability against moisture and oxygen. Therefore, it is important to estimate the permeability of the device to ensure the OLED display product's lifetime. The most frequently used method to estimate the barrier property is the calcium test (Figure 3.41). Calcium is reactive to water and oxygen. These reactions transform calcium, an opaque electrically conductive metal, to CaO or $Ca(OH)_2$, a transparent insulator, which can be measured optically and electrically so that the vapor transmission across the barrier layer can be estimated [24].

Though the calcium test can be applied very easily and gives good accuracy, it does not discriminate between oxygen and water permeation. To

Petitioner Samsung Ex-1009, 0105

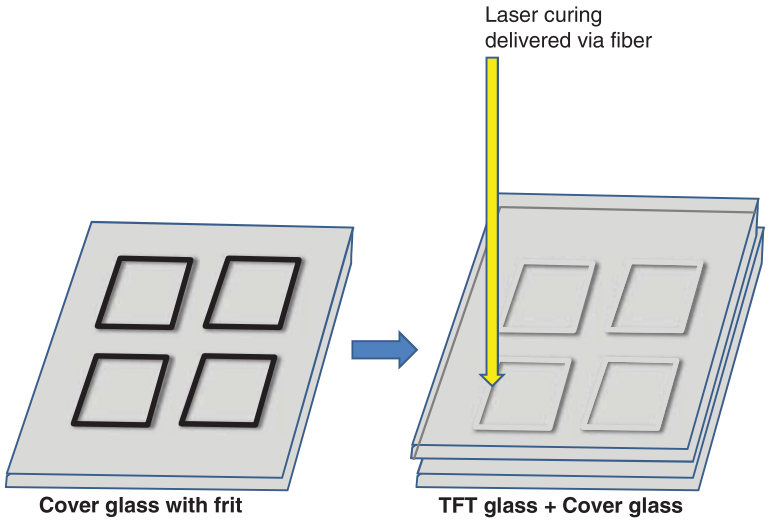


Figure 3.40 Examples of frit sealing encapsulation structure (bird's-eye view).

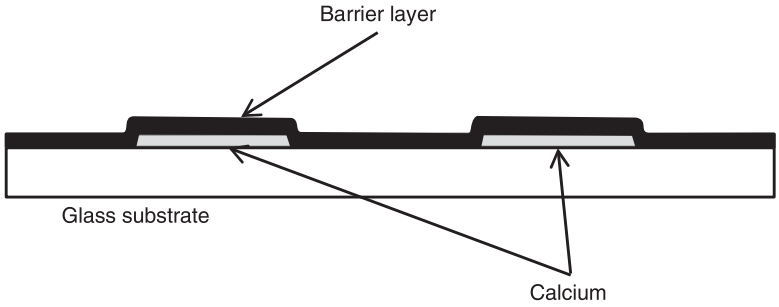


Figure 3.41 An example of sample structure for the calcium test.

get independent information about oxygen and water permeability, barrier property measurements are made using a vacuum system. Figure 3.42 shows the equipment used for the so-called Mocon method, for humidity transmittance measurement. Hundred percent humidity and low-humidity areas are separated by the barrier substrate, and the humidity transmitted through the barrier layer is detected by mass spectrometry. The detection limit of oxygen transmission is around 1×10^{-6} g/m^2·day with this method; however, it is hard to achieve a similar detection limit for water vapor transmission by the same method [24]. To make a better WVTR barrier property

Petitioner Samsung Ex-1009, 0106

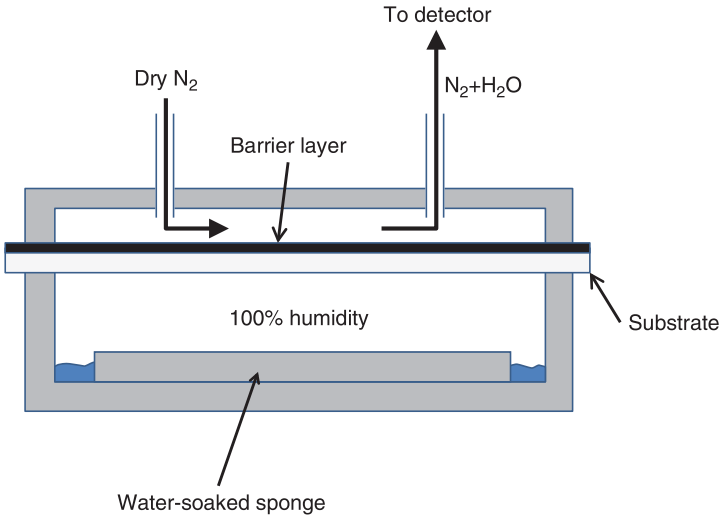


Figure 3.42 Equipment for the Mocon method of humidity permeation measurement [25].

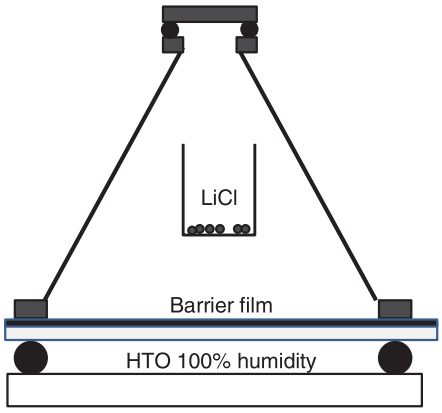


Figure 3.43 An example of HTO humidity measurement [26].

determination, the hydrogen–tritium–oxygen (HTO) method can be used. The HTO measurement uses similar equipment to the Mocon method but uses different moisture source and detector. The method uses HTO as the source of tritium and measures the tritium transmission rate (TTR). Figure 3.43 shows an example of barrier property measurement. The tritium transmitted through the barrier film is absorbed by LiCl. The LiCl is then dissolved in a scintillation cocktail, such as Perkin Elmer Ultima Gold LLT, and is measured by a scintillation counter [27]. The detection limit of the HTO method is below 1×10^{-6} g/m^2·day and is suitable for use in barrier property measurement for OLED devices.

Petitioner Samsung Ex-1009, 0107

3.4 PROBLEM ANALYSIS

When the properties of an OLED device seem to be defective, it is necessary to analyze the components of the device itself or the material remaining in the crucible to determine the cause of the problem. Methods used to troubleshoot and analyze the problem are discussed in the following sections.

3.4.1 Ionization Potential Measurement

As discussed in Section 2.3.6, it is very important to match the electrode workfunction to the energy level of organic materials (HOMO and LUMO) to obtain high efficiency and low-voltage emission of the OLED device. An ionization potential analyzer is used for this purpose.

An ionization potential analyzer measures the relationship between the wavenumber of incident UV light and the number of photoelectrons that are emitted from the sample surface under this irradiation. The x-intercept of this relationship gives the workfunction (i.e., the minimum energy required to move an electron to a point at infinity; see Figure 3.44) and the semiconductor's ionization potential (the energy required to remove an electron to form an ion, also called *ionization energy*).

In the case of a metal, when the UV light energy is lower than the workfunction energy, no photoelectrons are emitted, and when it is higher, photoelectrons are emitted. A semiconductor behaves similarly; only when the energy of UV light is higher than the ionization potential are photoelectrons emitted. Thus, an energy potential analyzer measures the workfunction and ionization potential by these procedures.

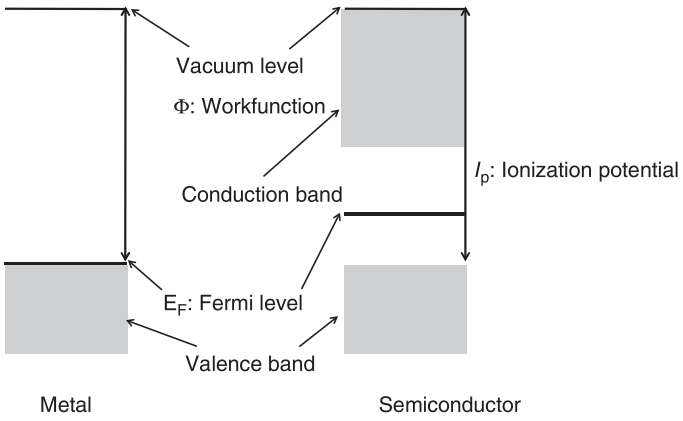


Figure 3.44 Schematic representation of workfunction and ionization potential.

Petitioner Samsung Ex-1009, 0108

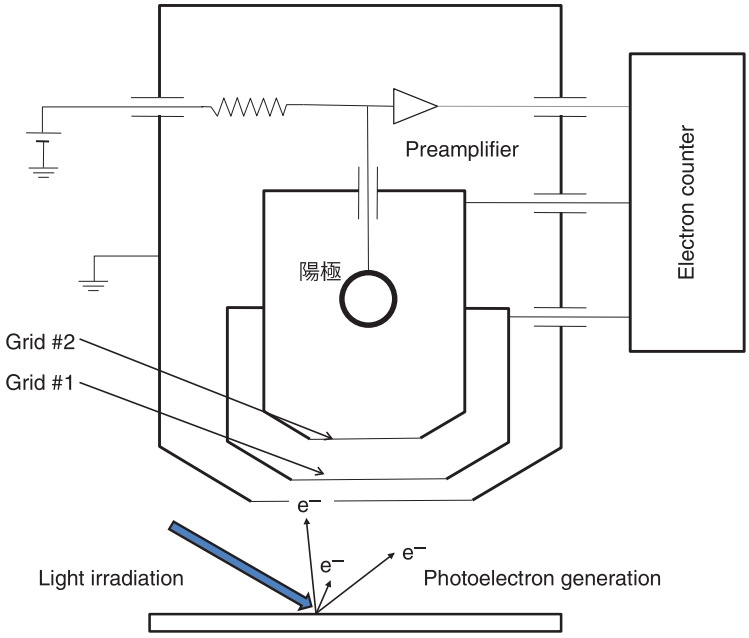


Figure 3.45 Schematic representation of operating principle of an ionization potential analyzer.

In the ionization potential analyzer shown in Figure 3.45, electrons emitted by the photoelectron effect due to UV light irradiation are captured by an oxygen molecule during their travel to the grid. Those electrons arrive at the anode after passing grids 1 and 2. When an ion approaches the anode, an electron avalanche occurs due to the presence of a strong electric field; one electron is amplified to approximately 10^5–10^7, and the discharge signal is provided to the preamplifier.

The number of electrons emitted depends on the energy of the irradiated light (Figure 3.46). The intercept of the graph in Figure 3.46 indicates the work-function, and for the semiconductor, it gives the ionization potential, namely, HOMO energy level. This method is called photoemission spectroscopy (PES).

When an OLED device exhibits characteristics of fluctuation, or when a fabricated device does not manifest its intended characteristics, energy level measurement of the electrode and organic materials is very useful and sometimes leads to solution of the problem.

3.4.2 Electron Affinity Measurement

As discussed in Section 3.4.1, HOMO level can be measured using PES. However, it was not very easy to measure LUMO level until recently. To obtain LUMO level, three methods are reported [28].

Petitioner Samsung Ex-1009, 0109

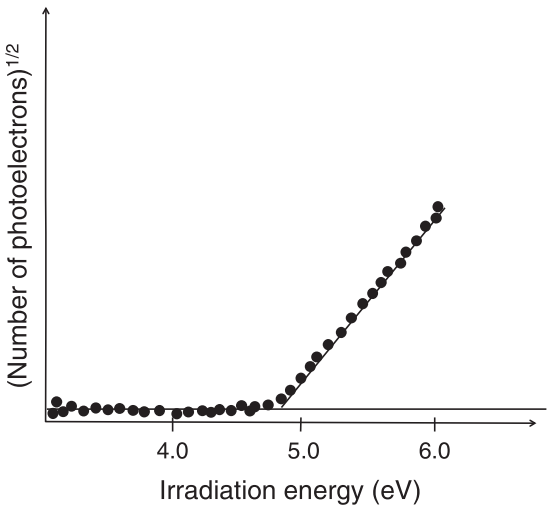


Figure 3.46 Graphical example of ionization potential analyzer measurement.

1. Reduction potential measurement by cyclic voltammetry (CV) method
2. Adding optical bandgap value to the HOMO level, which is measured by PES method
3. Inverse PES (IPES).

There were pros and cons for each measurement. CV method is carried out in solution, so it may not show accurate values. The second method can be carried out in solid phase; however, the optical bandgap measured by light absorption is often smaller than actual energy gap for an exciton.

IPES is an inverse process of PES method. PES method (Section 3.4.1) irradiates light onto the material and measure the outgoing electron. IPES process injects electron onto the sample and measures outgoing light. It can be carried out in solid phase. However, there are two major issues: measurement resolution and sample damage because the cross section of IPES is lower than that of PES by several orders of magnitude. Yoshida's method in *Chemical Physics Letters* [29] used low-energy electron; as a result, sample damage was avoided and also the resolution was dramatically improved because the outgoing light of Yoshida's method is near ultraviolet, different from the conventional IPES case, which used vacuum ultraviolet.

Due to the improvement of IPES method, direct LUMO level measurement has become possible without sample damage.

3.4.3 HPLC Analysis

High-performance liquid chromatography (HPLC; also called *high-speed liquid chromatography*) is frequently used to analyze impurities in OLED evaporation material and any residue material remaining in the crucible.

Petitioner Samsung Ex-1009, 0110

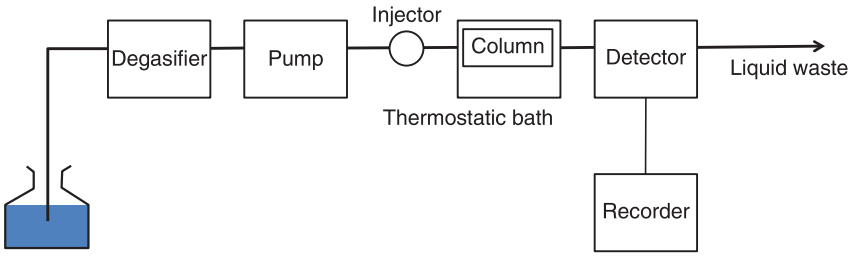


Figure 3.47 Flowchart of HPLC analysis equipment.

Figure 3.47 shows the equipment used for HPLC analysis. The typical components are a degasser, a pump, an injector, a thermostatic bath, a column, a detector, and a recorder.

First, the carrier solvent is transferred to the equipment from the carrier solvent bottle by a pump. (If pump pulsing occurs, a damper is sometimes used.) A degasser is necessary, as the presence of gases such as oxygen in the carrier solvent causes noise during detection when it is delivered to the equipment by a pump.

Next, liquefied samples are prepared for analysis by means of syringe injection and are delivered to the column. In the column, the samples are separated by partition between the flowing solvent and fine particles (e.g., 3–15 μm) of a stationary phase (often referred to as a gel; e.g., silica gel, polymer [polystyrene, polymethylmethacrylate, polyhydroxyethylmethacrylate, polyvinylalcohol, etc.] gel) supported in a stainless steel tube. As the separation process of the sample material is sensitive to temperature variation, the column is maintained in a thermostatic bath. The electrical signals provided by the detector after the separation process are detected and recorded (by the detector and recorder components, as shown in Figure 3.47).

There are many types of columns, such as reversed-phase columns, normal-phase columns, ion exchange columns, ligand exchange columns, ion exclusion columns, gas frontal chromatography (GFC) columns, and gel permeation chromatography (GPC) columns [30].

3.4.4 Cyclic Voltammetry

The cyclic voltammetry (CV) method, which measures potential and electric current simultaneously, is useful for analyzing electrochemical reactions by determining parameters such as electron transfer speed, reversibility, and chemical dissociation during reaction. Figure 3.48a shows a typical voltage sweep example for the measurement, and Figure 3.48b shows the corresponding electric current–voltage curve (cyclic voltammogram).

The electrode potential is controlled to ensure that the electrode is swept from a voltage higher than that of the oxidation–reduction potential to a lower

Petitioner Samsung Ex-1009, 0111

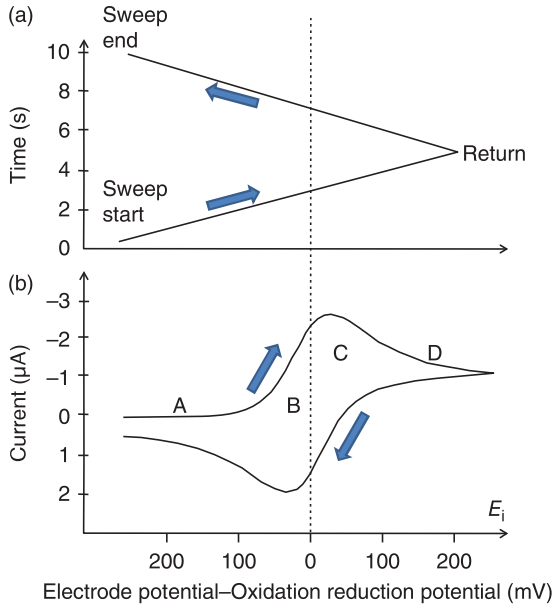


Figure 3.48 Schematic example of a cyclic voltammogram.

voltage and then swept back to the higher voltage again (see Figure 3.48a). In region *A*, there is almost no material to be oxidized, so the electric current is almost zero. In region *B*, the system undergoes reduction, so the electrons move toward the oxide, and the electric current thus rapidly increases.

In region *C*, when the voltage is slightly under the oxidation–reduction potential, the material near the electrode is almost completely reduced, so reduction no longer takes place, and the electric current starts to decrease. Gradually, the electric current created by reduction of material close to the electrode decreases, and the electric current is limited by reduction of material diffusing to the electrode from the bulk of the solution.

If the reduced material is stable, then when the voltage is swept from a lower value to a voltage higher than that of the oxidation–reduction potential, a reverse reaction takes place and the current–voltage curve shows complete charge symmetry; however, when the system is irreversible, a nonsymmetric *I–V* curve is created.

In some cases, this type of sweep is measured repeatedly. Also, dependence of the *I–V* curve on sweep speed is measured to enable analysis of the electron transfer mechanism in the submicrosecond range. This method provides information on the change in molecular structure with respect to electron transfer and electron mobility.

During the OLED operation, there occur surplus electrons or holes in the device system, which causes reduction or oxidation stress to organic molecules. To avoid such stress to cause reliability issue, tolerant molecule against such

Petitioner Samsung Ex-1009, 0112

stress must be chosen. CV provides important insights to check such tolerance of molecules.

References

1 S. Son, S.-H. Yoon, J.-G. Jang, M.-S. Kang, and S.-Y. Jeon, Pure aluminum metal as an anode for high performance OLEDs, *SID 2004 Digest*, p. 52 (2004).

2 T. Yamada, T. Yoshimotod, and G. Ono, Organic EL devices using a novel hole-injection material, *Eurodisplay* 2002, p. 847 (**2002**).

3 J. Blochwitz, M. Pfeiffer, T. Fritz, and K. Leo, Low voltage organic light emitting diodes featuring doped phthalocyanine as hole transport material, *Appl. Phys. Lett.* **73**(6):729 (1998).

4 C. Adachi, M. A. Baldo, S. R. Forrest, and M. E. Thompson, Blue electroluminescence from phosphorescent benzoxazole doped OLEDs, *Proc. Materials Research Society* (1999 fall meeting), p. 12 (1999).

5 C. T. Brown, B. Owczarczyk, T. K. Hatwar, and D. Kondakov, High efficiency red emitting electroluminescent devices with exceptional stability, *IDRC 2003 Digest*, p. 42 (2003).

6 S. R. Forrest, M. A. Baldo, J. J. Brown, B. D'Andrade, Y. Kawamura, R. Kwong, M. E. Thompson, and S. Yanagida, Electrophosphorescent organic light emitting devices, *SID 2002 Digest*, p. 1357 (2002).

7 T. Nakayama, K. Hiyama, K. Furukawa, and H. Ohtani, Development of phosphorescent white OLED with extremely high power efficiency and long lifetime, *SID 2007 Digest*, p. 1018 (2007).

8 T. Tsuji, S. Kawakami, S. Miyaguchi, T. Naijo, T. Yuki, S. Matsuo, and H. Miyazaki, Red-phosphorescent OLEDs employing bis(8-quinolinolato)-phenolato-aluminum(III) complexes as emission-layer hosts, *SID 2004 Digest*, p. 900 (2004).

9 T. Tominaga, paper presented at 87th spring meeting, The Chemical Society of Japan, 2007, 1B1-38.

10 H. Kanno, Y. Hamada, K. Nishimura, K. Okumono, N. Saito, K. Mameno, and K. Shibata, Reduction in power consumption for full-color active matrix organic light-emitting devices, *Jpn. J. Appl. Phys.* **45**:L947–L950 (2006).

11 M. Ichikawa, T. Kawaguchi, K. Kobayashi, T. Miki, T. Obara, K. Furukawa, T. Koyama, and Y. Taniguchi, Bipyridyl oxadiazoles as a new class of durable and efficient electron-transporting materials, *SID 2005 Digest*, p. 1652 (2002).

12 T. Tohma, S. Yamazaki, and D. Wzorek, The future of active-matrix organic LEDs, *Information Display*, p. 20 (2001).

Petitioner Samsung Ex-1009, 0113

13 S. Van Slyke, A. Pignata, D. Freeman, N. Redden, D. Waters, H. Kikuchi, T. Negishi, H. Kanno, Y. Nishio, and M. Nakai, Linear source deposition of organic layers for full-color OLED, *SID 2002 Digest*, p. 886 (2002).

14 J. W. Hamer, A. Yamamoto, G. Rajeswaran, and S. A. Van Slyke, Mass production of full-color AMOLED displays, *SID 2005 Digest*, p. 1902 (2005).

15 S. F. Lim, L. Ke, W. Wang, and S. J. Chua, Correlation between dark spot growth and pinhole size in organic light-emitting diodes, *Appl. Phys. Lett.* **78**(15):2116 (2001).

16 Y.-F. Liew, H. Aziz, N.-X. Hu, H. S.-O. Chan, G. Xu, and Z. Popovic, Investigation of the sites of dark spots in organic light-emitting devices, *Appl. Phys. Lett.* **77**(17):2650 (2000).

17 M. Schaer, F. Nüesch, D. Berner, W. Leo, and L. Zuppiroli, Water vapor and oxygen degradation mechanisms in organic light emitting diodes, *Adv. Funct. Mater.* **11**(2) (2001).

18 G. Nisato, M. Bouten, L. Moro, O. Philips, and N. Rutherford, Thin film encapsulation for OLEDs: evaluation of multi-layer barriers using the Ca test, *SID 2003 Digest*, p. 88 (2003).

19 W. Prins, J. J. Hermans, *J. Phys. Chem.* **63**:716 (1959).

20 T. Tsujimura and T. Miyamoto, Wire breakdown method for evaluating metal taper shape, International Display Workshop 1997 Digest, p. 219 (1997).

21 D. H. Levy, S. F. Nelson, and D. Freeman, Oxide electronics by spatial atomic layer deposition, *IEEE/OSA J. Display Technol.* **5**(12):484–494 (2009).

22 S. Hong, C. Jeon, S. Song, J. Kim, J. Lee, D. Kim, S. Jeong, H. Nam, J. Lee, W. Yang, S. Park, Y. Tak, J. Ryu, C. Kim, B. Ahn and S. Yeo, Development of commercial flexible AMOLEDs, *SID 2014 Digest*, Vol. 38, Issue 1, pp.1701–1704 (2014).

23 L. Zhang, S. Logunov, K. Becken, M. Donovan, and B. Vaddi, Impacts of glass substrate and frit properties on sealing for OLED lighting, *SID 2010 Digest*, Vol. 41, Issue 1, pp. 1890–1893 (2010).

24 J.-S. Park, H. Chae, H. K. Chung, and S. I. Lee, Thin film encapsulation for flexible AM-OLED: a review, *Semiconductor Science and Technology* **26**(034001):1 (2011).

25 F. McCormick, Barrier Films & Device Encapsulation, Council for Chemical Research OLED Materials for Lighting and Displays Workshop Session 4 (2011).

26 M. D. Groner, S. M. George, R. S. McLean, and P. F. Carcia, Gas diffusion barriers on polymers using Al_2O_3 atomic layer deposition, *Appl. Phys. Lett.* **88**(051907):88 (2006).

27 A. A. Dameron, S. D. Davidson, B. B. Burton, P. F. Carcia, R. S. McLean, and S. M. George, Gas diffusion barriers on polymers using multiple layers fabricated by Al_2O_3 and rapid SiO_2 atomic layer deposition, *J. Phys. Chem. C* **112**:4573–4580 (2008).

Petitioner Samsung Ex-1009, 0114

28 H. Yoshida and K. Yoshizaki, Electron affinities of organic materials used for organic light emitting diodes: a low-energy inverse photoemission study, *Org. Electron.* **20**, 24 (2015).
29 H. Yoshida, Near-ultraviolet inverse photoemission spectroscopy using ultra-low energy electrons, *Chem. Phys. Lett.* **539–540**, 180–185 (2012).
30 S. Denko, Distribution measurement and analysis of additives by GPC solvent separation column. *Shodex Chromato News* **70** (1998).

Petitioner Samsung Ex-1009, 0115

4

OLED Display Module

4.1 COMPARISON BETWEEN OLED AND LCD MODULES

Figure 4.1 compares the components that are necessary for production of liquid crystal display (LCD) and OLED display modules.

An LCD consists of many components because it must convert backlight emission to uniform area emission and switch on and off the light with a liquid crystal shutter, which is positioned between two polarizers.

A typical LCD uses multiple LEDs or a cold-cathode fluorescent tube (CCFL). Two types of LED are used: (1) that emits short wavelength emission, which is converted to longer wavelengths by means of a fluorescent material (downconversion) and (2) that emits the three color primaries (red–green–blue [RGB]). Thus, the light source for an LCD is either linear (fluorescent tube) or point, so the light must be converted to the area form to be used as a backlight unit. The light reflected by the reflector passes through the light guide and is diffused. A light guide is made of high refractive index material, such as an acrylic polymer, which delivers the light by total internal reflection due to the refractive index difference between it and the surrounding air. The light guide structure is designed such that uniform luminance distribution across the area of the display can be achieved. Light exiting from the light guide is transmitted through the prism sheet and diffuser and is then polarized by the rear polarizer. The polarization state of the light is altered by the birefringent LC layer and controlled by the voltage applied to it. The RGB components of the light are selected by a color filter aligned with the primary color subpixels of the display, and the exit polarizer transmits the required intensity of light—according to its polarization—toward the viewer.

In OLED displays, light emission takes place in an OLED device fabricated on the surface of a glass substrate. When the display is observed in a bright environment, the reflection from the display surface causes deterioration of

OLED Display Fundamentals and Applications, Second Edition. Takatoshi Tsujimura.
© 2017 John Wiley & Sons, Inc. Published 2017 by John Wiley & Sons, Inc.

Petitioner Samsung Ex-1009, 0116

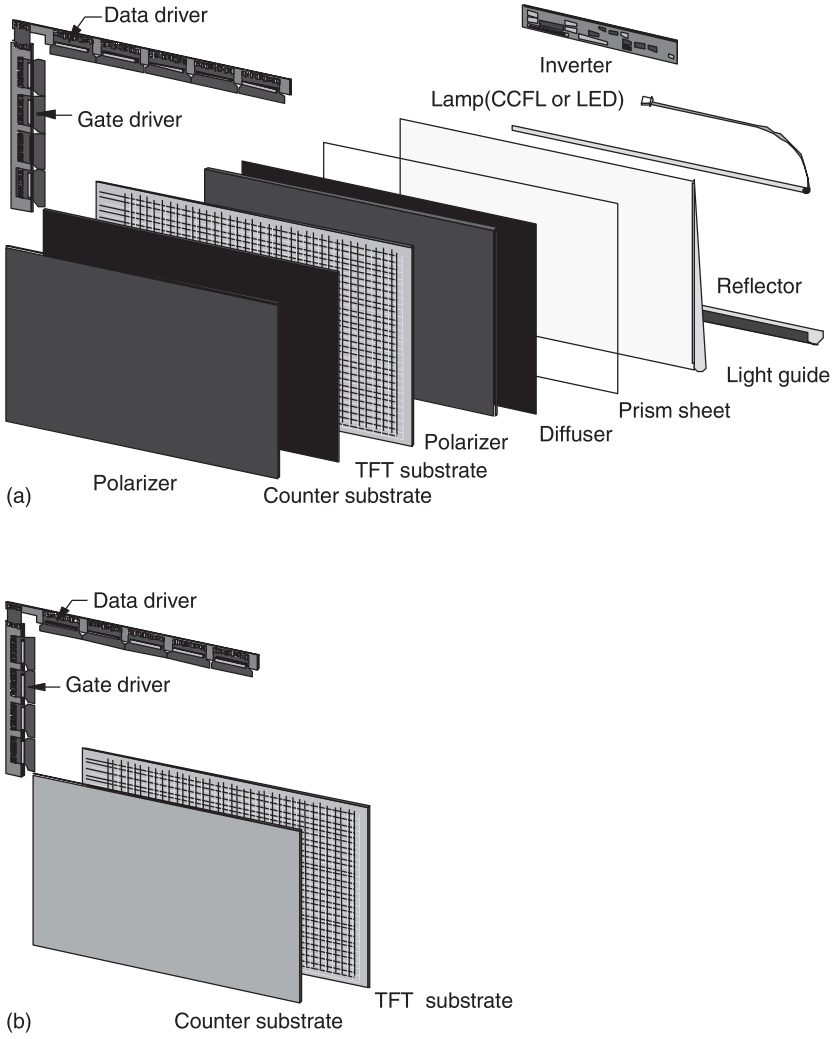


Figure 4.1 Examples of display components used in LCD (a) and OLED (b) television sets.

the contrast ratio, so a circular polarizer is often used (see Section 4.4.3 for further details), which reduces the luminance of the display by about 50%. For example, a 45% transmittance polarizer is sometimes used. LCDs also have an ambient light reflection problem. In an LCD, a black matrix is used to enhance the ambient contrast ratio. Generally, the reflection is more serious in the case of OLED because reflective electrode is used for OLED when transmissive LCD uses transparent electrode for both sides.

Petitioner Samsung Ex-1009, 0117

In all cases, OLED displays require fewer components than LCDs. O'Regan et al. [1] report the cost structure comparison between LCD and OLED. The paper ascribes the major reason of OLED's high cost to the low material utilization, which is typically 5% by evaporation methods. Even assuming a significantly higher cost of TFT backplane and driver IC than LCDs and also assuming a lower yield of OLED than LCD by 10–20%, the total cost of OLED would become 30% cheaper if a high material utilization processing technique is used, such as a solution-based technique. Recently, it was reported by a display research company that 5-in. full-HD AMOLED display cost became lower compared to that of a similar LCD display [2]. OLED TV is also showing significant cost reduction these days due to yield improvement by white + color filter architecture and also due to the adoption of large mother glass size. It is reported that the display research company is expecting OLED TV to reach a premium of 10% over LCDs [3].

4.2 BASIC DISPLAY DESIGN AND RELATED CHARACTERISTICS

To design a high-quality display, many factors must be considered. Designers need to understand how intended specifications, such as luminance, color reproduction, and luminance uniformity, can be achieved through display design.

4.2.1 Luminous Intensity, Luminance, and Illuminance

The radiometric (energy) values taking spatial and temporal considerations into account are called radiant quantities, and radiometric values weighted by physiological functions related to the wavelength sensitivity of the eye (spectral luminous efficacy) are called photometric quantities. Luminous intensity, luminance, and illuminance are the most well-known photometric quantity units.

4.2.1.1 Luminous Intensity

Here we assume that the luminous flux from a point light source traverses the areas between dm_1 and dm_2 as shown in Figure 4.2. Let us assume that the luminous intensity values are P_1 and P_2. The luminous flux values Φ (in lumens [lm]) of areas dm_1 and dm_2 are the same:

$$d\Phi = P_1\, dm_1 = P_2\, dm_2 \tag{4.1}$$

If the solid angle is $d\omega$, then the luminous flux per unit solid angle P is

$$P = \frac{d\Phi}{d\omega} \tag{4.2}$$

This parameter is called *luminous intensity*, measured in cd (candelas) = lm/sr (where sr is steradian, the unit for solid-angle measurement).

Petitioner Samsung Ex-1009, 0118

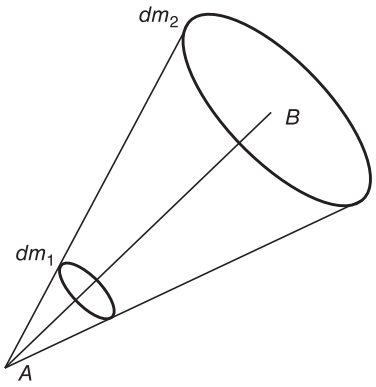


Figure 4.2 Relationship between luminous flux and luminous intensity.

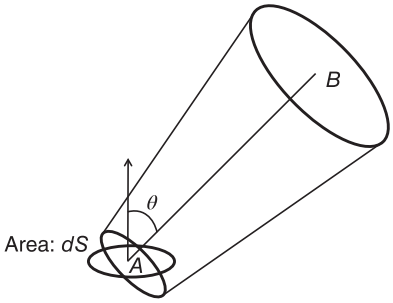


Figure 4.3 Relationship between luminous flux and luminance of an area light source.

4.2.1.2 Luminance

Luminous intensity can be measured in terms of a point light source, but measurement of an area light source requires another metric. As an area light source can be quantified as a multipoint light source, the luminous flux of an area light source is much larger than that of a point light source. The luminous intensity of the area light source is called *luminance*, and the measurement unit is $\mathrm{cd/m^2} = \mathrm{lm/(sr \cdot m^2)}$. ($\mathrm{cd/m^2}$ is sometimes called "nit," but it is not an officially acknowledged unit name.) As shown in Figure 4.3, when the angle between the normal line of face A and the A–B line is θ, the area of face A is regarded as $dS \cos\theta$ from the location on line A–B, so the luminance L can be expressed as follows:

$$L = \frac{dP}{dS \cos\theta} \tag{4.3}$$

Here, using 4.2, we obtain

$$L = \frac{d\Phi}{dS \cos\theta \, d\omega} \tag{4.4}$$

It should be noted that the luminance and the brightness are not the same (discussed in Section 4.2.1.5).

Petitioner Samsung Ex-1009, 0119

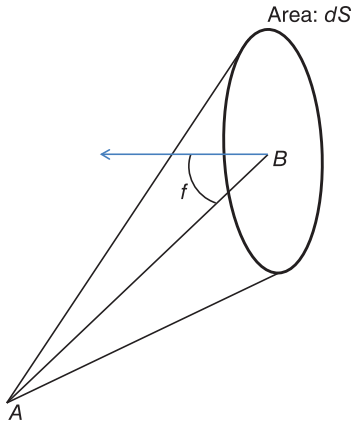


Figure 4.4 Relationship between luminous flux and illuminance of point light.

4.2.1.3 Illuminance

In Section 4.2.1.2, we noted that the luminous flux emitted per unit solid angle is called *luminous intensity*. Similarly, the luminous flux incident per unit area is called *illuminance*, and the measurement unit is lux (lx) (1 lx = 1 lm/m^2). We can use the same equation (Eq. 4.4) to calculate the *luminous exitance*, which is the luminous flux that exits from the source per unit area.

Illuminance E (luminous exitance) can be expressed as

$$E = \frac{d\Phi}{dS} \tag{4.5}$$

where, as shown in Figure 4.4, dS is the area on the incident face of luminous flux $d\Phi$.

Now let us consider how illuminance E of face B is defined. If the angle between face B and line A–B is ϕ, then the area of face B can be regarded as $dS \cos\phi$ from line A–B. If the distance between points A and B is d_{AB}, the solid angle $d\omega$ that is occupied by this space can be expressed as follows:

$$d\omega = \frac{dS\cos\phi}{d_{AB}^2} \tag{4.6}$$

For the point light source (Figure 4.4), using Eq. (4.2), we obtain

$$d\Phi = \frac{PdS\cos\phi}{d_{AB}^2} \tag{4.7}$$

Therefore, the illuminance E for a point light source is

$$E = \frac{d\Phi}{dS} = \frac{P\cos\phi}{d_{AB}^2} \tag{4.8}$$

Petitioner Samsung Ex-1009, 0120

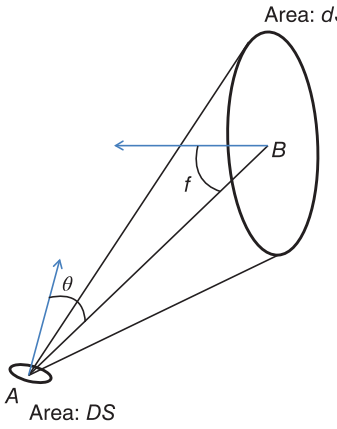


Figure 4.5 Relationship between luminous flux and illuminance of area light.

For the area light source (Figure 4.5), the area denoted by ΔS, the following formula can be derived using ΔS instead of dS in (Eq. 4.4):

$$\begin{aligned} d\Phi &= L\,\Delta S\cos\theta\, d\omega \\ &= \frac{L\,\Delta S\cos\theta\, dS\cos\phi}{d_{AB}^2} \end{aligned} \tag{4.9}$$

Therefore, the illuminance of an area light source is

$$\begin{aligned} E &= \frac{d\Phi}{dS} \\ &= \frac{L\,\Delta S\cos\theta\cos\phi}{d_{AB}^2}. \end{aligned} \tag{4.10}$$

Illuminance is the parameter used to quantify the brightness of an environment.

4.2.1.4 Metrics Summary

The four quantities discussed in the preceding section can be summarized as follows:

- *Luminous flux* is the psychophysical (in terms of spectral sensitivity of observers' eyes) visible light intensity per unit time, emitted by a light source.
- *Luminous intensity* is the luminous flux emitted per unit solid angle.
- *Luminance* is the luminous flux per unit solid angle emitted per unit area as projected on a plane normal to the line of sight.
- *Illuminance* is the luminous flux incident per unit area on a surface.

The equations and units used to calculate these quantities are summarized in Table 4.1.

Petitioner Samsung Ex-1009, 0121

Table 4.1 Summary of Photometric Parameters

Parameter	Quantification Equation	Unit
Luminous flux	$\Phi = \frac{dQ}{dt}$	Lumen (lm)
Luminous intensity	$P = \frac{d\phi}{d\omega}$	Candela = lumen/steradian (cd = lm/sr)
Luminance	$L = \frac{d\Phi}{dS\cos\theta\, d\omega}$	Candela per square meter = lumen per steradian per square meter ($cd/m^2 = lm/[sr \cdot m^2]$)
Illuminance	$E = \frac{d\Phi}{dS}$	Lux ($lx = lm/m^2$)

The steradian (sr) is the unit for determining solid angle. (A steradian means the solid angle that occupies the area equal to the square of the spheric radius, on the sphere surface. The solid angle for a full sphere is 4π.) When the surface reflection of a specific display is discussed, illuminance and luminance are often compared to calculate the contrast ratio in a lit environment as follows.

If perfect diffusion is assumed for surface A, illuminance at point B can be expressed as

$$E_B = \frac{dI(\theta)\cdot\cos^2\theta}{(2r\cdot\cos\theta)^2} = \frac{dI(\theta)}{4r^2}$$

As the illuminance is uniform at all points on the surface of the circle with radius r, total luminous flux can be calculated as

$$\Phi = \frac{I_0\cdot 4\pi r^2}{4r^2} = \pi\cdot I_0$$

As surface A is perfectly diffusive, luminance of reflective light on surface A can be described as

$$L_{\text{perfect}} = \frac{E}{\pi}$$

E is the illuminance on surface A.

If reflectivity of surface A is K, this equation can be written as

$$L_{\text{reflection}} = \frac{K\cdot E}{\pi}$$

The living room contrast ratio, discussed in Section 4.4.3.1, can be calculated by

$$CR_{\text{livingroom}} = \frac{L_{\text{display}}}{L_{\text{reflection}}} = \frac{\pi\cdot L_{\text{display}}}{K\cdot E}$$

Petitioner Samsung Ex-1009, 0122

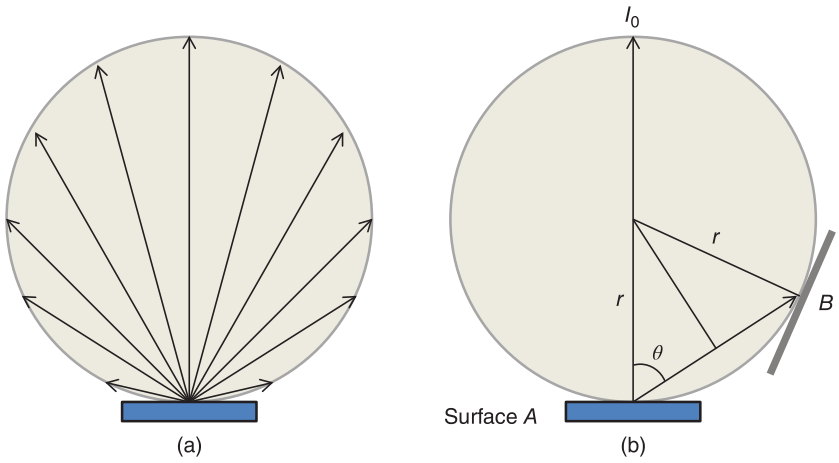


Figure 4.6 (a) Perfect diffusion surface; (b) incident light from a perfect diffusion surface. (Lambertian distribution.)

Normally, $E = 200$ (lx) is used for living room contrast ratio calculation. See Figure 4.6.

4.2.1.5 Helmholtz–Kohlrausch Effect

It is known that visual perception is subjected to the viewing condition. For example, when the colors are kept the same and the ambient light is changed, the perceived brightness and color change (Purkinje effect) [4]. Similarly, it has been reported that the characteristics of OLED display, such as high contrast and large color gamut, is affecting the perceived performance of the display.

It is known that perceived brightness is increased as the color is saturated. This is called Helmholtz–Kohlrausch effect (also called "H–K effect") [5, 6]. As many modern displays have a large color gamut, it can be perceived as brighter [7]. It is known that darker backgrounds makes human feel brighter (Bartle-son–Breneman effect [8]). Here, it should be noted that brightness and luminance have different meaning. Brightness is a subjective attribute of light, which human perceives. On the other hand, luminance is luminous intensity per unit area projected in a given direction. It is reported that, due to psychological effect, OLED display's brightness can be perceived 25% higher than LCDs with the same measured luminance [9].

4.2.2 OLED Current Efficiencies and Power Efficacies

When multiple OLED devices or OLED processes are compared or controlled, it is much easier to compare the efficiency metric than to compare actual measurement curves with many data points. The concepts of current efficiency and power efficacy (luminous efficacy) are discussed as follows.

Petitioner Samsung Ex-1009, 0123

(Readers should note that there is an ongoing discussion whether "efficiency" or "efficacy" should be used for this topic. Standardization committee, especially for lighting field, such as in IEC: International Electrotechnical Commission and in DOE: Department Of Energy, are promoting the use of "luminous efficacy." The main reason is that the word "efficiency" should be dimensionless and the word "efficacy" can carry the meaning of physiological quantity such as the eye response curve. "Current efficiency/efficacy" is also under discussion, but still no clear answer is yet. So, in this book, the author uses "luminous efficacy," "power efficacy," and "current efficiency" throughout.)

Let us assume monochromatic light first. The luminous flux $\Phi(\lambda)$ (measured in lm/m^2) at wavelength λ can be expressed as

$$\Phi(\lambda) = PK_{\mathrm{m}}y(\lambda) \tag{4.11}$$

where P is emission intensity (W/m^2), $y(\lambda)$ is the relative luminosity at wavelength λ, and K_{m} is the maximum luminosity factor 683 (lm/W). An actual emission has spectral width, so an integral that can be applied for all wavelengths is

$$\Phi(\lambda') = PK_{\mathrm{m}}y(\lambda')\frac{F(\lambda')}{\int F(\lambda)d\lambda} \tag{4.12}$$

Luminous flux Φ for all wavelengths can be calculated by integrating for all λ' as follows:

$$\Phi = PK_{\mathrm{m}}\frac{\int F(\lambda)y(\lambda)d\lambda}{\int F(\lambda)d\lambda} \tag{4.13}$$

Then the luminance L (cd/m^2) can be expressed as

$$L = \frac{\Phi}{\pi} \tag{4.14}$$

The power efficacy (lm/W; also called luminous efficacy) can be expressed as

$$\eta_{\mathrm{e}} = \frac{\Phi}{W} = \frac{PK_{\mathrm{m}}y(\lambda)}{S}\cdot\frac{S}{IV} = \frac{PK_{\mathrm{m}}y(\lambda)}{IV} \tag{4.15}$$

On the other hand, current efficiency η_{c} (cd/A) is defined as the luminance divided by the current density:

$$\eta_{\mathrm{c}} = \frac{L}{J} = \frac{PK_{\mathrm{m}}y(\lambda)}{\pi\cdot I} \tag{4.16}$$

An actual current–voltage (I–V) curve of an OLED device is illustrated in Figure 4.7, which shows that the electric current flows when the voltage is positive but does not when it is negative, which means that the OLED device

Petitioner Samsung Ex-1009, 0124

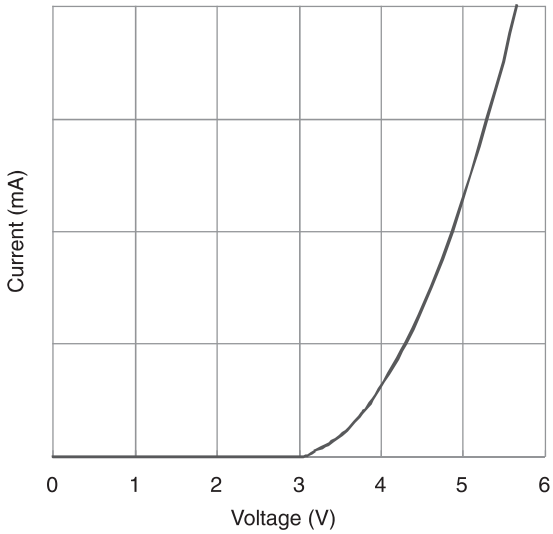


Figure 4.7 Example of a current–voltage curve of an OLED device.

exhibits diode characteristics. For nonuniformity compensation of a display (described in Section 6.4.4), many pixel circuitry requires to stop the OLED current flow while the threshold voltage of driver TFT is measured, so an additional TFT serially connected to OLED was used in the past. The diode feature of OLED can be utilized to remove the additional TFT, as it impedes the current flow of the driver TFT by applying negative voltage, which obstructs the detection of the driver TFT characteristic fluctuation to be compensated by a pixel circuitry.

A luminance–voltage curve is shown in Figure 4.8. This curve is also called the L–V curve. Similarly, luminance–current–voltage measurement is sometimes called L–I–V measurement. (It should be noted that L means luminance here, not inductance.)

As shown in Figure 4.9, the luminance is almost proportional to the electric current. The correlation between current efficiency and voltage is plotted in Figure 4.10. Thus, the efficiency is subjected to the voltage (due to concentration quenching, described in Section 2.4.2.4; densely generated excitons by larger current cause more chance of losing energy by collision to the quencher or other excitons), which needs to be taken into account in the display design. In particular, in the case of a phosphorescent device, collision between two triplet excitons causes quenching (as the high current generates many excitons by which many triplet excitons collide with each other to form a singlet state). This is called *triplet–triplet* (T–T) *annihilation* (discussed in Section 2.4.2.4), which can significantly reduce efficiency in the high-current region. This efficiency reduction is referred to as the *rolloff phenomenon*.

Petitioner Samsung Ex-1009, 0125

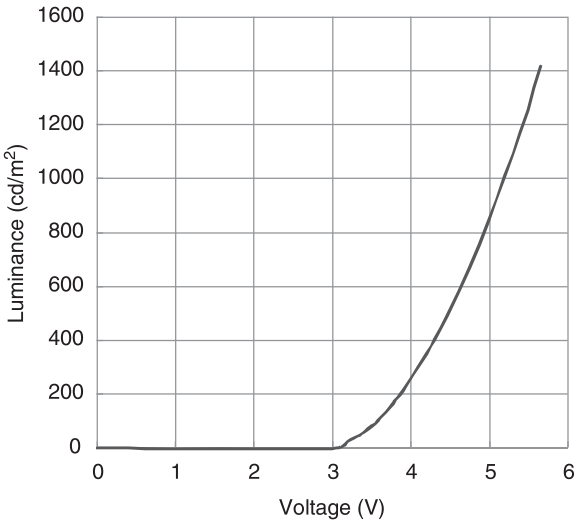


Figure 4.8 Example of a luminance–voltage curve of an OLED device.

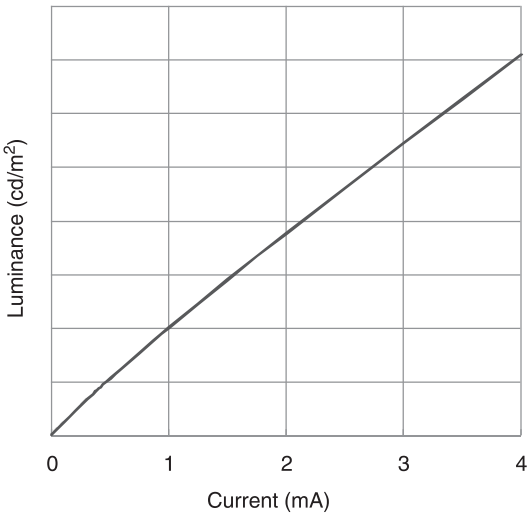


Figure 4.9 Example plot of luminance versus current.

4.2.3 Color Reproduction

Color reproduction is an important factor in ensuring color fidelity, especially for photo images. Large-scale color reproduction can be achieved by applying display schemes containing the primary colors red, green, and blue, as discussed below. Emission spectra of red, green, and blue subpixels are shown in Figure 4.11.

Here we assume that the emission spectrum is $S(\lambda)$ and the color matching functions (sensitivity of the human eye to each wavelength; see the appendix for

Petitioner Samsung Ex-1009, 0126

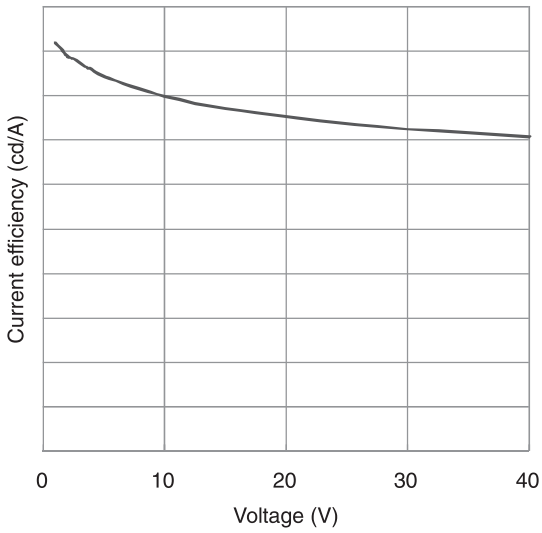


Figure 4.10 Graph showing dependence of voltage on current efficiency.

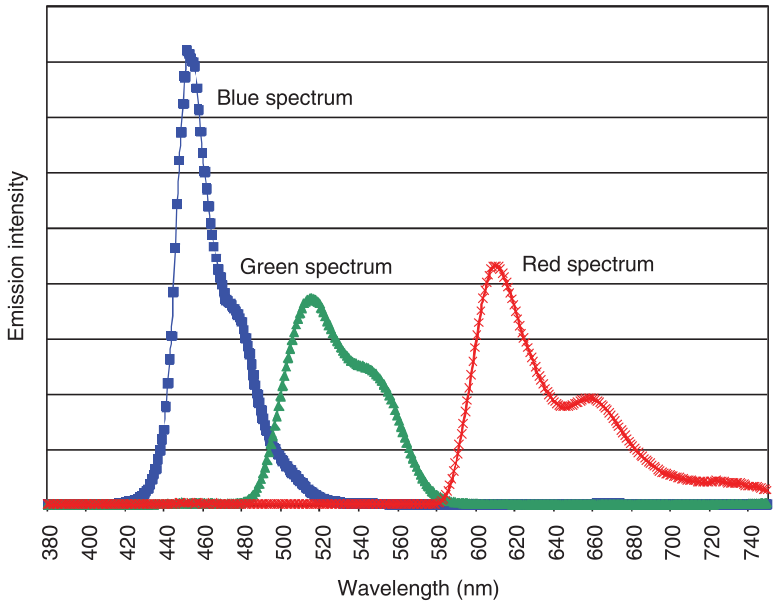


Figure 4.11 Example of emission spectrum of RGB (red+green+blue) subpixels.

Petitioner Samsung Ex-1009, 0127

actual values) are $\overline{x}(\lambda)$, $\overline{y}(\lambda)$, $\overline{z}(\lambda)$; we can then express the tristimulus values (a parameter set, derived from human eye responses to three color primaries, designed so that all weight factors are positive; standardized as the CIE1931 color space) as follows, using an integral ranging from 380 to 780 nm.

$$X = K\int_{380}^{780} S(\lambda)\overline{x}(\lambda)d\lambda \tag{4.17}$$

$$Y = K\int_{380}^{780} S(\lambda)\overline{y}(\lambda)d\lambda \tag{4.18}$$

$$Z = K\int_{380}^{780} S(\lambda)\overline{z}(\lambda)d\lambda \tag{4.19}$$

Here, we define the K so that calculated Y is equal to the display luminance.

Using the CIE1931-XYZ value, the (x, y) locus (generally used to indicate the display color reproduction capability) can be expressed as follows:

$$x = \frac{X}{X+Y+Z} \tag{4.20}$$

$$y = \frac{Y}{X+Y+Z} \tag{4.21}$$

This (x, y) value set can be calculated for red, green, and blue, respectively, as (x_R, y_R), (x_G, y_G), and (x_B, y_B).

The actual measurement results of an OLED emitter are shown in Figure 4.12. The color range that can be shown by the combination of these three color primaries is found within the triangle that is made by the three color primaries in the (x, y) coordinate. This area is called the *color gamut*. To determine the color reproduction capability of a display, the metric NTSC% is often used (NTSC = National [US] Television System Committee) (Figure 4.13). It is defined as the ratio of the area of the triangle achievable by the display divided by the area of the standard NTSC triangle, expressed as a percentage. For example, XEL-1, the 11-in. OLED television commercialized in 2007, claimed a color gamut of 110%.

Although NTSC was introduced as a cathode ray tube (CRT) television standard, eventually most CRT fluorescence materials were designed with emission color coordinates close to the European Broadcasting Union (EBU) standard or the Rec709 standard (the international standard for HDTV studios), which are much smaller in area than that of the NTSC triangle (Figure 4.14).

On the other hand, digital cameras and computers often use the s-RGB standard, which is shown in Figure 4.14 (it has the same color coordinates as EBU and Rec709). The Joint Photographic Experts Group (JPEG) standard also normally uses the s-RGB color coordinate standard; however, as the s-RGB triangle is not large enough to reproduce high fidelity colors, a new header standard

Petitioner Samsung Ex-1009, 0128

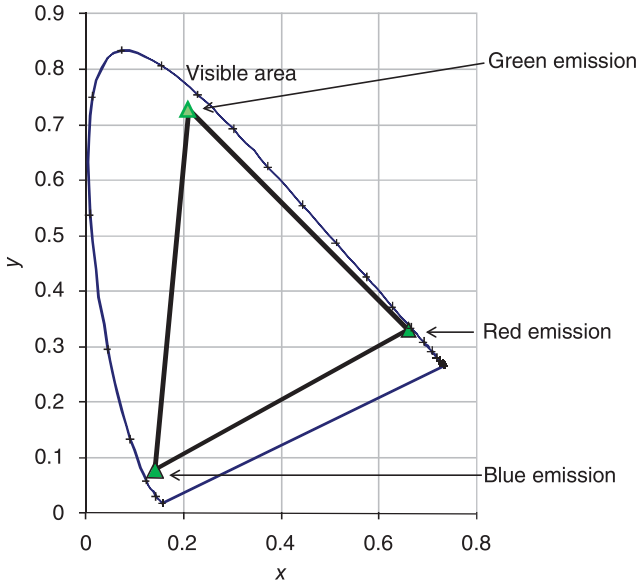


Figure 4.12 Plot of the area reproducible by RGB color mixture.

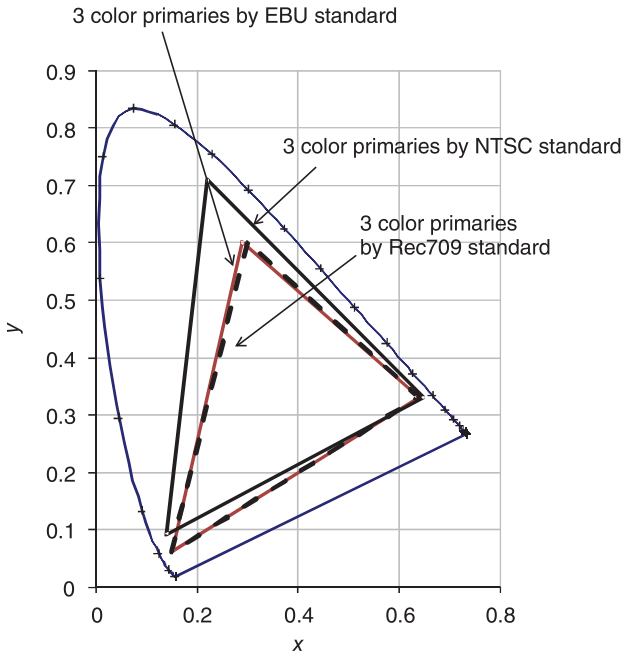


Figure 4.13 Graphical representation of the three color standards applied in television manufacture.

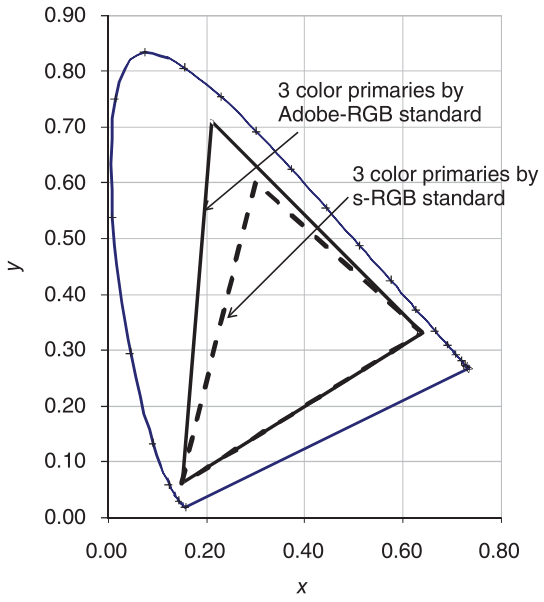


Figure 4.14 Graphical representation of the three color standards applied in digital camera manufacture.

EXIF2.2 has introduced the s-Ycc standard, which uses an extended dynamic range with grayscale values that extend from negative values to values greater than 255, while normal s-RGB uses 0–255 to express grayscales. The newer header standard EXIF2.21 can also handle the Adobe-RGB standard, which is popular in the publishing industry (Figure 4.14).

For better user experience, color reproduction enhancement of displays is attracting attention. Especially for the latest "Super Hi-Vision" standard, very wide color description BT-2020 is applied, which covers 99% of the so-called, "Pointer's color" region, which was introduced by Pointer that describes the area of surface object colors in real world [10]. DCI-P3 standard intended for digital movie projection is also becoming prominent, which covers most of the Pointer's color regions.

The (x, y) color coordinates for four of these standards are listed in Table 4.2.

To ensure color fidelity, s-RGB can reproduce most colors realistically because there are not many vivid colors outside the s-RGB triangle in the real world, as illustrated in Figures 7.2 and 7.3. However, although highly saturated colors rarely occur, they have an intense impact on a viewer, so a color gamut wider than that of s-RGB is useful for showing such colors.

In the television industry, the image boosting technique, which converts an original image into a more impressive image, such as one with more vivid colors, by means of graphic engine IC chips or a graphics processing unit (GPU), is often used to enhance the image impression. A wider color gamut is useful for such an application as well (discussed in Section 4.2.6).

Petitioner Samsung Ex-1009, 0130

Table 4.2 (x, y) Coordinate of Color Primaries for Each Standard

Standard	Red	Green	Blue
NTSC	(0.670, 0.330)	(0.210, 0.710)	(0.140, 0.080)
Rec-709 (HDTV)	(0.640, 0.330)	(0.300, 0.600)	(0.150, 0.060)
EBU	(0.640, 0.330)	(0.290, 0.600)	(0.150, 0.060)
s-RGB	(0.640, 0.330)	(0.300, 0.600)	(0.150, 0.060)
Adobe-RGB	(0.640, 0.330)	(0.210, 0.710)	(0.150, 0.060)
BT-2020	(0.708, 0.292)	(0.170, 0.797)	(0.131, 0.046)
DCI-P3	(0.680, 0.320)	(0.265, 0.690)	(0.150, 0.060)

As discussed earlier, the (x, y) coordinate is popular as a display color metric; however, there are problems with using the standard. Distance in the (x, y) coordinate is not proportional to differences in perception of the human visual system, so a larger area does not always mean better display capability. Figure 4.15 shows 10 times the perception limits of the human eye in different regions of the (x, y) color space reported by McAdam et al. [11]; this is known as the "McAdam ellipse." As it is an ellipse, not a circle, the human eye does not have the same sensitivity for the x axis and the y axis. Also as shown in Figure 4.15, the human eye is very sensitive to blue colors (left bottom of the graph) but is less sensitive to red (right bottom) and is very insensitive to green colors (top). This illustrates that human eye sensitivity depends on the location on the (x, y) coordinate. Therefore, it is not very meaningful to discuss the area to judge the display capability on the basis of an (x, y) coordinate system.

The issues discussed above explain why many display companies and research institutes have used (u', v') color coordinates to express display capability. The CIE1976 color space coordinates (u', v') can be expressed as

$$u' = \frac{4x}{(-2x + 12y + 3)} = \frac{4X}{(X + 15Y + 3Z)} \tag{4.22}$$

$$v' = \frac{9y}{(-2x + 12y + 3)} = \frac{9Y}{(X + 15Y + 3Z)}. \tag{4.23}$$

Performance comparisons using the (u', v') color coordinates indicate how a color display color can actually be perceived by the human eye. For this reason, there is an increasing number of studies in the literature, calculating color gamut by (u',v').

Also, uniform color space is sometimes factored into any discussion of display capability because the defective criteria (such as the luminance variation limit or the image burning limit according to lifetime test discussed in

Petitioner Samsung Ex-1009, 0131

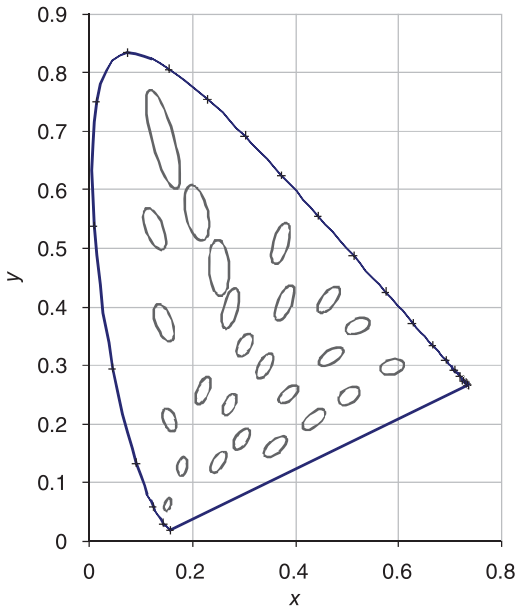


Figure 4.15 Graphical representation of McAdam ellipse, showing the human eye's perception limit (at 10° magnification).

Section 2.5, uniformity criteria discussed in Section 6.4.4, or the metal bus design discussed in Section 6.4.3) should be determined according to the limit of human perception.

4.2.4 Uniform Color Space

CIE-LAB and CIE-UV are two well-known uniform color spaces. On these uniform color spaces, lightness and color can be treated equally so that the length = 1 on the color space is almost equal to the human eye perception limit.

In CIE-LAB uniform color space (Figure 4.16), lightness L^* is defined as

$$L^* = 116f\left(\frac{Y}{Y_n}\right) - 16$$

$$a^* = 500\left\{f\left(\frac{X}{X_n}\right) - f\left(\frac{Y}{Y_n}\right)\right\}$$

$$b^* = 200\left\{f\left(\frac{Y}{Y_n}\right) - f\left(\frac{Z}{Z_n}\right)\right\}$$

In the case of $t > \left(\frac{6}{29}\right)^3$, $f(t) = t^{1/3}$. In other cases, $f(t)$ is $\frac{1}{3}\left(\frac{29}{6}\right)^2 t + \frac{4}{29}$.

Plotting a^*, b^*, and L^* on a three-dimensional graph, the angle of the line made by the plotted point and the original point in plane a^*–b^* shows the hue, and the distance between the plotted point and the original point in plane a^*–b^*

Petitioner Samsung Ex-1009, 0132

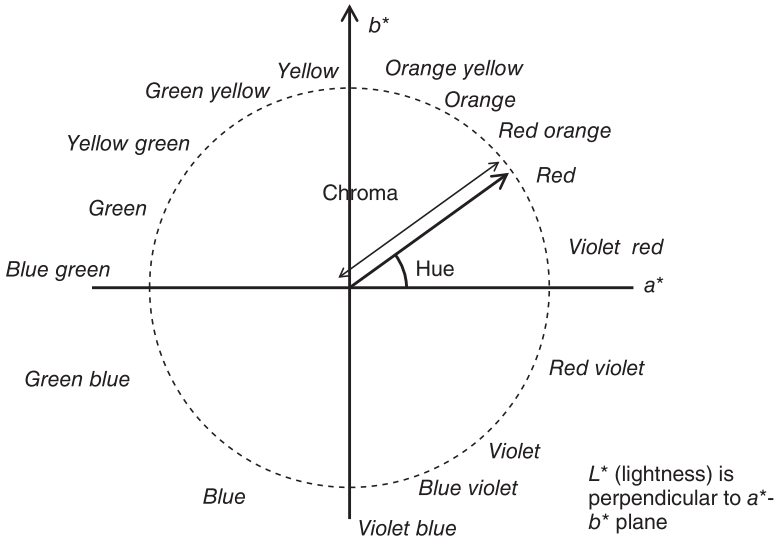


Figure 4.16 CIE-LAB uniform color space.

is the chroma, as in the Munsell color system widely used in color science. In this color space, the color difference (including lightness difference) is defined as ΔE_{ab} by the following equation:

$$\Delta E_{ab} = \sqrt{\Delta L^{*2} + \Delta a^{*2} + \Delta b^{*2}}$$

For CIE-LUV uniform color space, the (u^*, v^*) coordinate is defined by the following equations:

$$u^* = 13L^*(u - u'_n)$$
$$v^* = 13L^*(v - v'_n)$$

Color difference can be expressed for CIE-LUV uniform color space as follows:

$$\Delta E_{uv} = \sqrt{\Delta L^{*2} + \Delta u^{*2} + \Delta v^{*2}}$$

Color difference $\Delta E = 1$ is known to be close to the human perception limit and is a useful criterion for determining parameters for display design, such as

- Acceptable display white point variation
- Acceptable lifetime and viewing angle
- Acceptable image sticking level.

4.2.5 White Point Determination

To display a white image, all red, green, and blue subpixels need to emit light. The white color changes the impression of a display quite a bit. The color should be selected according to the purpose of the display.

Petitioner Samsung Ex-1009, 0133

When tristimulus values of red, green, and blue are (X_R, Y_R, Z_R), (X_G, Y_G, Z_G), (X_B, Y_B, Z_B) respectively, then

$$X_{white} = X_R + X_G + X_B \tag{4.24}$$

$$Y_{white} = Y_R + Y_G + Y_B \tag{4.25}$$

$$Z_{white} = Z_R + Z_G + Z_B \tag{4.26}$$

Then, the (x, y) coordinate of the white emission can be calculated as follows:

$$x_{white} = \frac{X_{white}}{X_{white} + Y_{white} + Z_{white}} \tag{4.27}$$

$$y_{white} = \frac{Y_{white}}{X_{white} + Y_{white} + Z_{white}}. \tag{4.28}$$

The white coordinate (white point) is expressed by the CIE coordinates as well as by the blackbody radiation temperature.

To express the color of white emission, a blackbody temperature is often used. Radiant intensity from a black object having temperature T at the wavelength between λ and $d\lambda$ can be expressed as (Planck radiation law)

$$P(\lambda) = \frac{8\pi hc^2}{\lambda^5} \cdot \frac{1}{e^{\frac{hc}{\lambda k_B T}} - 1}$$

(P, total radiant intensity from a black object toward all directions; c, speed of light; h, Planck constant; k_B, Boltzmann constant. It is necessary to pay attention to a potentially confusing definition. "Warm" color temperature, which normally means a color coordinate closer to red, has a low color temperature, while "cold" color temperature, normally a color coordinate closer to blue, has a high color temperature.)

Figure 4.17 shows the spectrum of the radiant intensity for various color temperatures.

Figure 4.18 shows the CIE coordinate of each blackbody temperature. (The line that the color coordinate follows when temperature is changed is called Planckian locus or blackbody locus.)

In television applications, a temperature of 6500 K (designated as D65) is used to display the white point, which has been introduced by the SMPTE-170M standard in the United States and many other countries. On the other hand, Asian countries such as Japan are using high-temperature color points. For example, Japan is using 9300 K (D93) as a target, which was introduced by NHK, a Japanese broadcasting organization. D65 is $(x, y) = (0.3127, 0.3290)$ and D93 is $(x, y) = (0.283, 0.297)$ on the CIE coordinate. For computer monitors, three color point temperatures are sometimes available: 5000, 6500, and 9300 K.

When designing OLED displays, it is necessary to adjust the red, green, and blue primary color intensities to ensure adequate white balance.

Petitioner Samsung Ex-1009, 0134

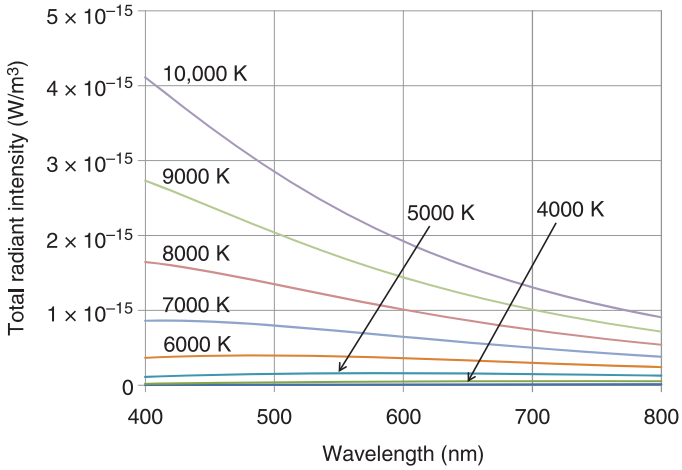


Figure 4.17 Blackbody emission spectrum for each color temperature.

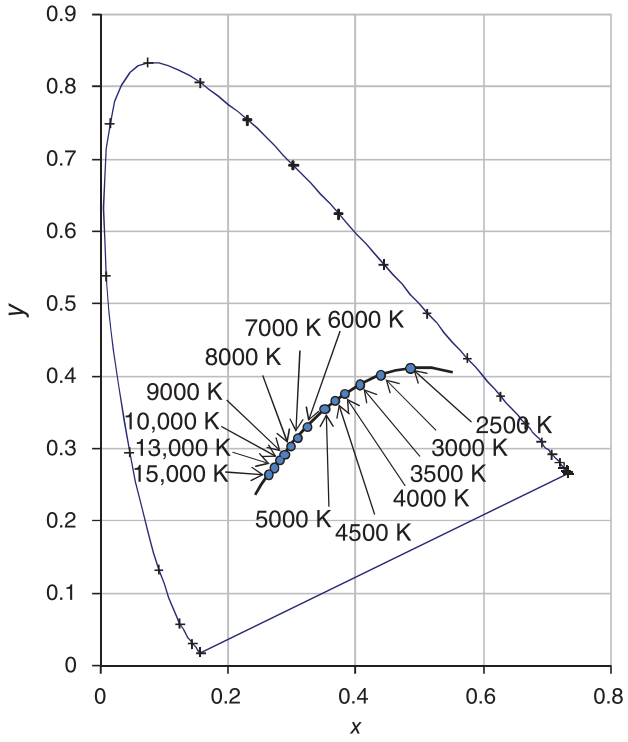


Figure 4.18 Graphical representation of blackbody versus color temperatures.

Petitioner Samsung Ex-1009, 0135

4.2.6 Color Boost

As discussed in Section 4.2.3, a trend exists to aim for wider color reproduction to enhance the user's viewing experience. There was a case that achieved 190% color gamut compared to Rec-709 standard by means of laser scanning television [12]. Then the question arises whether a television with a wider color gamut is always better.

For fidelity, if a television system is using EBU standard, wider color reproduction than EBU color point does not make sense. A still image on PC using s-RGB standard with zero to 255 values (which is representing grayscales by 8-bit, namely, $2^8 = 256$ colors) does not need a wider gamut for fidelity color reproduction. As discussed in Section 7.4.1.2, as the color is saturated (as the coordinate goes the outer direction), the probability to have the color point is significantly decreased, especially outside the EBU triangle.

The reasons why people want to use a wider color gamut is one of the following cases or both.

(1) A display that needs to reproduce rare saturated colors
(2) A display with color boosting for better viewer experience.

In option (1) without color boosting, the viewers seldom see the color outside the EBU triangle. It should be noted though such rare colors seldom appear in real world, it remains much stronger impression than frequent colors. The purpose of having a wider color gamut in such systems is to have impressive color reproduction for rare images.

Option (2) is a more realistic implementation of wider color reproduction. It is using human's preference of converted object colors to more vivid images. Hisatake et al. made an analysis on human's preference on the color conversion [13]. Figure 4.19 shows the allowable limit and optimal limit of color conversion. In most cases, color conversion to less vivid direction (inward conversion in the figure) is not acceptable, but conversion to more vivid direction is more acceptable (outward direction). It was also pointed out that wider color conversion within the allowable limit is preferred by the viewers. (It can be also seen that the color conversion near the skin color is not preferred, very much different from other colors.) From the result, a certain level of color conversion to more vivid colors within allowable limit improves the viewing experience. Wider color gamut display helps to make this happen.

Generally speaking, a display with wider color reproduction delivers better viewing experience through color boosting and the capability to show rare colors. Said that, it should be noted that the effectiveness is limited beyond 100%

Petitioner Samsung Ex-1009, 0136

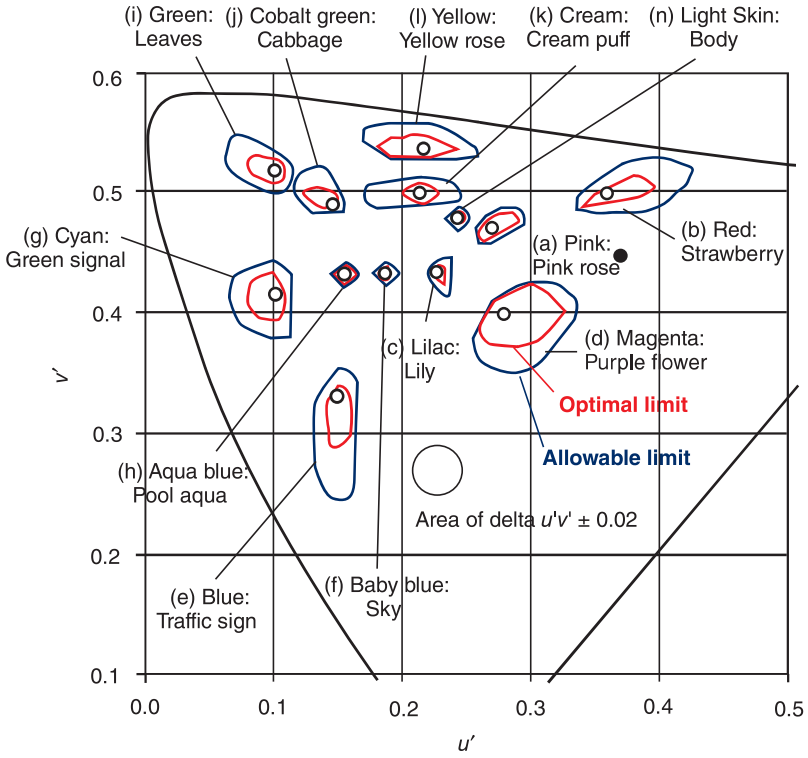


Figure 4.19 Optimum and limit of color boosting (Courtesy by Y. Hisatake).

NTSC. At the same time, as the vivid primary colors have less human eye's sensitivity, the power consumption is increased as the display color gamut is increased. It is reasonable to design an OLED display taking the trade-off into account.

4.2.7 Viewing Condition

Kubota et al. made a survey analysis on the viewing condition of CRT display in home use environment for 50 Japanese households [14]. The data shows the following:

1. Illuminance on the display was 27–327 lx and average was 108 lx.
2. Luminance of display was 72–530 cd/m^2, average was 260 cd/m^2.
3. Viewing angle was ±60° for horizontal direction and was ±30° for vertical direction. Moriguchi et al. reported that there is an acceptable viewing angle limit due to the geometrical distortion of a display [15].

Petitioner Samsung Ex-1009, 0137

Tanton et al. also made a survey in England by 102 people regarding the viewing distance in 2004. The mode value of 50 households was 8H, 8 times the display screen height [16]. Noland et al. reported that the display size is increasing without much change in the viewing distance, so the latest viewing distance has become 5.5H, much smaller than Tanton's number [17].

When display technologies are discussed and compared, people tend to compare by the catalog specification, such as viewing angle. However, the survey of viewing condition shows that none watches television from 170°angle direction. To make real high-performance display happen, it is important to consider the range of viewer's location and maximize the display performance, such as contrast ratio, for it.

4.3 PASSIVE-MATRIX OLED DISPLAY

Actual display design methodologies are discussed in the following chapters. There are several forms of OLED displays, such as segment displays (involving formation of electrodes by photolithography to create a pattern where the emission needs to take place and no matrix is formed), passive-matrix displays [18–22], and active-matrix displays. The passive-matrix display design is discussed here.

4.3.1 Structure

Figures 4.20 and 4.21 show passive-matrix OLED (PMOLED) displays (also called *passive OLED displays*). The data line, which is oriented vertically, and scan line, which is oriented horizontally, are formed, and the OLED devices are fabricated between the lines. Red, green, and blue subpixels are allocated to specific lines; data lines are driven by data drivers, and scan lines are driven by scan drives. (Data line and scan line can also be driven by a display controller chip to reduce cost in actual case.)

Figure 4.22 shows a microscopic view of a passive-matrix OLED display. When voltage is applied to data and scan lines, current flows in the target pixel and emission takes place.

The most common OLED device patterning method involves the shadow masking process (discussed in Section 5.1.1). For cathode patterning, an overhanging photoresist (cathode separator) can be applied with cathode self-alignment as shown in Figure 4.23. The pixel definition layer (PDL; also called "edge cover" or "edge insulator") is also described in Figure 4.23. It is used (1) to avoid defective pinhole formation made by the steep anode edge, which sometimes causes an electric short between anode and cathode and (2) to apply accurate pixel area definition by photo patterning, which can facilitate more accurate positioning of the patterning edge than shadow masking. The PDL is normally made of photoresist.

Petitioner Samsung Ex-1009, 0138

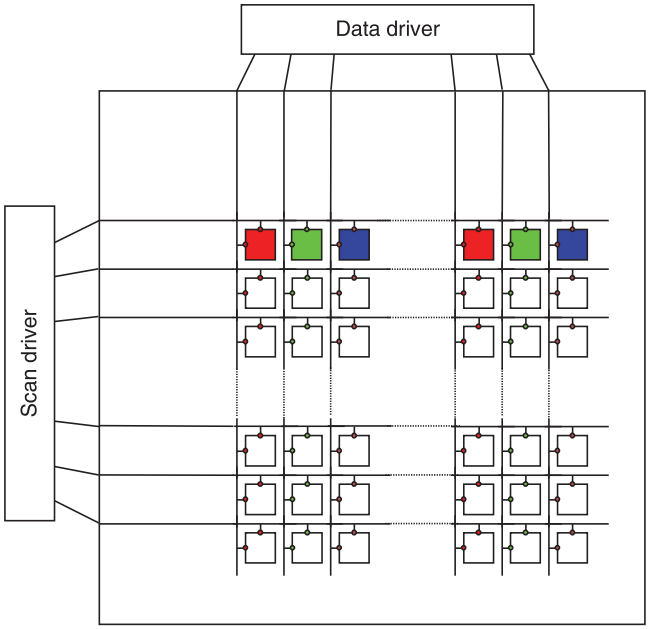


Figure 4.20 Matrix driving of a passive-type OLED display.

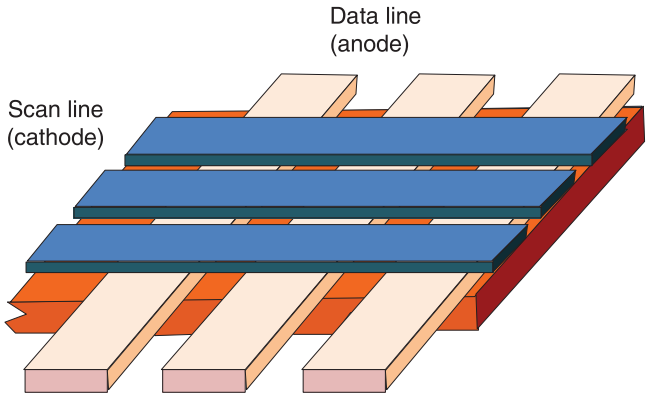


Figure 4.21 Structure of a passive-matrix OLED display.

4.3.2 Pixel Driving

The equivalent circuit of an OLED device is depicted in Figure 4.24, with a diode having parasitic capacitance. When the organic layer thickness is ~100–200 nm, and if the pixel area is 0.2 mm^2, the capacitance is somewhere in picofarads. The capacitance charge/discharge current does not contribute

Petitioner Samsung Ex-1009, 0139

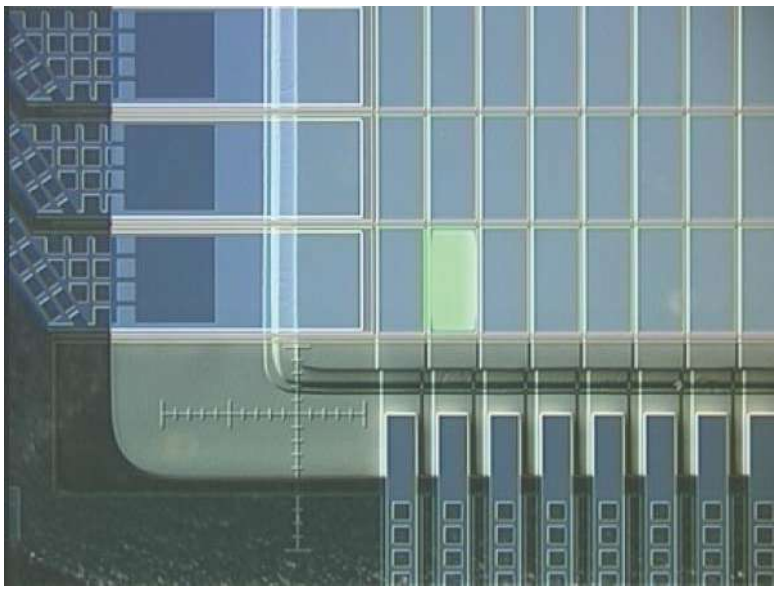


Figure 4.22 Microscopic view of a passive-matrix OLED display.

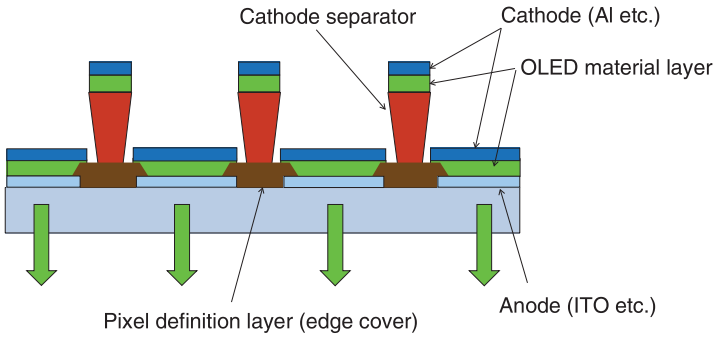


Figure 4.23 A passive-matrix display employing the cathode separator patterning method.

to the OLED emission, so it can increase the power consumption and reduce the emission period. Therefore, it is very important to minimize the parasitic capacitive current when designing passive-matrix OLED displays.

When driving a pixel as shown in Figure 4.22, it is possible to transfer charge (precharging) from the most recently addressed pixels to the next row of pixels by applying a voltage lower than the threshold voltage to "off" lines. In this way, crosstalk is avoided and the charging period is reduced by avoiding unnecessary charging.

Petitioner Samsung Ex-1009, 0140

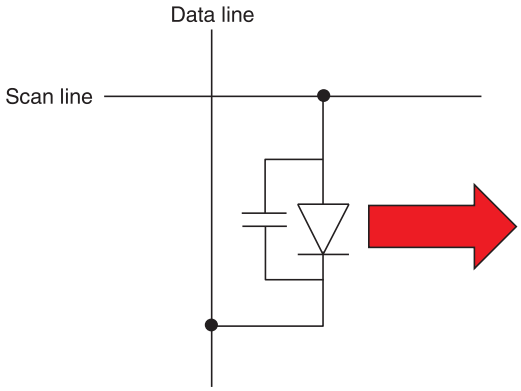


Figure 4.24 Pixel circuit of a passive-matrix OLED display.

Also, crosstalk (luminance error due to unintended signals) takes place according to the precharging situation difference. To avoid this phenomenon, the data line and the scan line are connected together electronically, at the onset of every frame period, to prepare for emission in order to reset the precharging levels.

With simple scanning of a passive-matrix OLED display, emission of OLED devices takes place only for one selected line. For example, if the number of the scan line is N, the emission period in one timeframe ($t_{\text{timeframe}}$) is $t_{\text{timeframe}}/N$, and is very short. Normally, the OLED device lifetime is proportional to $1/L^n (n = 1.2–1.9$, where L is luminance (see discussion in Section 2.5), so higher resolution can shorten the OLED device lifetime. To correct this problem, multiline scanning, which drives multiple lines at the same time, is used (Figure 4.25).

Figures 4.26 and 4.27 show examples of actual passive-matrix OLED display products. Thus far, passive-matrix OLED displays have been used more for lower-resolution displays than high-resolution displays because of the following:

- High luminance (needed for high resolution) required due to short emission time, which diminishes lifetime
- Insufficient charging period for high-resolution displays, due to the time loss caused by the charging of the huge parasitic capacitance of passive-matrix OLED displays
- Insufficient data line capacitance discharging in a short time, which makes inaccurate low grayscale presentation.

Currently, passive-matrix OLED displays are used mainly for the applications that do not require high resolution, such as car audio systems and MP3 players.

Petitioner Samsung Ex-1009, 0141

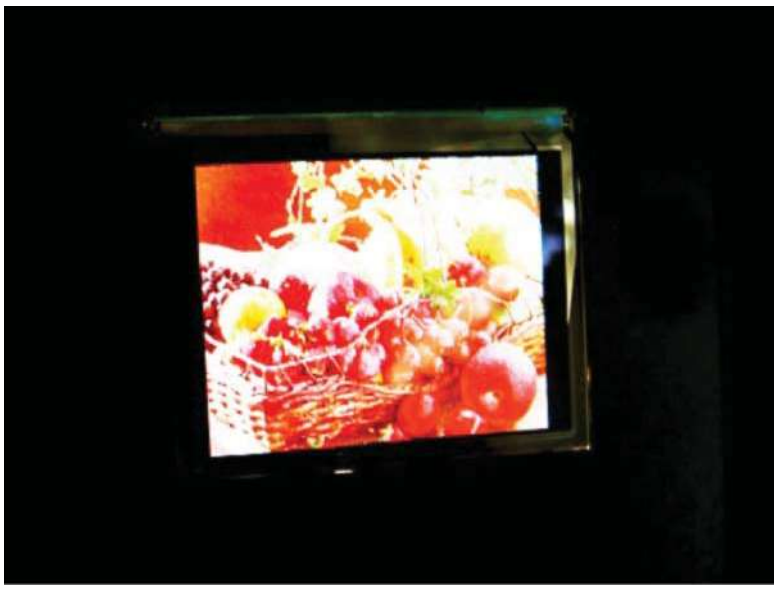


Figure 4.25 A passive-matrix OLED display prototype employing a multiline scanning method (2.2-in.-scale demonstration by TDK at CEATEC 2009).

4.4 ACTIVE-MATRIX OLED DISPLAY

As discussed in the preceding section, active-matrix driving is necessary when larger or higher-resolution displays are needed. Active-matrix OLED display design techniques are discussed in this section.

4.4.1 OLED Module Components

Figure 4.28 shows an example of an active-matrix OLED (AMOLED) product. Active-matrix OLED display includes the following components:

- TFT (thin-film transistor) substrates (also called *backplane substrates*; discussed in Chapter 6)
- Encapsulation glass (discussed in Section 3.3)
- Driver integrated circuits (IC) (discussed in Sections 6.4.4 and 6.4.5)
- Circular polarizers (may be unnecessary in certain applications).

As TFT is manufactured in large scale due to LCD needs, its cost is reduced enough compared with other components. Various TFT technologies have been tried for OLED driving, such as laser-crystallized polysilicon TFT [23],

Petitioner Samsung Ex-1009, 0142



Figure 4.26 A passive-matrix OLED display product (FOMA N2001).

metal-induced polysilicon TFT [24], amorphous silicon TFT [25], microcrystalline silicon TFT [26], oxide TFT [27], and organic TFTs [28]. For the mobile display applications, laser-crystallized polysilicon technology is dominant due to several merits, such as reduced number of electrical connection, narrow boarder, peripheral circuit cost reduction, and low power operation, brought by the CMOS circuit integration capability of polysilicon TFTs. For the large television, oxide TFT is dominant because it can be manufactured with almost the same mature equipment infrastructure of amorphous silicon TFTs, while equipping with much better mobility and stability than amorphous silicon.

Petitioner Samsung Ex-1009, 0143



Figure 4.27 A white monochrome passive-matrix OLED display product (EDIROL R09 digital audiorecorder).

The details are discussed in Chapter 6.

For the reduction, the main focus for active-matrix should be encapsulation, driver ICs, and material utilization.

4.4.2 Two-Transistor One-Capacitor (2T1C) Driving Circuit

Figure 4.29 shows an example of the OLED pixel emission of an actual product. To control the luminance of an OLED device, TFT needs to be serially connected to OLED. There are two types of connection of TFT and OLED as shown in Figure 4.30, depending on placing TFT in (a) higher-voltage side like

Petitioner Samsung Ex-1009, 0144



Figure 4.28 A smart phone with round-shape bezel by flexible OLED display (in SID Display Week 2015 exhibition by LG display).

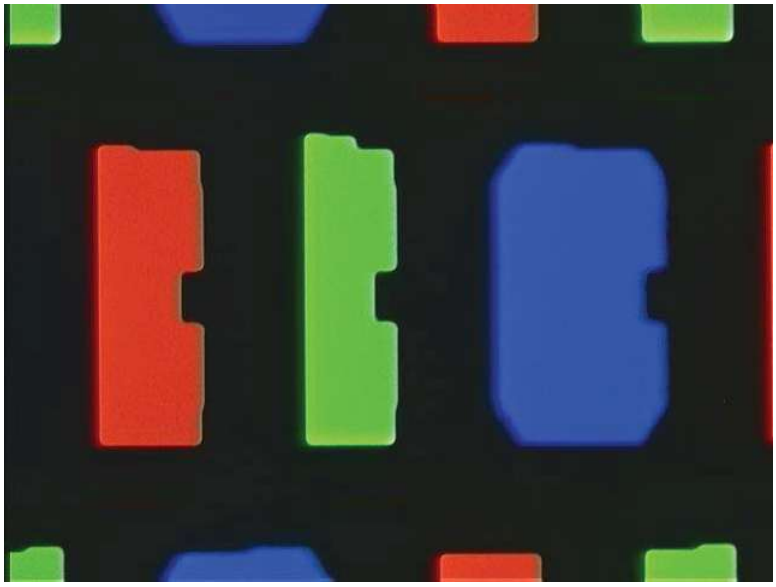


Figure 4.29 An example of an OLED pixel used in an actual product.

Petitioner Samsung Ex-1009, 0145

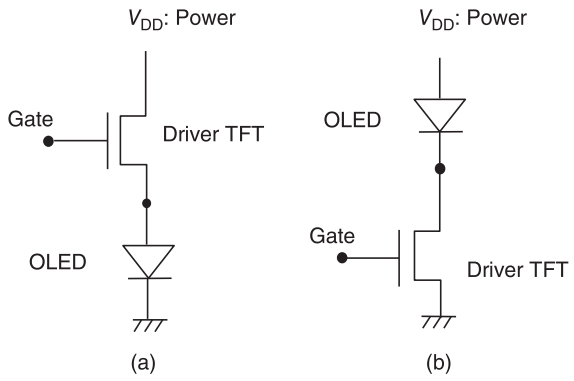


Figure 4.30 Two ways of OLED-TFT connection.

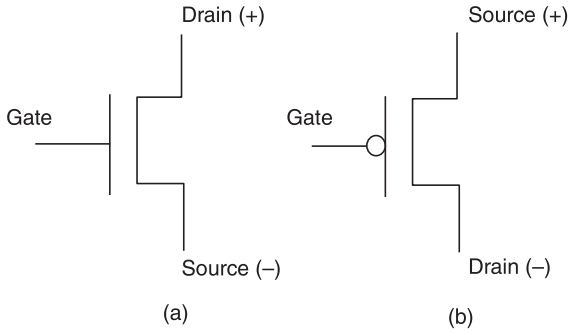


Figure 4.31 Expression of NMOS FET and PMOS FET.

or (b) lower-voltage side like. As commonly used, NMOS FET and PMOS FET are described as shown in (a) and (b) of Figure 4.31, respectively.

In most of the displays, scan lines are selected and then deselected one after another. For example, 720 progressive (720p) display format driven at 60 Hz, 720 lines are selected and deselected one by one in 1/60 s. Therefore, the selected period of one scan line is 1/720/60≅20 μs. If the OLED-TFT connection such as active-matrix LCDs is simply applied to the display matrix as shown in Figure 4.32, OLED in a pixel emits light for only 20 μs in one frame = 1/60 s in the case of 720p, which cannot make high luminance display performance happen. The paper by Brody et al. in 1975 employed two TFTs and one capacitor (called 2T1C circuit) as shown in Figure 4.33 [29]. With this pixel circuit, the signal data is stored in pixel capacitor during selected period and the stored voltage drives the driver TFT for a frame period, which dramatically improve the emission time that promises the high luminance OLED display operation. This 2T1C circuit is still used as the basis of most pixel circuit of OLED displays.

As mentioned above, this acronym is derived from the fact that the circuit contains two transistors and one capacitor. Other pixel circuits are equipped

Petitioner Samsung Ex-1009, 0146

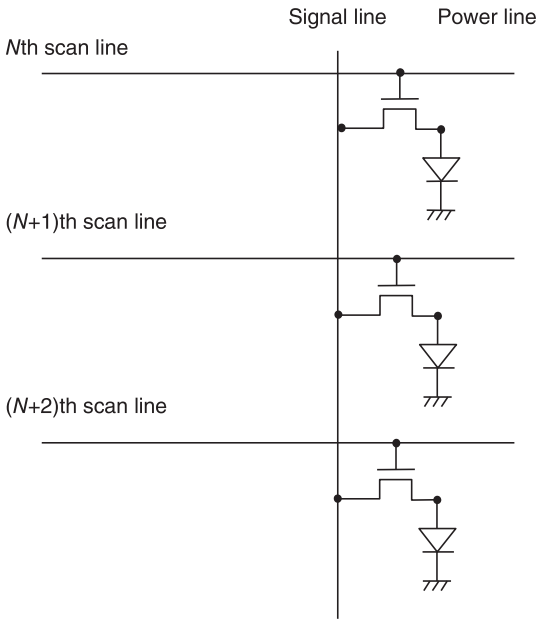


Figure 4.32 Active-matrix driving by one TFT per pixel approach.

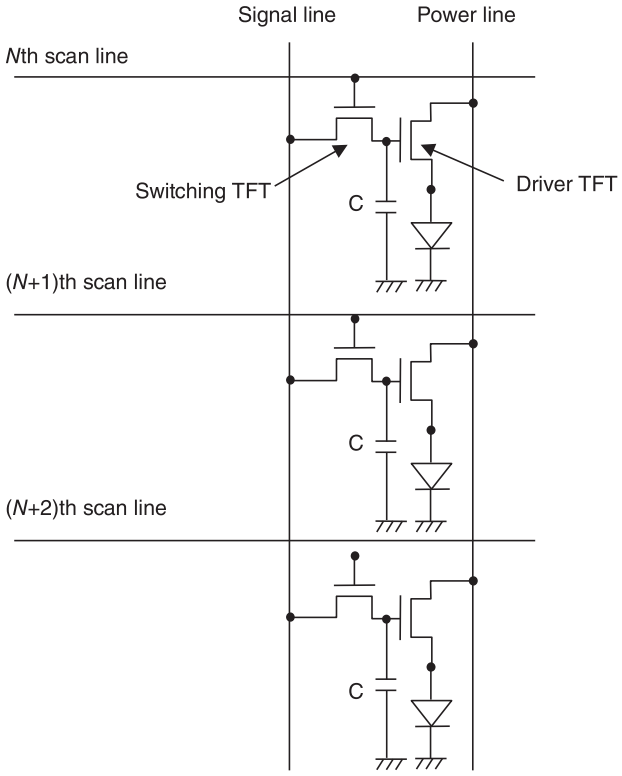


Figure 4.33 Active-matrix driving by two TFT and one capacitor (2T1C) per pixel approach.

Petitioner Samsung Ex-1009, 0147

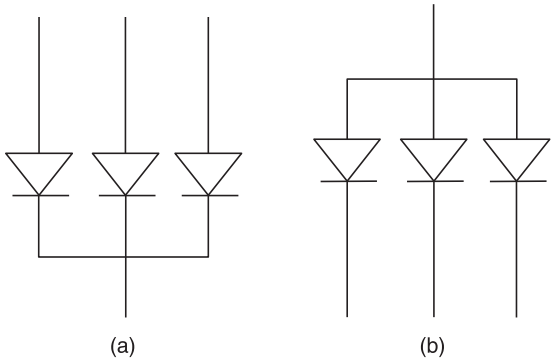
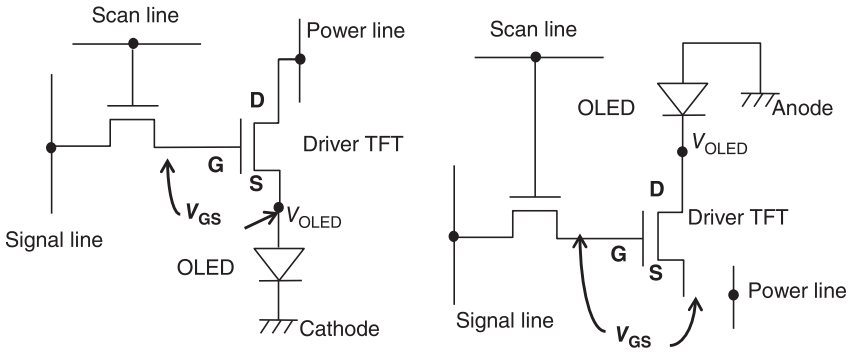


Figure 4.34 Common-cathode and common-anode connection.

with two TFTs and one capacitor; however, the designation 2T1C normally indicates a circuit configuration as shown in Figure 4.33.

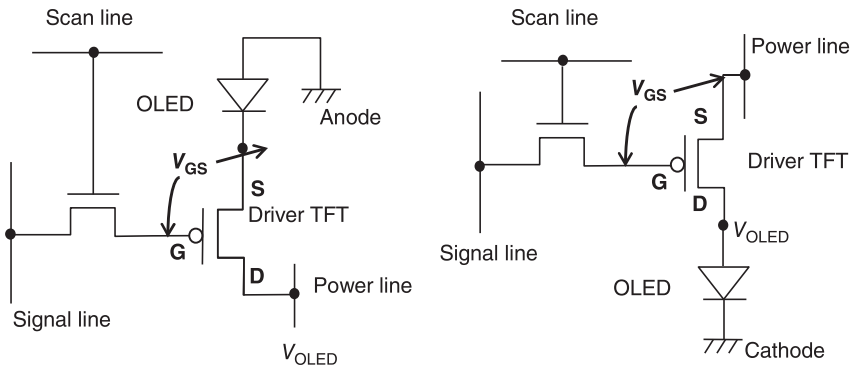
Figure 4.34 shows the so-called "Common-cathode" and "Common-anode" configuration, which is frequently used in the electronic circuit. In a display using 2T1C pixels, the circuit can be formed by either of these two connections. The driver TFT, which drives the OLED current, can be either NMOS or PMOS type, so there are four kinds of 2T1C circuit, as shown in Figures 4.35 and 4.36. In the case of "NMOS + common cathode" (Figure 4.35a) and "PMOS + common anode" (Figure 4.36a), gate-to-source voltage V_{GS}, which determines the OLED current, is subjected to the OLED driving voltage variation. This configuration is called source-follower type. On the other hand, the case of "NMOS + common anode" (Figure 4.35b) and "PMOS + common cathode" (Figure 4.36b) V_{GS} is kept the same regardless of OLED voltage variation, which assures the constant OLED current. These four configurations



(a) Source-follower circuit (b) Constant-current circuit

Figure 4.35 Two ways of pixel configuration using NMOS driver TFT (omitting capacitor to avoid complexity).

Petitioner Samsung Ex-1009, 0148



(a) Source-follower circuit (b) Constant-current circuit

Figure 4.36 Two ways of pixel configuration using PMOS driver TFT (omitting capacitor to avoid complexity).

have a possibility to be used for either top emission or bottom emission with RGB-pixelation or with White + Color Filter method. It is important to carefully consider the pros and cons of each technology combination when a new OLED display is designed.

Currently, most of the OLED devices on the market is using anode as the bottom electrode and cathode as top electrode. (It is known that the top anode structure gives worse performance compared to top cathode structure. There are several papers reporting the performance improvement of top anode structure [30, 31].) Naturally, it makes the situation simpler if the anode is connected to TFT electrodes. In that sense, constant-current type "PMOS + common cathode" device (Figures 4.36b and 6.13) and source-follower type "NMOS + common cathode" (Figures 4.35a and 4.37) are more commonly used. Former is an industry-standard technology for mobile displays and the latter is also an industry standard for large OLED television using oxide semiconductors (Section 6.5.5).

As discussed, in the case of source-follower-type pixel configuration, the OLED current is altered by an OLED voltage increase, which happens after driving stress. To avoid the source-follower-type configuration using NMOS TFT, TFT structure as shown in Figure 4.38 is necessary. In Figure 4.38, TFT electrode is connected to the cathode of NMOS TFT via hole and overhanging photoresist structure. In this implementation, the anode is made of aluminum and forming as a low resistive line. (Anode line structure.)

Though the V_{GS} fluctuation of source-follower-type is sometimes regarded as disadvantageous, there are actually some merits using it. In the case of constant-current configurations regardless of NMOS or PMOS, the source electrode is connected to the power line, as shown in Figures 4.35b and 4.36b.

Petitioner Samsung Ex-1009, 0149

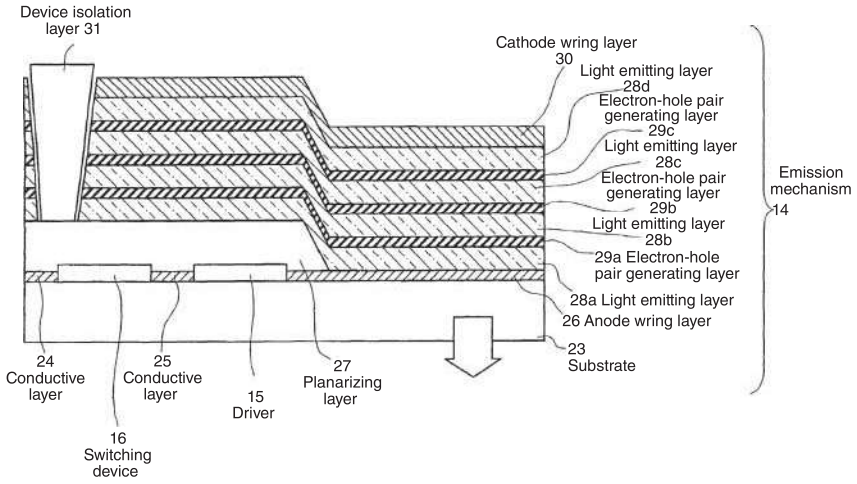


Figure 4.37 An example of common-cathode tandem white OLED pixel configuration by NMOS TFT [32].

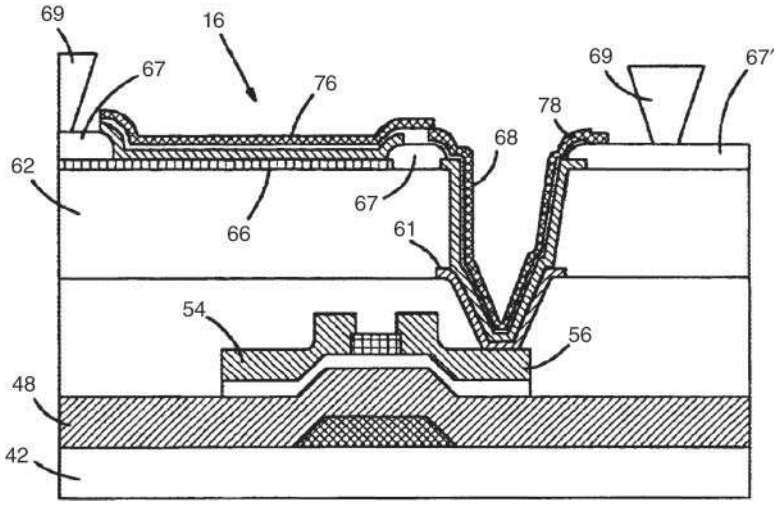


Figure 4.38 An example of common-anode pixel configuration by NMOS TFT [33].

Due to this reason, the OLED current is subjected to the voltage drop of the power line. However, in the case of source-follower configuration, the source node is not connected to the power line, which decreases the sensitivity to the power line voltage drop.

There is another merit of source-follower type. In the case of constant-current circuit, when I–V curve of OLED device is fluctuated, the OLED current would

Petitioner Samsung Ex-1009, 0150